
# Production of Biogasoline from Waste Cooking Oil as an *Environmentally Friendly* Alternative Liquid Fuel

*Submitted by*

**Mampuru, Madinoge Bridgiliah (361967)**

A Dissertation submitted to the Faculty of Engineering and the Built Environment, University of the Witwatersrand, Johannesburg, South Africa, in fulfillment for the degree of Master of Science.

**Supervisor: Dr. Diakanua Bavon Nkazi**

Johannesburg, 20th of September 2017

## DECLARATION

I declare that this thesis titled *"Production of Biogasoline from Waste Cooking Oil as an Environmentally Friendly Alternative Liquid Fuel"* is the result of my own unaided research work, except as cited and acknowledged in the references. This thesis has not been submitted for any degree.

Name: Mampuru, Madinoge Bridgiliah

Student Number: 361967

Signature: .....

Date: 18-September-2017.....

## DEDICATION

This work is dedicated to:

My dear parents Mr L.M. and Mrs E.M. Mampuru,

my beloved siblings Lennies Nkgabe, Sharol Diphale,

Collins Matime and Bradley Segatle

## ACKNOWLEDGEMENTS

The successful completion and outcomes of this study were possible through of the collective efforts and support I have received. I will like to acknowledge and express my sincere gratitude to the following individuals and organizations that have contributed positively to the work done during my study:

First and foremost, I would like to express my sincerest gratitude and honour to Almighty God, Father, for his Love, Mercy and Grace throughout this journey. Thank you for keeping me going when the going got tough. Thank you Daddy for walking with me until the finish line of this journey.

To my supervisor, Dr Diakanua Bavon Nkazi, your work ethic is admirable and phenomenal. Thank you for your support and dedication every step of the way. Without your much needed and received support, this work will never have been possible. Your commitment towards the start and completion of this project has made it all possible, and I am very grateful and honoured to have worked with you as my supervisor.

Special thanks to my parents, Mr. L.M. Mampuru and Mrs. E.M. Mampuru; and siblings, Lennies Nkgabe, Sharon Diphale, Collins Matime and Bradley Segatle Mampuru, thank you for your support and being patient with me during my academic endeavors. Thank you for allowing me to confidently go after my dreams and achieving all that I have always wanted to.

I express my full gratitude to the South African Nuclear Human Asset and Research Programme (SANHARP) under the National Research Foundation (NRF) for financial support for the duration of this study.

To Prince Matayo, founder of Matayo Biofuels (Pty) Ltd, thank you very much for the significant contribution and value you have added to this work.

To the School of Chemical and Metallurgical Engineering workshop staff, thank you very much for your willingness to assist with most of the laboratory experimental work set-up. Your assistance is very much appreciated.

- Thank you to Miss Swathi Burla and Mrs Zamashinga Mthabela for assistance with TGA.

Thank you to the following staff from the faculty of Sciences (Schools of Chemistry, Microbiology and Physics) for specifically assisting me with the following analysis:

- Prof. N.J. Coville and his students Tumelo Phaahlamohlaka and Lerato Lehlekelele for assisting me with FT-IR spectrometry and BET characterisations.
- Dr. Manoko Maubane from the Microscopy and Microanalysis Unit for your assistance with SEM analysis, your contribution is very much appreciated.
- Dr. Rudolph Erasmus for availing himself to assist with Raman spectroscopy.
- Mr Thapelo Mbhele for assisting with GC-MS.
- Mr Chuene Mokgehle for assistance with ICP-OES.

To Kudzai Mabika, our collaborations during the course of our respective studies have brought forth some meaningful contributions to the impacts of this work. I thank you.

## ABSTRACT

Energy is an important utility to human kind. Since the beginning of human civilization, human beings have become acquainted with travelling and transportation of goods. The use of conventional energy fuels for automobile engines is no longer sustainable due to finite crude oil reserves available in the world, of which many are facing the crisis of being depleted. The use of conventional fuels is a major contributor to environmental concerns such as global warming. Therefore there is an urgent need to explore alternative sources of fuel energy that are sustainable and environmentally friendly. The production of biofuels has been receiving increased academic and industrial attention as practical alternative fuel sources that can partially or completely replace conventional fuels.

A study of the production of biogasoline from waste cooking oil as an alternative and re-usable source of liquid fuel was conducted in this project. This work focused on the variety of parameters that would deliver the optimum conversion and yield of biogasoline. The waste cooking oil was converted through catalytic hydrocracking in the presence of an acid activated Ni-Mo/$Al_2O_3$ catalyst and constant hydrogen gas pressure of 0.5 kPa. A number of Ni-Mo/$Al_2O_3$ catalysts were synthesized with varying Ni-loadings from 5-25 wt. % and calcination temperatures from 300 °C to 700 °C.

The catalysts were characterised using ICP-OES, TGA, BET, SEM, FT-IR and Raman spectroscopy. Catalyst characterisation results revealed that the catalyst with 5 wt. % Ni possessed the greatest thermal strength, with the maximum BET surface area of 61.61 $m^2/g$ and high dispersion of the active species in the catalyst. The optimal calcination temperature range for this catalyst was found from 500 °C to 600 °C.

The effects of reaction temperature, reaction time, catalyst: oil ratio, catalyst calcination temperature and Ni-loading (wt. %) were investigated. The highest percentage of produced biogasoline was 59.50 wt. % at a reaction temperature of 250 °C, catalyst: oil ratio of 1:75, reaction time of 1 hr with a catalyst loaded with 5 wt. % Ni and calcinated at 300 °C.

The use of stainless steel reactors that can handle higher reaction temperatures and pressure is recommended for future studies that will allow more severe cracking of the raw material into

lighter hydrocarbons. The Ni-Mo/$Al_2O_3$ catalyst can also be modified with boron or fluorine to enhance its catalytic activity.

## NOMENCLATURE

| | |
|---|---|
| $Al_2O_3$: | Alumina |
| Ar: | Argon |
| BET: | Brunauer-Emmet-Teller |
| BFPL: | Biomass Flash Pyrolysis Liquid |
| CHMT: | School of Chemical and Metallurgical Engineering |
| $CO_2$: | Carbon Dioxide |
| DF: | Distilled Fraction |
| EN: | European Standard |
| EU: | European Union |
| FFA: | Free Fatty Acid(s) |
| FAE: | Fatty Acid Esters |
| FT-IR: | Fourier Transform Infrared Spectra |
| GC-MS: | Gas Chromatography and Mass Spectrometry |
| GHG: | Greenhouse Gases |
| HDS: | Hydrodesulphurization |
| $H_2$: | Hydrogen |
| L: | Litre |
| LHSV: | Liquid Hourly Space Velocity |
| Mo: | Molybdenum |
| MT: | Mega-Ton |

| | |
|---|---|
| Ni: | Nickel |
| $N_2$: | Nitrogen |
| NOx: | Nitrogen Oxides |
| OLP: | Organic Liquid Products |
| RON: | Research Octane Number |
| RPM: | Revolutions per Minute |
| SEM: | Scanning Electron Microscopy |
| T: | Ton |
| TIC: | Total Ion Chromatogram |
| UK: | United Kingdom |
| USA: | United States of America |
| WCO: | Waste Cooking Oil |
| wt. %: | Weight Percentage |

## Table of Contents

## List of Figures

## List of Tables

# CHAPTER 1: INTRODUCTION

## 1.1 Introduction

The United Nations Framework Convention on Climate Change (UNFCCC) reported in 2006 (Blodel *et al.*, 2006) that the energy sector accounted for 83 % of the global anthropogenic greenhouse gas (GHG) emissions. Carbon dioxide ($CO_2$), methane ($CH_4$) and water vapour ($H_2O$) constituted approximately 94 %, 5 % and 1 %, respectively (Pandey, 2011). These gases occur naturally in the atmosphere and form part of a natural temperature control system. However, the concentration of these gases in the atmosphere has increased significantly. The increase in concentration of greenhouse gases in the atmosphere is partly as a result of the combustion of fossil fuels. Of the greenhouse gases, $CO_2$ is said to be the main cause of global warming (Olivier *et al.*, 2012). Global warming creates drastic social and economic challenges. The challenges brought upon by global warming include melting glaciers, rising sea levels and drastic negative impacts on agricultural activities (Gupta & Demirbas, 2010). To mitigate such challenges, the energy production sector can potentially shift from fossil sources to carbon-emission free energy sources (Pandey, 2011).

The sustainable use of carbon-emission free resources, such as biomass, as an alternative raw material for the production of biofuels has recently been a subject to which various global research activities are giving attention and focus. From the range of biomass resources available, the use of vegetable oils has been a common topic (Nasikin *et al.*, 2009). Vegetable oils have become an attractive resource because they are free of nitrogen and sulphur compounds, giving them an advantage over fossil fuels (Taufiqurrahmi & Bhatia, 2011). Biofuels also release $CO_2$ during combustion. However, they are considered to be $CO_2$ neutral. This implies that the $CO_2$ emitted gets used up by plants during the process of photosynthesis (Taufiqurrahmi & Bhatia, 2011).

However, vegetable oils are also used within the food supply chain. It then becomes a challenge to use them as feedstock for the production of biofuels. To counteract this challenge, using waste cooking oil (WCO) is seen as a possible solution. Using waste cooking oil from households and food supply industries will mitigate the problem of waste cooking oil disposal. According to

given statistics, in China alone, as much as 4-8 million tons (MT)/year of oil are disposed (Fu *et al.*, 2008). In the USA and Canada, 1.4 MT/year and 150 000 T/year of waste cooking oil are discarded, respectively (Chhetri *et al.*, 2008). In other statistics, the European Union (EU) countries dispose 700,000 to 1 MT/year (Jacobson *et al.*, 2008). As reported by Chhetri *et al.* (2008) and Phan and Phan (2008), the United Kingdom (UK) and Japan disposes off 200,000 to 1 MT/year and 400,000 to 1 MT/year of oil, respectively. In South Africa, the National Recycling Forum (2013) reported that approximately 73,000 T/year of used cooking oil is collected for recycling (National Recycling Forum, 2013).

## 1.2 Motivation

The continued and eventually successful advances for improving biofuel technology applications are necessary tools that can effectively be used to combat energy security issues, environmental concerns, foreign exchange savings and socio-economic issues (Mohd Addli, 2009).

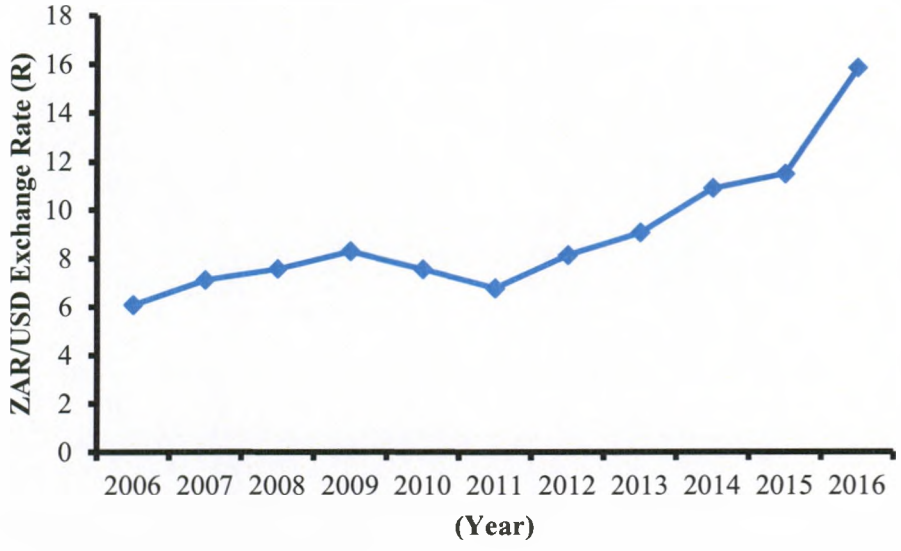


**Figure 1: ZAR/USD Exchange Rate from 2006 to 2016 (extracted from BusinessTech.co.za, 2016a)**

In the local context, South Africa currently relies heavily on foreign suppliers for liquid fuel energy in the form of crude oil. This brings about drastic fuel price hikes as a result of the continually weakening South African Rand (ZAR) against the US Dollar (USD). It can be observed from Figure 1 that the ZAR/USD exchange rate has increased significantly over the

past decade, which means that South Africa's reliance on importing foreign goods has become very expensive over the years. The exchange rate over the course of the past 10 years has increased by more than 160 %. Since the year 2011, the exchange rate has increased continually. The worst performance of the ZAR against the USD was experienced in 2016, with more than 34.9 % increase compared to an average increase of 14.3 % over the 5 preceding years. Therefore a need arises for investing efforts into exploring alternative sources of liquid fuels that can be accessed and produced locally.

The use of vegetable oils as fuel sources has received attention as a topic for academic researches. Vegetable oils consist mainly of triglycerides, which are hydrocarbon molecules with three fatty acids attached to carbon atoms on a propane molecule. The triglycerides molecules exhibit quite a similar structure to those found in crude oil (Nasikin *et al.*, 2009). Numerous studies for producing biodiesel from used vegetable oils have proven to be successful and this has led to the commercialization of biodiesel production. It is therefore necessary to explore the possibilities of producing biogasoline from waste cooking oil. Mohd Addli (2009) highlighted the fact that over 50 % of petroleum crude oil gets converted into gasoline, as compared to other petroleum-based products. This means that gasoline or petrol has the highest demand and price cost to its consumers. It is therefore worthwhile to invest extensive research efforts into the exploration of biogasoline production possibilities.

Figure 2 shows that the increase in the price of petrol has been significantly more than that of diesel. Before the year 2009, the prices of petrol and diesel were competitive. It can be seen from Figure 2 that from 2009, there was a significant difference in the costs of petrol and diesel. This trend carried on to recent years, but there was a decrease in the difference between the average price of petrol and diesel from 17.5 % in 2015 down to 11.3 % in 2016. It can also be observed that the high octane Unleaded 95 was quite cheaper than its lower octane counterpart, Unleaded 93. This suggests that the demand for Unleaded 93 is higher than that of Unleaded 95, thus it came at a bit higher price.

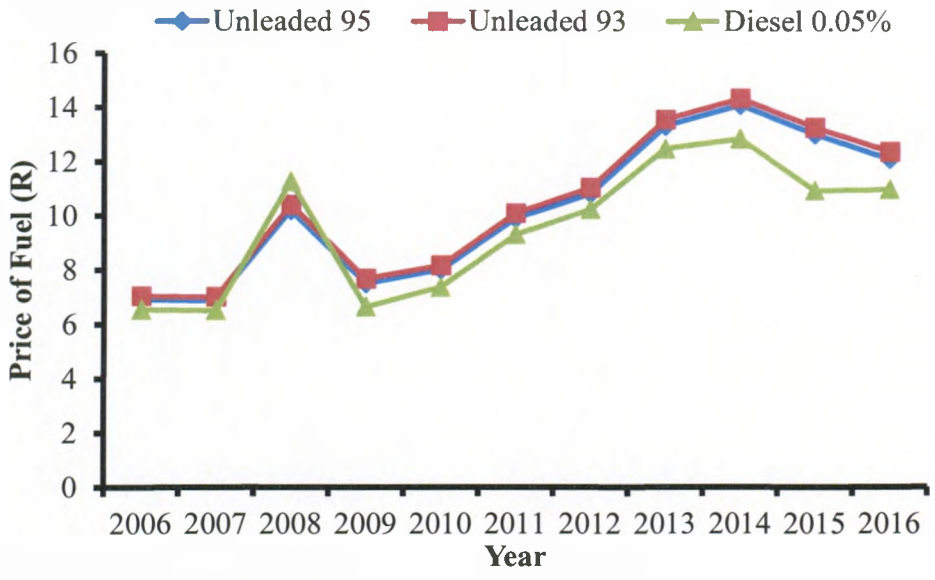


**Figure 2: Prices of Petrol vs Diesel in South Africa between 2006 and 2016 (extracted from BusinessTech.co.za, 2016 b)**

A number of scientific research studies have been conducted on different types of vegetable oils to produce biogasoline. Nasikin *et al.* (2009) conducted a study on the production of biogasoline from palm oil. The study was done through simultaneous catalytic cracking and hydrogenation over a bifunctional Ni-Mo/zeolite catalyst (Nasikin *et al.*, 2009). They studied the effect of reaction temperatures at 300 °C and 320 °C. Their reactions had contact times of 1 hr, 1.5 hrs and 2 hrs for both investigated temperature, using a catalyst: reactant ratio of 1:75. From their study, it was found that cracking of the oil into lighter fractions indeed occurred. Their conclusions were made by comparing the density and boiling point of oil before and after the hydrogenation process; in which both were reduced.

The advantage of using waste cooking oil is its lower cost compared to virgin oil, and absence of sulphur components. Sulphur is a major air pollutant that may be emitted from the combustion of petroleum liquid fuels in automobile engines. It is for this reason that strict environmental regulatory measures are being enforced on petroleum refineries. The U.S. Environmental Protection Agency (EPA) has adopted regulations that require petroleum refineries to produce gasoline/petrol with a low sulphur content from 500 to 30 ppm in 2007 (Liu *et al.*, 2007). The use of non-sulphur containing liquid petroleum fuels mitigates the costs incurred on expensive technologies and catalysts employed for the desulphurization processes.

## 1.3 Project Feasibility

The production of biogasoline is a highly feasible project within the South African context. Extensive research located a local South African biodiesel production company; Matayo Biofuels (Pty) Ltd. Contact was made with the founder of the company to request raw material data and pricing logistics. It was found that there is about 60 000 L to 140 000 L of collectable waste cooking oil being traded at a price of R6.50/L. The selling price for biodiesel in 2016 was R10.96/L. Using the statistic presented in Figure 2 and assuming that the price ratio of Unleaded 95 to diesel of 0.05 % is the same to that of biogasoline and biodiesel, the selling price of biogasoline was estimated. The selling price of biogasoline was estimated to be R12.18, based solely on the cost of the main raw material. The calculation of the price of biogasoline in 2016 was based on equation 1.1. This makes the biogasoline a market competitive commodity.

$$\frac{Selling\ Price\ of\ Unleaded\ 95\ in\ 2016}{Selling\ Price\ of\ diesel\ 0.05\%\ in\ 2016} = \frac{Selling\ Price\ of\ biogasoline\ in\ 2016}{Selling\ Price\ if\ biodiesel\ in\ 2016} \quad (1.1)$$

## 1.4 Aim of the study

The aim of this study is to investigate the feasibility of converting triglycerides and fatty acids into light biofuel. In particular, this study aims to produce biogasoline (biopetrol) that is as compatible as petroleum-based gasoline, and thus can be used as liquid fuel to power automobile engines. In order to be able to achieve this purpose, the biogasoline must be produced such that its physical and chemical properties are closely similar to those of petroleum-based gasoline. Catalysts and catalytic processes have also been investigated to optimize the production of biogasoline from waste cooking oil.

## 1.5 Objectives of the Study

The objective of this study was to investigate parameters that will optimally convert triglycerides and fatty acids from vegetable oils into gasoline (petrol) carbon range hydrocarbons. This study will focus on the following objectives:

a. To investigate the chemical and physical characteristics of waste cooking oil that make it to be as compatible a fuel production feedstock as crude oil.
b. To synthesize catalytic hydrocracking catalysts to be used for the production of biogasoline from waste cooking oil.

c. To investigate the effect of catalyst Ni-loading (wt. %) and calcination temperature on the catalyst's activity and performance.
d. To investigate the effects of reaction temperature, contact time and catalyst: oil ratio on the production of and selectivity towards biogasoline.
e. To investigate the optimal reaction parameters that give the optimum production of biogasoline from WCO.

## 1.6 Outline of the Dissertation

The dissertation is outlined as follows:

**CHAPTER 1**: Introduction- This chapter gives an introductory insight into the research work that this project will be focusing on. The motivation, aim and objectives of the study are included in this chapter.

**CHAPTER 2**: Literature Review- This chapter gives further insight and feedback from literature studies that have done work on the same or similar scope of study. The focus was on production of biofuels, particularly biodiesel, bioethanol and biogasoline and the catalysts used for cracking catalysis of fuels.

**CHAPTER 3**: Experimental Procedure- This chapter outlines the experimental procedures followed for synthesizing the Ni-Mo/$Al_2O_3$ catalyst and production of biogasoline from waste cooking oil. The characterisation methods used in this study are also outlined and described in this chapter.

**CHAPTER 4**: Results and Discussions- This chapter presents the results obtained from the characterisation of the catalysts and the liquid products. The results are discussed and interpreted as far as possible.

**CHAPTER 5**: Conclusions and Recommendations- This chapter concluded on the outcomes of this study based on the overall results obtained. Recommendations for future works relating the same or similar study field are given.

# CHAPTER 2: LITERATURE REVIEW

This chapter looks into literature studies associated with the production of biofuels and the catalysis employed. A review of previous studies that worked on the same or similar research field is done and presented. The review focuses on the feedstock used for the production of biofuels, employed catalysts and methods of production. The aim of this study is to investigate the possibility of replacing conventional petroleum-based gasoline with biogasoline to have a positive impact towards the global environment.

## 2.1 Biofuel Technology Applications

In recent years, significant efforts in the search for alternative, renewable automobile fuel energy have been devoted to the production of biofuels. Biofuels as alternative source of transportation liquid fuels enhances sustainability and economic growth (Bezergianni & Kalogianni, 2009). This section briefly overviews some examples of biofuels from bio-sources, namely biodiesel, bioethanol and biogasoline.

### 2.1.1 Biodiesel

Biodiesel is by far one of the biofuels that has been extensively researched, and ultimately successfully produced commercially. In their brief review paper, Owolabi *et al.* (2012) highlighted that the major reason for focusing on biodiesel more than other bio-sourced fuels was that in addition to biodiesel exhibiting defined chemical and physical properties that meet diesel engine application demands, biodiesel is currently being produced on an industrial scale as a fuel (Owolabi *et al.*, 2012). In South Africa, one such example of a company that successfully produces biodiesel on an industrial scale is the Matayo Biofuels, situated in Benoni in the East Rand, Johannesburg.

The major feedstock for biodiesel production is animal fat and plant oils. Rapeseed oil, sunflower oil, soybean oil, palm oil, etc., are some of the oils being used as feedstock for biodiesel production in countries such as the United States of America (USA), Brazil, France and Italy. Production of biodiesel occurs mainly through three processes, namely pyrolysis, micro-emulsification and trans-esterification (Owolabi *et al.*, 2012). The commonly practiced process is

trans-esterification. In this process, the oil, being free of any impurities either by being pre-treated or using virgin oil, is reacted with a suitable alcohol such as ethanol, methanol, butanol, etc. The three main parameters affecting the yield and quality of the biodiesel are, namely, reaction temperature (T), reaction time (t) and ratio of oil to alcohol (Owolabi *et al.*, 2012).

### 2.1.2 Bioethanol

Alcohols have been used as viable fuels for engines since the inception of automobiles (Balat *et al.*, 2008). Bioethanol is another biomass-derived fuel (biofuel) that has been receiving much interest and attention as an alternative liquid fuel for completely and/or partially replacing petroleum-based fossil fuels. In most instances, the alcohol is used as a blending component with gasoline to enhance the properties and performance of gasoline in gasoline engines (Cardona & Sánchez, 2007). Balat *et al.* (2008) highlighted that bioethanol can potentially replace 353 L of gasoline/petrol if used in E85 fuel, which is a blend of 85 % bioethanol and 15 % gasoline. The interest in bioethanol arises from its potential to reduce the net contribution of GHGs to the atmosphere. In comparison to gasoline, bioethanol has a higher octane number (Balat *et al.*, 2008). Ethanol (bioethanol) has a positive net energy balance, i.e., the energy content of the fuel is more than the energy consumed for its production (Kim & Dale, 2004).

The three main feedstocks available for the production of bioethanol come from plant materials that contain sucrose, starchy materials and lignocellulosic biomass. Common plant materials used for the production of bioethanol are crops such as corn, sugar cane, rice, maize, wheat, grass, etc. (Balat *et al.*, 2008; Kim & Dale, 2004). On a global scale, 94% of biofuels produced is attributed to the production of bioethanol, which increased from 12.1 billion gallons (45.7985 billion liters) in 2005 to 13.5 billion gallons (51.0975 billion liters) in 2006 (Balat *et al.*, 2008). South Africa was featured among the top ten global producers of bioethanol by Balat *et al.*, (2008), as shown in Table 1.

**Table 1: Top ten bioethanol producers (in billion gallons) (adapted from Balat *et al.*, 2008)**

| Country | 2004 | 2005 | 2006 |
|---|---|---|---|
| **USA** | 3.54 | 4.26 | 4.85 |
| **Brazil** | 3.99 | 4.23 | 4.49 |
| **China** | 0.96 | 1.00 | 1.02 |
| **India** | 0.46 | 0.45 | 0.50 |
| **France** | 0.22 | 0.24 | 0.25 |
| **Germany** | 0.07 | 0.11 | 0.20 |
| **Russia** | 0.20 | 0.20 | 0.17 |
| **Canada** | 0.06 | 0.06 | 0.15 |
| **South Africa** | 0.11 | 0.10 | 0.10 |
| **Thailand** | 0.07 | 0.08 | 0.09 |

There are a number of important advantages that comes with the use of bioethanol as an automobile engine fuel. When used in blended fuel mixtures, bioethanol reduces the consumption of petroleum-based gasoline, and ultimately the consumption of crude oil. With a 35 % oxygen content, this oxygenated fuel reduces NOx and particulate emissions from combustion (Balat *et al.*, 2008). It is, however, worthwhile also mentioning that there are some disadvantages to the production of bioethanol that prohibit its exploitation for maximum human benefit. A major set-back relating to the production of bioethanol is the cost of production, which is higher than the cost of production of gasoline (Cardona & Sánchez, 2007). This set-back is as a result of the high volatility of the prices of the feedstock, which on its own accounts for 60 % of the cost of production. Given that the raw materials used as feedstock for bioethanol production become available seasonally, it is a challenge to keep up with supply throughout the year. The most common bioethanol producing crops such as sugar cane and corn cause soil erosion and use more nitrogen fertilizer in comparison to other crops. Particularly for corn-derived bioethanol, there are large amounts of $CO_2$ produced that contribute to the amount of

GHGs contained in the atmosphere, thus promoting environmental pollution and global warming (Balat *et al.*, 2008).

### 2.1.3 Biogasoline

Various studies have been conducted and their outcomes have shown the possibilities of producing biogasoline from a number of different feedstock. In a study by Samolada *et al.* (1998), biogasoline was produced through hydrogen processing and catalytic cracking. The feedstock used for this study was biomass flash pyrolysis liquids (BFPLs), which were upgraded to biogasoline range quality to meet the EU specifications. The biogasoline produced from this study had a high research octane number (RON) of 96 (Samolada *et al.*, 1998). In another study by Tsuchida *et al.* (2008), biogasoline with a RON of 99 was achieved. The feedstock for this specific study was plant-derived, dehydrated ethanol. The biogasoline produced from this study mainly contained hydrocarbons with a carbon range number of $C_6$-$C_{10}$ (Tsuchida *et al.*, 2008). Nasikin *et al.*, (2009) conducted a study on the production of biogasoline from palm oil through simultaneous cracking and hydrogenation over Ni-Mo/zeolite catalyst. Their work was done using a liquid phase batch reactor at atmospheric pressure. By taking note of the decreased density and boiling point of the palm oil before and after the reactions took place, it was proven that cracking of long chain, heavy triglyceride molecules occurred. The biogasoline produced contained hydrocarbons within the carbon range number of $C_8$-$C_{15}$ (Nasikin *et al.*, 2009).

A study by Wang *et al.* (2013) looked into producing biogasoline by co-cracking the distilled fraction of bio-oil and ethanol through over a H-ZSM-5 catalyst. Prior to the production of the biogasoline, the bio-oil was pre-treated to obtain and concentrate the distilled fraction (DF) through multiple molecular distillation. The study achieved a maximum biogasoline phase yield of 29.9 wt. % at a reaction temperature of 400 °C, pressure of 2 MPa and a DF/ethanol ratio of 0:1. This study confirmed that alcohols have a high catalytic cracking stability. The lowest yield was obtained from a reaction temperature of 400 °C, pressure of 0.1 MPa and a DF/ethanol ratio of 1:2. An increase in conversion of the reactants and deoxygenation efficiency was observed with an increase in reaction temperature (Wang *et al.*, 2013).

Doronin *et al.* (2012) studied the use of bi-zeolite catalysts to crack vegetable oils into liquid products containing gasoline and light olefins range fractions. The study was successful as it was found out that the highest yield of gasoline and gaseous products was achieved by cracking on a

H-ZSM-5 zeolite. By incorporating the bi-zeolite effects of Y and H-ZSM-5 catalysts, an improvement in the yield of the gasoline and $C_2$-$C_4$ fraction hydrocarbons was observed. The gasoline obtained from this study was said to have a high octane number. The authors reporting on this study suggested that a high selectivity and yield of light olefins and gasoline range hydrocarbons depends on the composition of the feedstock oils. Oils with an increased concentration of saturated fatty acids are most beneficial (Doronin *et al.*, 2012).

## 2.2 Vegetable oils as sustainable sources of liquid fuel energy

Vegetable oils are composed of triglycerides containing fatty acids with 14 to 22 carbon atom chains (Kubička & Kaluža, 2010). The demand for gasoline/petrol has been rising steadily in all economies (industrialized and developing), for more than a century (Inkpen & Moffett, 2011), therefore alternative and sustainable sources and processes of producing gasoline range hydrocarbons must be explored. The oils can successfully be used as feedstock for catalytic cracking processes for the production of liquid fuels. The acids in the oils have a high cracking performance and high reactivity (Wang *et al.*, 2013). The advantage of using vegetable oils is the absence of sulphur and nitrogen compounds in their chemical composition, thus they eliminate the release of hazardous fumes into the atmosphere (Doronin *et al.*, 2012). A study in literature has concluded that reaction pressure and temperature play a vital role in the conversion of triglycerides and fatty acids into liquid fuel hydrocarbons (Sotelo-Boyás *et al.*, 2012).

The triglycerides and fatty acid molecules in vegetable oil are made up of linear paraffinic carbon chains with sixteen (16) to eighteen (18) carbon chains (Sotelo-Boyás *et al.*, 2012). Sunflower oil is composed of linoleic acid (60 wt. %), oleic acid (27 wt. %), palmitic acid (6.5 wt. %), stearic acid (5.8 wt.%) and trace amounts of palmitoleic and linolenic acids (both at 0.2 wt.%). The main constituents of this oil, i.e. oleic and linoleic acids have side chains with one (1) and two (2) carbon-carbon double bonds, respectively. Hydrocracking of the vegetable oils involves the cracking and hydrogenation of the higher molecular weight triglycerides and fatty acid molecules into lighter hydrocarbons (Sotelo-Boyás *et al.*, 2012). This implies that high hydrogen pressure and temperature in the presence of a bi-functional catalyst are required to transform triglycerides and fatty acids into hydrocarbons (Liu *et al.*, 2011).

Transformation of triglycerides and fatty acids into hydrocarbons follow different combinations of some common reaction pathways, namely decarboxylation, decarbonylation, hydro-

deoxygenation, cracking, isomerization and cyclization. The different combinations of the afore mentioned processes enhance the saturation of double bonds, cracking of long chain C-C bonds and removal of heteroatoms (sulphur, oxygen and nitrogen) (Morgan *et al.*, 2012).

## 2.3 Waste cooking oil

The use of waste cooking oil as a feedstock for biofuels production is a sustainable technology owing to a number of benefits for the economy and the environment. Waste cooking oil usage mitigates the costs associated with the use of virgin oil and the social challenges associated with food competition. Waste and non-edible oils come at a low and stable price because of the absence in food competition (Liu *et al.*, 2011). This feedstock has been proven to have a high calorific value. Other attractive properties include low moisture and low heavy metal content. Most vegetable oils are composed of palmitic and oleic acids, and these fatty acids can potentially be cracked into hydrocarbons (Khalisanni *et al.*, 2008).

### 2.3.1 Biogasoline production from Waste Cooking Oil

In a study by Tsuchida *et al.* (2008), biogasoline was produced from plant-derived ethanol over a hydroxyapatite catalyst. In this study, biogasoline with a research octane number of 99 was produced, and it was composed of hydrocarbons within the range of $C_6$-$C_{10}$ (Tsuchida *et al.*, 2008). In another study by Nasikin *et al.* (2009), biogasoline was produced from palm oil through simultaneous cracking and hydrogenation reaction over Ni-Mo/zeolite catalyst. This study was conducted using a liquid phase batch reactor at atmospheric pressure. By noting the decrease in density and boiling point of the palm oil before and after the reaction, it was proven that cracking of the long chain triglyceride molecules took place (Nasikin *et al.*, 2009).

#### 2.3.1.1 Pre-Treatment of Waste Cooking Oil

Waste cooking oil, like petroleum crude oil, is composed of complex molecules combined together. It is therefore crucial that the oil get pre-treated and refined before it is of any value to the transportation industry. The pre-treatment stage of the WCO is very vital because the untreated oil has a high FFA content which gives processing challenges due to the formation of soap, yield loss and increased difficulty in product separation (Chai *et al.*, 2014). Prior to hydrocracking, pre-treatment of the oil enables the removal of the double bonds and heteroatoms in the oil (Bezergianni & Kalogianni, 2009).

Untreated oil has a high water content that leads to saponification, which, like a high FFA content, causes the oil to be soapy, and thus foamy (Pandey, 2011). If the water in the oil is not removed, the saponification will result in a decrease in the biofuel yield in the later stages of production and the ultimate deactivation of the catalyst (Knothe *et al.*, 2010). The oil has an increased content of inorganic water –soluble salts, which therefore implies that the oil needs to be de-salted as part of the pre-treatment stage (Fahim *et al.*, 2010).

Liquid fuels derived from biological matter (biofuels) tend to have a high oxygen content in comparison to crude oil derived petroleum liquid fuels (Pandey, 2011). Vegetable oils used in cooking/frying get exposed to heat at temperatures of 60 °C-200 °C and oxygen dissolves into the cooking oil, resulting in an increase in the occurrence of oxygenated groups within the oil (Kulkarni & Dalai, 2006). Oxygenation of the oil is a process that follows reaction (2.1), as depicted below.

$$CnHmOH + H2 \rightarrow CnHm + H2O \qquad (2.1)$$

where $n$ and $m$ are the number of carbon and hydrogen atoms, respectively.

High oxygen content reduces the heat content of molecules and gives them a high polarity. It is therefore a necessity to eliminate specific oxygenated groups from the oil in order to improve their stability (Laurent & Delmon, 1994; Pandey, 2011).

## 2.4 Catalysis

Fogler (2006) defines catalysis as the occurrence, study, and use of catalysts and catalytic processes. By definition, "a catalyst is a substance that affects the rate of a reaction but emerges from the process unchanged". The change in reaction rate is achieved "by promoting a different molecular path or mechanism for the reaction" (Fogler, 2006). Chemical reactions primarily convert raw material of no or less value, into products of a higher value. However, during these chemical reactions, other undesired reactions occur, resulting in undesired product. Therefore it is crucial that the catalysts used for a particular reaction promotes the selectivity and yield of the desired product.

For the purpose of this work, three catalytic processes for the conversion of liquid fuels were studied from the production of gasoline from heavier liquid oil, and will thus be considered for

the production of biogasoline. The processes are thermal cracking, catalytic cracking and catalytic hydrocracking. Of the three processes, catalytic cracking is considered to be the most efficient method for producing biofuels, especially biogasoline (Taufiqurrahmi & Bhatia, 2011).

### 2.4.1 Petroleum Refining Catalysts

In any catalytic process, the catalyst plays an important role, and therefore the type of catalyst used is a key point to investigate and interrogate for an optimized process (Sotelo-Boyás *et al.*, 2012). This section will look into discussing the various types of catalysts that are used for the refining of petroleum fuel.

#### 2.4.1.1 Metals-on-Support Catalysts

Catalysts can be synthesized and manipulated in order to intensify their properties to increase yield and selectivity. As such, some catalysts have the ability to be bi-functional, i.e., they perform the role of cracking and hydrogenating. Such catalysts are synthesized by loading and dispersing a pure metal or metal oxide onto a less active or inert material, which acts as the support. Supported catalysts usually have three phases, namely the active phase, support and promoter (Bartholomew & Farrauto, 2011). When metals are deposited onto a support, the metals are considered as the active sites/phase of the catalyst (Fogler, 2006). The active phases are certain transition metals in the form of their oxides, sulphides, carbides and nitrides. The use of transition metals is attributed to their possession of multiple low energy electronic states. Because of this feature, transition metals, while making or breaking bonds, can easily and readily donate or accept electrons (Bartholomew & Farrauto, 2011).

Catalyst supports are also referred to as carriers. These materials are highly porous metal oxides or carbons with high surface areas. They provide a significant pore volume and capacity for preparing and preserving stable catalytic phases that are well dispersed during reactions (Bartholomew & Farrauto, 2011). A common material used as a support for bi-functional catalysts is alumina, which has been widely used because of its excellent mechanical and dispersion properties (Ferdous *et al.*, 2007). It is because of its surface acidity with surface hydroxyl groups that it is capable of acting as a moderately acidic catalyst/support. Alumina possesses a number of well-characterised amorphous or crystalline structures (Bartholomew & Farrauto, 2011). Alumina is employed as a support for a number of catalysts used for the refining

of petroleum hydrocarbons. Platinum-on-alumina ($Pt/Al_2O_3$) is used for obtaining high octane rating gasoline from reformed petroleum naphtha (Fogler, 2006).

Catalyst promoters, on the other hand, play a role of enhancing both the support and active phases of the catalyst. They ensure that the catalytic-active phases are well dispersed and remain so during the course of the reactions. Such are referred to as textural promoters. Promoters can also play a role of enhancing the activity or selectivity of a specific reaction towards the desirable product(s), and such are known as chemical promoters (Bartholomew & Farrauto, 2011).

Certain metals are active enough to be loaded onto the support, while others are not as active and desirable. For instance, nickel has been noted to be a porous substance that actively promotes hydrogenation reactions. An example is the Raney nickel that is being used for the hydrogenation of vegetable oils and animal fat (Fogler, 2006). Most active metals for hydrogenation reactions are cobalt (Co), ruthenium (Ru), rhodium (Rh), Osmium (Os), palladium (Pd), nickel (Ni), Iridium (Ir) and platinum (Pt). These metals play an active catalytic role in the presence of hydrogen. On the other hand, metals such as molybdenum (Mo) and chromium (Cr) are only active in hydrogen reactions in the form of metal oxides, i.e., $MoO_2$ for the former and $Cr_2O_3$ for the latter (Fogler, 2006).

Hydro-treating processes need to employ environmentally friendly production materials and methods for upgrading low value petroleum oil fractions into those of a higher value. In this regard, extensive studies have been done on the catalytic activities of alumina supported Ni/Co and Mo catalysts, which are popular for taking part in many petroleum hydrogenation processes. Palcheva et al. (2012) studied the hydrodesulphurization (HDS) of 1-benzothiophene over an alumina catalyst impregnated with Anderson-type nickel heteropolyxomolybdate. The alumina catalyst was modified by the addition of Ni, Co or boron (B), in the form of $Ni\text{-}Mo/Al_2O_3$, $Co\text{-}Mo/Al_2O_3$ or $B\text{-}Mo/Al_2O_3$ in order to study the effect that these ions have on the catalytic activity of alumina. The outcomes of the study showed that there was an increase, to different extents, in the catalytic activity of alumina upon the addition of the above mentioned metals. In addition to the increased catalytic activity, the loaded metals influenced the phase composition of the support. For this work, the highest activity increase for HDS was observed with the support loaded with Ni (Palcheva *et al.*, 2012).

Table 2 gives a summarized comparison of the surface area, pore volume and pore diameter of common catalysts/supports.

**Table 2: BET surface area, pore volume and pore diameter of different catalysts/supports (adapted from Bartholomew and Farrauto, 2011)**

| Support/Catalyst | BET area ($m^2/g$) | Pore Volume ($cm^3/g$) | Pore Diameter (nm) |
|---|---|---|---|
| **Zeolites(molecular sieves)** | 500-1000 | 0.50-0.80 | 0.40-1.80 |
| **Silica gels** | 200-600 | 0.40 | 3-20 |
| **Activated clays** | 150-225 | 0.40-0.52 | 20 |
| **Activated alumina ($Al_2O_3$)** | 100-300 | 0.40-0.50 | 6-40 |

### 2.4.1.2 Zeolite Catalysts

Zeolites can be employed in cracking processes as catalysts because of their acidity, like it is the case with alumina. The faujasite-type zeolite catalyzes hydrocracking and catalytic cracking petroleum refining processes, with selectivity towards kerosene, jet fuel, benzene, toluene and xylene for the former, and gasoline and fuel oil for the latter (Bartholomew & Farrauto, 2011). Zeolite catalysts have been reported to have higher selectivity towards hydrocarbon production as a catalytic cracking acid catalyst when using palm oil as feedstock (Mohd Addli, 2009). In a study by Mohd Addli (2009), the researcher compared the yields of biogasoline from palm oil through thermal cracking and catalytic cracking. By keeping all other reaction parameters constant, thermal cracking gave a yield of 3 % to a maximum of 5 % by gradually increasing the amount of catalyst used. For catalytic cracking, yields of 9.1822 % up to 20.7210 % were reported (Mohd Addli, 2009). Zeolites are natural and are of the molecular sieve type. Zeolites are said to have the ability to control the placement of the reacting molecules at the desired active sites within the catalyst (Fogler, 2006).

### 2.4.1.3 Silica-Alumina Catalysts

Silica-alumina catalysts are very common and attractive for catalytic cracking. These catalysts are considered to be very porous, thus providing a high surface area onto which reaction can take place. Fogler (2006) stated that a typical silica-alumina cracking catalyst has a pore volume of

0.6 $cm^3/g$, an average pore radius of 4 nm, and a surface area of 300 $m^2/g$ (Fogler, 2006). Silica is relatively less acidic when compared to alumina. The advantage that silica based catalysts has over those without silica lies in that silica catalysts have a higher resistance towards surface sulphate species formation. Surface sulphates are undesirable because they cause the deactivation of the catalyst (Bartholomew & Farrauto, 2011).

#### 2.4.1.4 Activated Clay Catalysts

These types of catalysts are known as natural catalysts. Like zeolites, they are said to be of the molecular sieve type. This entails that they have pores so small that they selectively permit the entrance of certain small molecules to reach the active sites of the catalyst, while preventing the entrance of larger molecules. The small pores are advantageous to the reaction as they increase the retention time (Fogler, 2006).

### 2.4.2. Preparation of Catalysts

The method used for the preparation of catalysts has a significant impact on the catalytic activity. Different preparation methods are available for hydrocracking and hydrotreating catalysts, with the impregnation method being the conventional method employed commercially. The relatively low costs associated with this method is the reason it is widely used by mainstream, manufacturers of catalysts such as KF 757 (Co-Mo/$Al_2O_3$) and KF 848 (Ni-Mo/$Al_2O_3$) (Liu *et al.*, 2007).

### 2.4.3 Catalytic Hydrocracking

Hydrocracking is defined as the process of catalytic cracking of feedstock products with lower boiling points by reacting them with hydrogen (Fahim *et al.*, 2010). The number of carbon atoms in vegetable oils range within approximately $C_{16}$-$C_{20}$, which falls within the carbon number range of petroleum diesel, i.e. $C_{11}$-$C_{24}$ (Sotelo-Boyás *et al.*, 2012; Total Engineers Technical Handbook, 2014). The catalytic hydrocracking process will convert the waste vegetable oils (WCO) into lighter hydrocarbons that correspond to the carbon range of gasoline ($C_5$-$C_{10}$). The catalyst for the hydrocracking has an acidic matrix which will promote the isomerization reactions (Ginley & Kahen, 2012). During the hydrocracking process, the value of the research octane number (RON) of the biogasoline reduces. The isomerization stage is essential to correct this imbalance, thus increasing the octane number.

### 2.4.4 Cracking for Biofuel Production

The hydroconversion of natural triglycerides into fuel liquid products must be a cost effective process if it is to be economically feasible and sustainable. The use of Ni-Mo and Co-Mo based catalysts is more suitable for the hydroconversion of natural triglycerides because of their low costs in comparison to other metals such as Pt and Pd. Their higher conversion and deoxygenation capabilities give them an added advantage (Veriansyah *et al.*, 2012).

#### 2.4.4.1 Ni-Mo/$Al_2O_3$ Catalyst

The use of Ni-Mo/$Al_2O_3$ catalysts has found extensive applications for catalytic hydrotreating processes for the production of biofuels. Krár *et al.* (2009) studied the conversion of triglycerides into a diesel carbon range liquid product over a Ni-Mo/$Al_2O_3$ commercial catalyst using sunflower oil as feedstock. The results presented a high paraffin containing product mixture, composed mainly of primary $C_{15}$-$C_{18}$ n- and *iso*-paraffins. The study found that maximum yield was obtained when a high pressure of 60 bars, reaction temperatures of 360 °C -380 °C and a low LHSV of 0.5-1.0 $h^{-1}$ were used. After distillation of the liquid product, the target product had a high cetane number higher than 80. The cold flow properties of the diesel were unimpressive, of which it was suggested that selective isomerization of the product be performed (Krár *et al.*, 2009). An alternative way for improving the cold flow properties of the diesel range hydrocarbons is by blending it with petroleum diesel (Sotelo-Boyás *et al.*, 2012).

The catalytic activity and promotion of the hydrocracking of rapeseed oil to produce diesel range hydrocarbon fuels were studied by Sotelo-Boyás *et al.* (2012) using three different catalysts, namely Ni-Mo/$Al_2O_3$, Pt/H-Y and Pt/H-ZSM-5. It was found that Ni-Mo/$Al_2O_3$ gave the highest yield of the target boiling range liquid hydrocarbon products in comparison to the zeolite based catalysts Pt/H-Y and Pt/H-ZSM-5. In addition it was found that the $MoS_2$ arising from the sulphided Ni-Mo/$Al_2O_3$ contributed to the saturation of the triglycerides (Sotelo-Boyás *et al.*, 2012). The use of Ni-Mo/$Al_2O_3$ to hydrocrack triglycerides has extended to the production of gas oil boiling range liquid products. The catalyst displayed competitive properties when compared to other hydrocracking catalysts, with a performance grading of Ni-W/$Al_2O_3$ < Ni-Mo/$Al_2O_3$ << Co-Mo/$Al_2O_3$ in a study by (Hancsók *et al.*, 2012). In a study to produce a paraffin rich mixture of hydrocarbons from hydroprocessing soybean oil, conversion by Ni-Mo/$Al_2O_3$ outperformed all the competing catalysts. The conversion performance of the catalysts was in the order of

sulphided Ni-Mo/γ-$Al_2O_3$ (92.9 %) > 4.29 wt. % Pd/γ-$Al_2O_3$ (91.9 %) > sulphided Co-Mo/γ-$Al_2O_3$ (78.9 %)>57.6 wt. % Ni/$SiO_2$-γ-$Al_2O_3$ (60.8 %) >4.95 wt. % Pt/γ-$Al_2O_3$ (50.8 %) >3.06 wt.% Ru/$Al_2O_3$ (39.7 %) at a constant catalyst: oil ratio of 0.044 (Veriansyah *et al.*, 2012). Veriansyah and co-workers reckon that the type of catalyst influenced the composition of the product and that the Ni-Mo/$Al_2O_3$ is favourable for hydrocracking processes owing to its high capabilities to remove oxygen and low costs (Veriansyah *et al.*, 2012).

Šimáček *et al.* (2010) used a commercial Ni-Mo/$Al_2O_3$ catalyst for hydroprocessing rapeseed oil into a hydrocarbon-based biodiesel. At reaction conditions of 360 °C, and hydrogen pressures of 7 MPa and 15 MPa, the study achieved oxygen-free hydrocarbon mixtures. The organic liquid products (OLP) were composed of 75 wt. % middle distillates in the form of n-alkanes $C_{17}$ and $C_{18}$. The biodiesel had a high cetane number, and like typical vegetable produced liquid hydrocarbons, it had poor flow properties. It is for this reason that it was only suitable for blending with petroleum-based diesel in automobile engines. Blends of 5 to 30 wt. % OLP were proven to meet European diesel fuel specification EN 590. The blends retained a high cetane index by 2-14 units (Šimáček *et al.*, 2010). Deoxygenation is an important process in the conversion of triglycerides into hydrocarbons. In fact, the removal of the oxygen heteroatom is the essence of transforming triglycerides into hydrocarbons. The deoxygenation reaction pathways for rapeseed oil were investigated by Šimáček *et al.* (2010) through catalytic processes. The results of this study showed that the degree of hydroconversion and deoxygenation of the triglycerides was in the order of Ni-Mo/$Al_2O_3$ < Mo/$Al_2O_3$ < Ni/$Al_2O_3$. This shows the increased catalytic activity achieved by the bi-functionality of Ni and Mo.

# CHAPTER THREE: EXPERIMENTAL PROCEDURE

The experimental methods followed in this research study are outlined in this chapter. The procedures are thoroughly explained, and chemicals and equipment used are hereby enlisted. This section comprises of five (5) main sub-sections. The first sub-section **3.1** looks at preparation and synthesis of the Ni-Mo/$Al_2O_3$ catalysts. It is then followed by sub-section **3.2**, which discusses the characterisation of the catalysts. Prior to conversion biogasoline, the WCO was pre-treated. This was discussed in sub-section **3.3**. Sub-section **3.4** details the production method of biogasoline from pre-treated WCO and sub-section **3.5** discusses the characterisation of the biogasoline.

## 3.1 Synthesis of Ni-Mo/$Al_2O_3$ Catalysts

The catalysts used in this study were prepared through the incipient wetness method. Following an investigation on alternative techniques available for hydrocracking catalysts preparation, the incipient wetness method was considered more applicable for the purposes of this study. For each catalyst, 4 g of $Al_3O_2$ powder was activated with acid by mixing with 5 ml of 1M sulphuric acid inside a 50 ml glass beaker. Thorough mixing was ensured by stirring over a magnetic stirrer at 300 rpm. The mixing was done just long enough that the $Al_3O_2$ was evenly dispersed into the acidic solution to create a consistent paste.. After the activation, the paste was dried in an oven at 120 °C to evaporate any excess water and other volatile species. The paste, which serves as a support for the catalysts, was then calcinated in air at a temperature of 520 °C for 5 hours inside a furnace. Once dry, the support was impregnated following the sequence show in Figure 3. To impregnate the acid activated $Al_3O_2$ support (Figure 3 a.), nickel and molybdenum salts were dissolved in distilled water and added onto the support in the form of aqueous solutions of nickel sulphate ($NiSO_4.7H_2O$) in Figure 3 b and ammonium molybdate tetrahydrate ($(NH_4)_6Mo_7O_{24}.4H_2O$) in Figure 3 c, respectively.

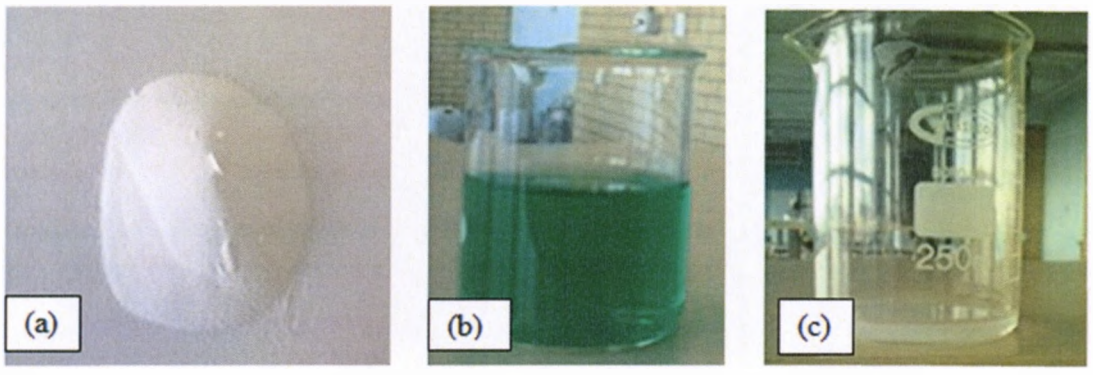


**Figure 3: The Catalyst Impregnation Procedure: (a) Dried Acid-activated Catalyst Support ($Al_2O_3$) (b) Aqueous Nickel salt, (c) Aqueous Molybdenum salt**

During catalyst impregnation, Ni salt was loaded first, and then followed with Mo salt. After addition of each aqueous salt solution, the mixture was stirred thoroughly with the paste to achieve an overall wet consistency. The catalyst – support system was than dried at 90 °C for 1 hour. The dried material was calcinated at 300 °C for 3 hours, except when the calcination temperature was investigated. The resulting product was an acid activated Ni-Mo/$Al_3O_2$ catalyst.

Different samples of catalysts of 4 g each were synthesized using the above described procedure, but with different Ni-loadings and calcination temperature from 300 °C to 700 °C. For all the catalysts-support prepared, an equal amount (50 wt. %) of catalyst support ($Al_3O_2$) was added. For the Ni-loadings investigation, the metal concentration varied at 5 wt. %, 10 wt. %, 15 wt. %, 20 wt. % and 25 wt. %, while keeping the calcination temperature at 300 °C. They were then taken for analysis to determine the catalyst with the most favourable properties. From the effect of Ni-loading results, which is presented and discussed in section (4.3), the catalyst with the maximum BET surface area was designated Catalyst A, chosen to be the most ideal for optimum production of biogasoline. Catalyst A was further used for calcination temperature studies. This investigation was performed at 400 °C, 500 °C, 600 °C and 700 °C, in addition to the 300 °C mentioned above. In addition, the synthesized catalyst was compared to the mimic Ni-Mi/$Al_2O_3$ as a standard, in term of catalyst specifications, catalytic activity and performance. The mimic catalyst was synthesized by specifications as reported by Kougionas *et al.* (1995). The catalyst was prepared with metal loadings of 9.3 wt. % Mo and 2.4 wt. % Ni, and the balance being $Al_3O_2$ (Kougionas *et al.*, 1995).

## 3.2 Catalyst Characterisation Techniques

The catalysts were characterised to determine various properties. The characterisation techniques that were use are ICP-OES, TGA, BET, SEM, FT-IR and Raman Spectroscopy.

### 3.2.1 Inductively Coupled Plasma Atomic Emission Spectroscopy (ICP-OES)

ICP-OES was employed to determine the composition of the catalysts. Of interest was the concentration of Ni for the catalysts with varying Ni-loadings (wt. %). To administer ICP-OES characterisation, the solid catalysts samples were first digested by mixing with 8 ml of nitric acid and 2 ml of sulphuric acid. Digestion was done inside a Microware ® at a constant pressure of 31 bars. The duration of the reactions was kept at 40 minutes for each sample. The digestion gave liquid samples, which were characterised with an ICP-OES Spectro Genesis. For the purposes of accuracy, the analyses were performed in 3 runs per sample and averaged.

### 3.2.2 Thermogravimetric analysis (TGA)

TGA was used to determine the thermal stability of the catalysts. Approximately 11.1690 mg samples of each catalyst were loaded into a mini-crucible. The sample holder was inserted into the instrument and zeroed. The samples were then heated at a rate of 20 °C/min in the presence of nitrogen gas. A SDT Q600 V20.9 instrument was used for the characterisation. The analyses had durations of 22 minutes per sample.

### 3.2.3 Brunauer-Emmet-Teller (BET)

The physical characteristics of a catalyst have an impact on its catalytic activity. BET analysis was performed on the catalysts in order to observe what effect Ni loading and catalyst calcination temperature have on the, pore size, BET surface area and pore volume of the catalysts. Catalyst samples of 0.4203 g were used and degassed at a temperature of 150 °C for 6 hours under a stream of nitrogen ($N_2$) gas. During this characterisation, $N_2$ adsorption-desorption occurs. The BET analyses were performed using a Micromeritics Tristar 3000 surface area and porosity analyzer (V6.05).

### 3.2.4 Scanning Electron Microscopy (SEM)

SEM was used to determine the morphology of the catalysts. Small amounts of the catalysts samples were mounted onto carbon resins. The solid catalyst particles were smeared and

flattened onto the sample holders. The samples were then taken for SEM characterisation using FEI Quanta 200 ESEM.

### 3.2.5 Fourier Transform Infrared (FTIR) Spectrometry

FT-IR was employed to study the chemical and molecular structure of the catalysts. A TriStar 3000 V6.05-A FT-IR spectrometer was used. Equal mass of 0.4203 g for each sample was analyzed in the presence of nitrogen and an analysis bath temperature of 195-800 °C.

### 3.2.6 Raman Spectroscopy

Raman spectroscopy was used to study the vibrational and rotational properties of the catalysts. Small amounts of each sample were mounted onto a glass slide and were illuminated with a laser beam. The analysis mechanism is such that the light reflected from the solid catalyst particles is sent through a monochromator after being collected by a lens. The wavelengths of the reflected light that are similar or close to that of the laser beam are filtered. The remaining are sent to a detector, which records a Raman spectrum (Maubane, 2011). Jobin-Yvon T64000 Raman spectrometer was used for the characterisation.

## 3.3 Pre-treatment of Waste Cooking Oil

Prior to the catalytic hydrocracking experiments, the WCO was pre-treated. The WCO was sieved to remove all solid particles. It was then mixed with distilled water in equal parts. The mixture was poured into a 500 ml Schott Duran glass beaker and stirred overnight at a speed of 200 rpm using Heidolph MR 3002 stirrer. The stirred mixture was then poured into a decanter and allowed the two phases to settle and separate. The low density phase (water phase) was then released through the bottom of the decanter, while being cautious not to allow the oil phase to pass through. The oil phase was then poured into a 500 ml canonical flask and heated inside an oil bath for 3 hours at a temperature of 120 °C to ensure the complete removal of the water molecules. The oil was then allowed to cool down to room temperature prior the catalytic hydrocracking reactions.

## 3.4 Catalytic Hydrocracking for Production of Biogasoline from Waste Cooking Oil procedure

The method followed in this study for producing biogasoline from hydrocracking triglycerides in waste cooking oil into hydrocarbons was designed by adaptation from the practical techniques

used in petroleum refineries, and from published research work. Biogasoline was produced from waste cooking oil by converting the oil through catalytic hydrocracking over Ni-Mo/$Al_2O_3$ catalyst in the presence of hydrogen gas. The reactions were conducted in a liquid phase batch reactor set-up inside a safety fume-hood, at a hydrogen pressure of 0.5 kPa.

For all the experimental runs, a fixed volume of 20 ml of the pre-treated oil was added into 200 ml glass beaker. The required amount of catalyst was then measured and transferred into the same beaker. The liquid-solid mixture was agitated using ultra-sonication for 60 minutes at 75 % rotation speed output, so as to achieve high and uniform dispersion of the solid catalyst particles throughout the oil. The mixture was then transferred into a three-neck round bottom flask with a stirring bar put into it. The round bottom flask was connected to a condenser, thermo-couple and a hydrogen/argon gas inlet nozzle, on each neck. The condenser was connected to a cooling water source with water circulating at a flowrate of approximately 7 ml/min. A gas purge line was also connected to the condenser to release excess gas and avoid pressure build-up within the reactor. The thermo-couple was put into the reactor through one of the necks such that it was able to read the temperature of the oil inside the reactor. The temperature of the oil bath was also measured by the thermos-couple.

Prior to the commencement of every run, an oil bath made up of a 2500 ml flask filled with 1000 ml paraffin oil was pre-heated on top of a heating mantle, while stirring at 300 rpm for uniform distribution of heat. The oil bath was covered with glass wool to reduce the amount of heat lost to the surroundings, thus providing insulation. For each run, the heating oil bath was pre-heated up to 10 °C more than the required experiment temperature so as to compensate for the drop in temperature upon submersion of the reactor into the oil. The experimental set-up is shown in Figure 4 and the detailed process flow diagram is shown in Figure 5.

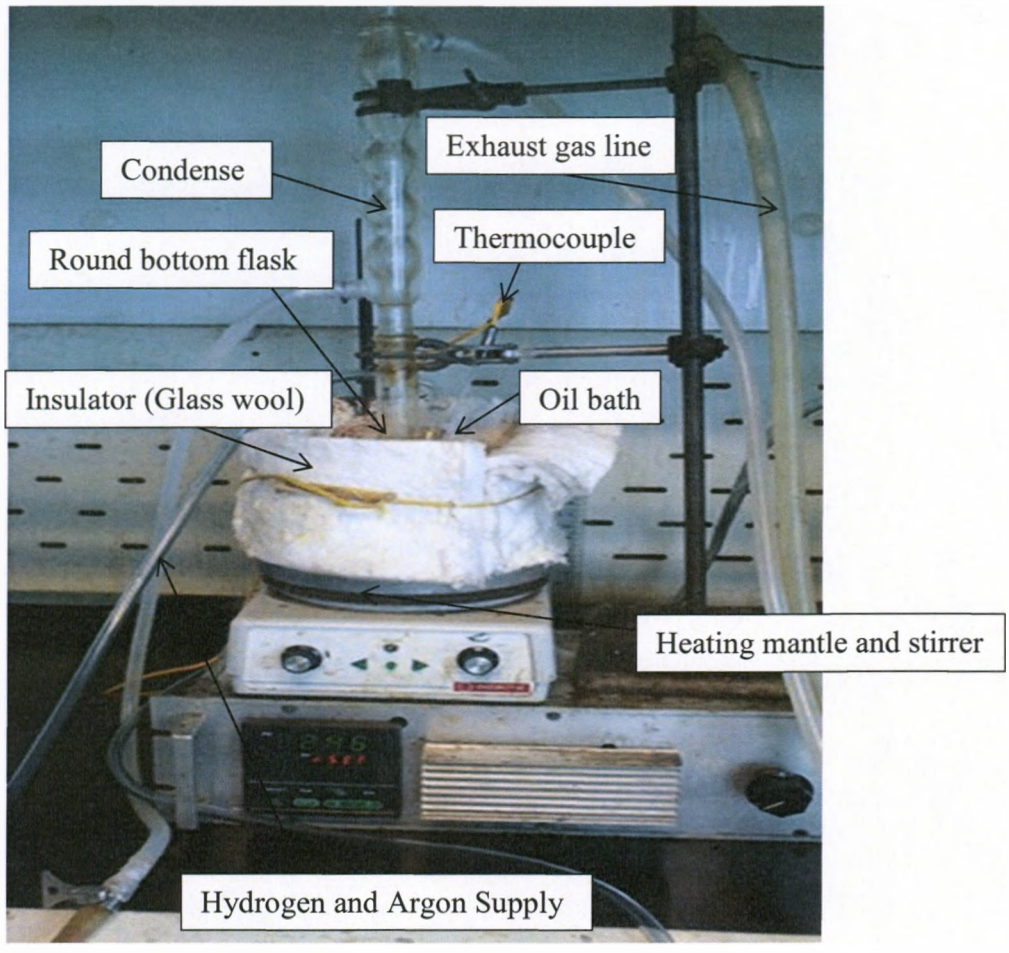


**Figure 4: Batch Reactor Set-up for Production of Biogasoline from Waste Cooking Oil**

Six different experimental runs were conducted, which looked into how the yield of biogasoline was affected when varying reaction temperature, contact time, catalyst: oil ratio, catalyst calcination temperature and Ni-loading (wt. %) in the catalyst. Characterisation results will be used to determine the best catalysts; which will be used for the rest of the experiments. The standard experiments were designed by a combination of reaction conditions that were found out to give optimum yield of biogasoline from previous studies in literature i.e. calcination temperature of catalyst of 300 °C, catalyst oil ratio of 1:75, reaction temperature of 250 °C and contact time of 1 hr (Nasikin *et al.*, 2009).

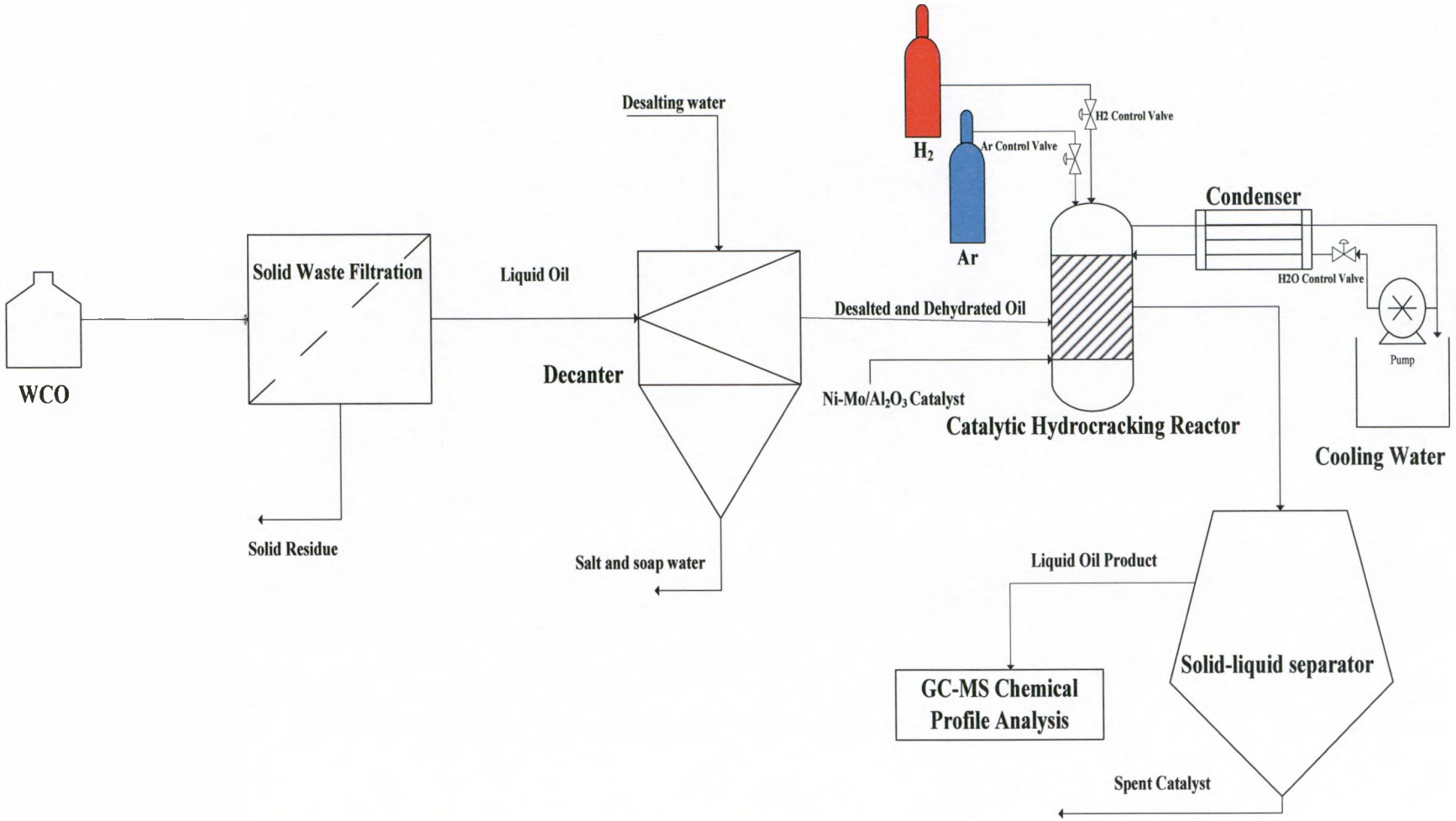


**Figure 5: Process Flow Diagram for Production of Biogasoline from Waste Cooking Oil**

### 3.5 Liquid Products Characterisation Technique (GC-MS)

The liquid products obtained from this study were taken for GC-MS analysis. To characterise the product samples, 10 μL of the sample was pipetted into Pasteur pipettes stuffed with cotton wool chunks that filter out any solid particles that may be present in the samples. The filtered sample was then transferred into a GC-MS sample holder, and into the same holder, 99.9 % dichloromethane solvent was filtered. The analysis was performed using Pagasus 4D GC× GC TOF MS from LECO: GC system Agilent 7890B. An Rxi-5SILMS column (30 m×0.25 μm ID ×250 μm) was used, with helium used as the carrier gas.

# CHAPTER FOUR: RESULTS AND DISCUSSIONS

## 4.1. Introduction

This chapter presents the results obtained from the experimental work done for this study. The techniques used for the characterisation of the synthesized catalysts and biogasoline are outlined and the results as received from each characterisation method are discussed.

## 4.2 Characterisation of Catalysts

### 4.2.1 Inductively Coupled Plasma Atomic Emission Spectroscopy (ICP-OES)

The ICP-OES analysis was performed on the catalysts to determine their actual Ni-loading (wt. %) and compare to their intended experimental compositions. The Ni-loading (wt. %) was varied and increased with every succeeding catalyst. The catalysts A-E were loaded with Ni at 5-25 wt. %, respectively, together with a commercially specified catalyst. The results obtained from the ICP-OES analysis are presented in Table 3.

**Table 3: ICP-OES Analysis for Catalyst Composition**

| Catalyst Identification | Experimental Composition (Ni-loading wt. %) | Actual Composition (Ni-loading wt. %) | Absolute Error | Relative Error (%) |
|---|---|---|---|---|
| **Commercial Catalyst** | 2.4 | 2.08 | 0.32 | 13.3 |
| **A** | 5 | 4.82 | 0.08 | 9.6 |
| **B** | 10 | 9.03 | 0.97 | 9.7 |
| **C** | 15 | 14.42 | 0.58 | 3.9 |
| **D** | 20 | 19.55 | 0.45 | 2.25 |
| **E** | 25 | 24.57 | 0.43 | 1.72 |

Table 3 shows that the actual Ni-loadings for all the catalysts are lower than the expected loadings with varying degrees of error. It can also be seen that the actual compositions for the commercially specified catalyst; and catalysts A and B have significant relative errors at 13.3 %,

9.6 % and 9.75 %, respectively. On the other hand, catalysts C, D and E are relatively close to the expected compositions with relative errors of 3.9 %, 2.25 % and 1.72 %, respectively. The errors in the Ni-loadings could be attributed to the loss of material during the preparations of the catalysts and transfer of materials between the equipment used. The first three catalysts show a significant loss because smaller amounts were measured for the loadings, thus the errors are more pronounced than for the catalysts with increased Ni-loadings.

### 4.2.2 Thermogravimetric Analysis (TGA)

The thermal stability of a catalyst plays a vital role in the activity and performance of a catalyst. For this study, TGA was performed on the synthesized catalysts with varying Ni-loadings (wt. %) and calcination temperatures to determine the maximum temperature up to which they can remain catalytically active for the duration of the experiments. Figures 6 and 7 show the degrading of the catalysts with increasing temperature.

#### 4.2.2.1. Effect of Ni-loading on Thermal Stability of Catalysts

Figure 6 presents the effect of Ni-loading (wt. %) on the thermal stability of the catalysts.

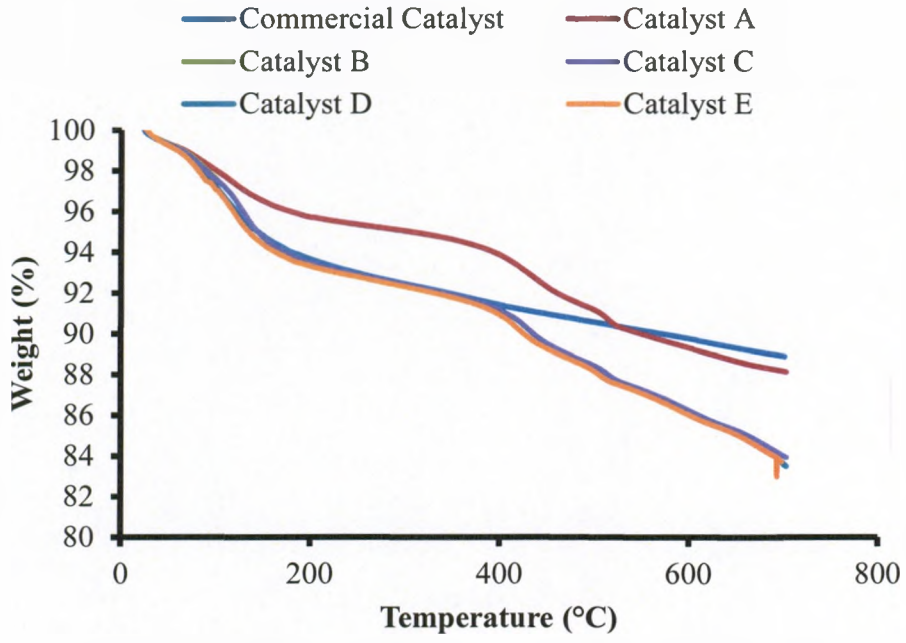


**Figure 6: TGA plots for catalysts with varying Ni-loading a) Commercial Catalyst (2.4 wt. % Ni), b) Catalyst A (5 wt. % Ni), c) Catalyst B (10 wt. % Ni), d) Catalyst C (15 wt. % Ni), e) Catalyst D (20 wt. % Ni) and f) Catalyst E (25 wt. % Ni)**

The overall trend observed from Figure 6 is the increased decomposition rate of the catalysts with increasing temperature. The catalysts were calcinated at a temperature of 300 °C for 3 hours each, prior TGA characterisation. The catalysts decomposed at a steady rate for temperatures below 100 °C. This trend is attributed to the release of moisture by the catalysts. The catalysts continued to degrade at a steady state until a temperature of approximately 150 °C, after which a plateau was observed, with an exception to catalyst A. Catalyst A displayed a different behaviour showing that it is the most stable at temperatures below 520 °C with a 5 wt. % Ni-loading. The

commercial catalyst, with a Ni-loading of 2.4 wt. % showed the highest thermal stability at temperatures above 520 °C. Catalyst E with highest N-loading at 25 wt. % experienced an accelerated degradation at temperatures above 700 °C, which suggests that high Ni-loadings result in weak thermal strengths. These results reveal that the catalysts with lower Ni-loadings have a higher thermal stability. It can be concluded that for the enhancement of a catalyst's activity by the use of promoters such as nickel for the purpose of increasing thermal stability is limited. The Ni-loading must be kept below 5 wt. % in order to give rise to increased thermal stability effects. Being calcinated at 300 °C, the catalysts displayed a high loss in weight with increasing temperature because of a higher moisture content retained due to the low calcination temperature. Chen *et al.* (2005) suggested that at relatively low calcination temperatures, a lower Ni-loading is an important factor to consider for improved catalytic performance.

#### 4.2.2.2 Effect of Calcination Temperature on Thermal Stability of Catalysts

The calcination temperature of the catalyst has an effect on its thermal stability. Catalysts F to G were generated from calcining Catalyst A at increased temperatures because of it outperformed the other catalysts in terms of thermal strength. Figure 7 shows the change of catalyst weight with increasing temperature for catalysts calcinated at varying temperatures. The catalysts display a similar and steady decrease in weight % with increasing temperature. This trend occurs until a temperature of approximately 100 °C during which there was a release in the moisture content, similarly to the trend observed from Figure 6. It can be seen that Catalyst F, calcinated at 400 °C, shows the highest thermal stability. This catalyst retained more than 96 wt. % of its initial mass up to a temperature of approximately 900 °C. Catalysts G, H and I; calcinated at 500 °C, 600 °C and 700 °C, respectively, display closely similar mass decomposition trends with increasing temperature. These catalysts retained more than 92 wt. % of their initial mass to a maximum thermal temperature of approximately 600 °C, above which there was a drastic decline in mass down to approximately 82 wt. % at 900 °C. At temperatures above 600 °C, Catalyst G showed a higher thermal stability than Catalysts H and I, while Catalyst H was more stable than Catalyst I at the same temperature conditions. From this trend, it can be seen that increasing calcination temperatures increases the Ni consumption during reactions between NiO and $Al_2O_3$ support. Therefore there was a reduction in the desired thermal stability effects that Ni promotes. The continued, steady weight loss with increased temperature, reflected by the steady horizontal

lines, was a result of sintering and agglomeration of various phases within the catalyst, which gradually allowed room for more moisture evaporation.

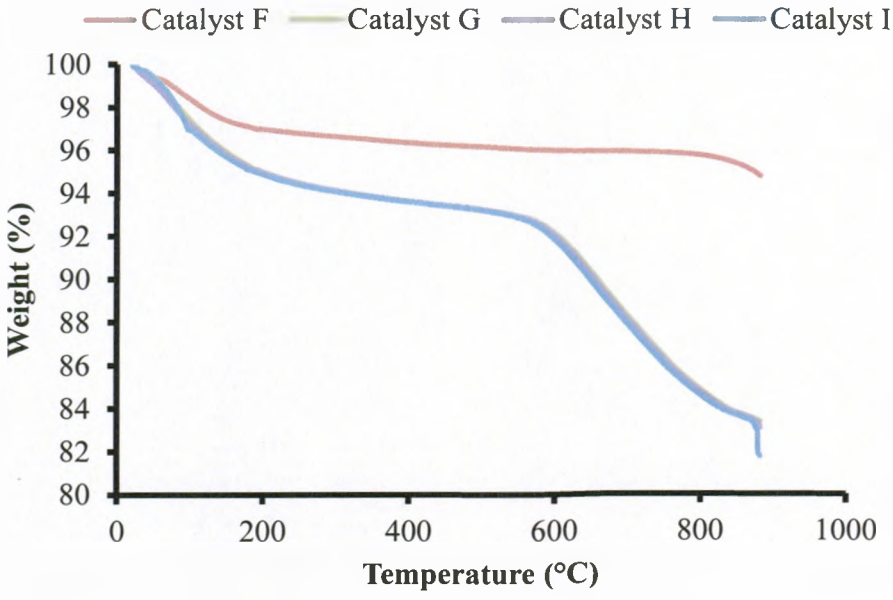


**Figure 7: TGA plots for Catalyst A with varying calcination temperatures a) Catalyst F (400 °C), c) Catalyst G (500 °C), d) Catalyst H (600 °C), and e) Catalyst I (700 °C)**

### 4.2.3 Brunauer-Emmet-Teller (BET)

Thermal and chemical treatment on catalysts affects their textural properties, physical structure and ultimate catalytic activity. BET characterisation was employed to investigate the effect Ni-loading (wt. %) and calcination temperature have on the catalysts.

#### 4.2.3.1 Effect of Ni-loading on Catalyst Pore Size, BET Surface Area and Pore Volume

The effect Ni-loading have on the pore size, BET surface area and the pore volume are presented and discussed. Literature studies reported that the metal loading has an effect on the textural properties of Ni-Mo/alumina catalysts (Priecel *et al.*, 2011). One study has shown that the loading of metals on catalyst supports such as alumina decreases the surface area of the support, and thus the entire catalyst (Priecel *et al.*, 2011). In another study, it was found that the loading of metal onto supports also decreases the pore volume and size (Kamyab, 2016).

**Table 4: Effect of Ni-loading on Catalyst Pore Size, BET Surface Area and Volume**

| Catalyst Identification | Ni-loading (wt. %) | BET Surface Area ($m^2/g$) | Pore Volume ($cm^3/g$) | Pore Size (nm) |
|---|---|---|---|---|
| A | 5 | 61.6146 | 0.0512 | 6.4597 |
| B | 10 | 41.4799 | 0.0583 | 7.4389 |
| C | 15 | 37.5360 | 0.0672 | 7.5001 |
| D | 20 | 30.7976 | 0.0765 | 7.5516 |
| E | 25 | 28.5987 | 0.0929 | 7.5734 |

Figure 8 and Table 4 presents the BET characterisation results for the effect of Ni-loading on the surface area of the pores. It can be seen from Figure 8 that the increase in concentration of the promoter (Ni), significantly decreased the BET surface area of the catalyst. This observed trend is the result of the increased concentration of the loaded metals filling up and plugging the pores. The decrease in the surface area of the pores with increased Ni-loading translates into a decrease in catalyst surface area available for reactions. The BET catalyst surface area decreased as a result of less nitrogen being adsorbed on the surface of the catalysts during analysis. Yin *et al.* (2013) studied the effect of increasing the Ni:Mo ratio on the surface area and pore volume of

unsupported Ni-Mo catalysts. They observed an increase in the surface area and pore volume after increasing the Ni:Mo ratio. It was suggested that the increase in both surface area and pore volume was due to increased NiO formation as a result of more Ni content. The results of the study done by Yin *et al.* (2013) are partially in agreement with the results of this study. Both studies resulted in an increase in the pore volume of the catalyst with increased Ni:Mo ratio. But the opposite effect was observed on the surface area of the catalysts. In this study, the surface area decreased with an increase Ni:Mo ratio. The different observation is attributed to the effect of the Ni-Mo interactions with the alumina support. The presence of the alumina resulted in reactions of the loaded metals with the support, giving rise to other chemical species that settled on the surface of the catalysts, thus reducing the surface area available for hydrocracking reactions.

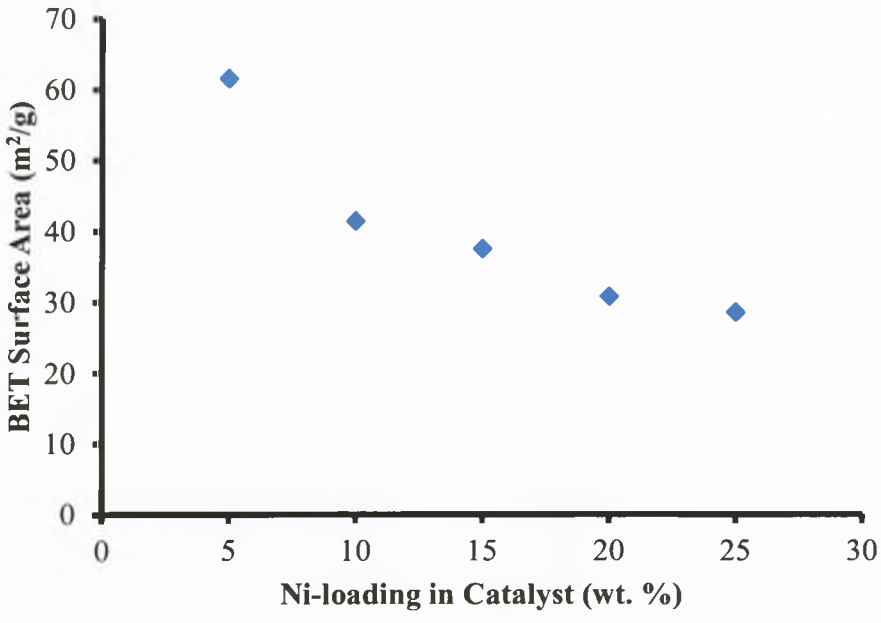


**Figure 8: BET Surface Area for varying Ni-loading (wt. %) in Catalyst**

Figure 9 and Table 4 show the effect Ni-loading has on the pore volume of the catalysts. A common trend is observed for the effect on pore size and volume. The pore volume increases with increasing Ni-loading. The volume increase was steady. At a Ni-loading of 5 wt. %, the pore volume was 0.051 $cm^3/g$. The volume increased to 0.058 and 0.067 $cm^3/g$ at loadings of 10 and 15 wt. %, respectively. There was an increase of volume by 13.73 % and 15.52 % in succession from 5 to 15 wt. %. At a loading of 20 and and 25 wt. %, the volume of the pores was

0.077 and 0.093 $cm^3/g$, respectively. The successive percentage increments were 12.98 % and 20.78 %, respectively. This means that the pore volume increase with increasing Ni-loading was non-linear and non-proportional. From Figures 8 and 9, it can be seen that the pore volume increases faster than the surface area. Therefore the surface area to volume ratio decreases with increasing Ni-loading.

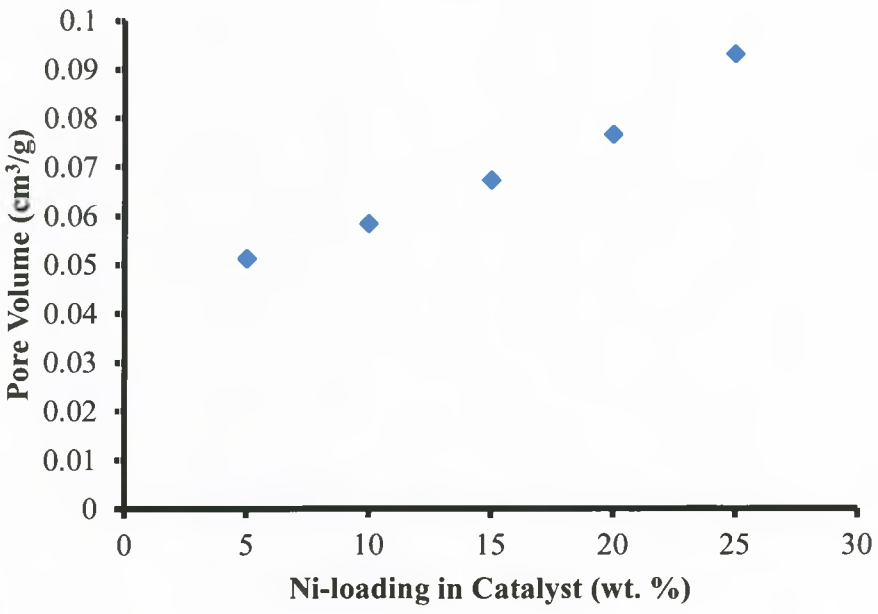


**Figure 9: BET Pore Volumes for Varying Ni-loading in Catalyst (wt. %)**

It is observed from Figure 10 and Table 4 that the catalyst pores size or diameter increased with increasing Ni-loading in the catalyst. The BET pores size of these catalysts is classified as mesoporous (Kamyab, 2016). The catalysts have an average pores size of 7.3047 nm. Catalyst A, having 5 wt. % of Ni-loading has a pore sizes of 6.4597 nm, which goes up to 7.4389 nm at a loading of 10 wt. %, increasing the pore size by 15.16 %. It can be seen that as the Ni-loading was increased from 7.4389 nm at 10 wt. % to 7.5734 nm at 25 wt. %, the effect on pore size became less drastic. The increase in pore size with increasing Ni-loading is attributed to the formation of Ni crystals resulting from the agglomeration of Ni grains. Higher agglomeration of Ni results in low catalytic activity and non uniform spherical morphology of the produced catalyst as seen in figure 14. It is desirable that a catalyst may have a high number of small sized

pores. Therefore it is advantageous to use high temperatures for the calcination of the catalysts as the sintered precursors will decompose and break down into smaller particles, creating a larger surface area on the catalyst for maximum contact with the reactants.

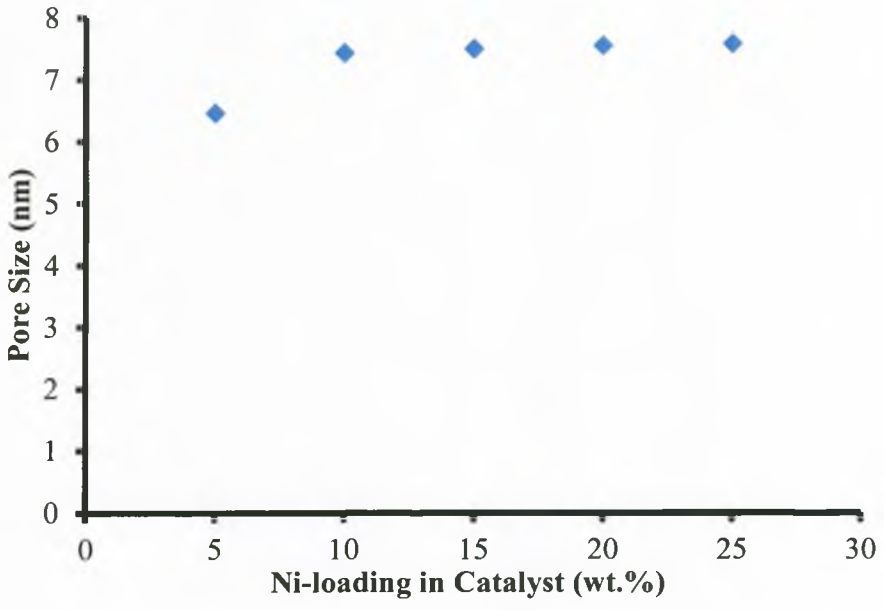


**Figure 10: BET Pore Sizes for Varying Ni-loading in Catalysts (wt.%)**

**4.2.3.2 Effect of Calcination Temperature on Catalyst Pore Size, BET Surface Area and Volume**

The effect calcination temperature has on the physical characteristics of the catalysts is presented in Table 5 and Figures 11-13.

**Table 5: Effect of Calcination Temperature on Catalyst Pore Size, BET Surface Area and Volume**

| Catalyst Identification | Calcination Temperature (°C) | BET Pore Surface Area ($m^2/g$) | Pore Volume ($cm^3/g$) | Pore Size (nm) |
|---|---|---|---|---|
| A | 300 | 61.6146 | 0.1329 | 6.4597 |
| F | 400 | 51.3941 | 0.1294 | 7.0414 |
| G | 500 | 45.5837 | 0.0986 | 8.4842 |
| H | 600 | 43.0596 | 0.0939 | 10.0274 |
| I | 700 | 40.7868 | 0.0938 | 10.5734 |

It is observed from Table 5 and Figure 11 that the BET surface areas of the catalysts decreased with increasing calcination temperature.

Catalyst A, which was calcinated at a temperature of 300 °C, has the highest BET surface area of 61.61 $m^2/g$. The surface area decreased gradually with calcination temperatures reducing in intervals of 100 °C. Catalyst I, being calcinated at the highest temperature of 700 °C experienced the highest reduction in BET surface area. The small difference in surface area of 2.27 $m^2/g$ between Catalysts H and I, in comparison to the difference between Catalysts A and F of 10.22 $m^2/g$ indicate that higher temperatures are effective in removing moisture and organic matter contained in the samples. The calcination of catalysts at high temperatures may possibly cause an increase in the size of the catalyst particles. Ferdous *et al.* (2004) suggested that during sintering at elevated temperatures, there is sintering of the alumina support. This sintering results in the alumina transforming into $Al_2(MoO_4)_3$, which contributes to the increase in size of the catalyst particles (Ferdous *et al.*, 2004). Large particles result in reduced catalyst surface area available for reactions.

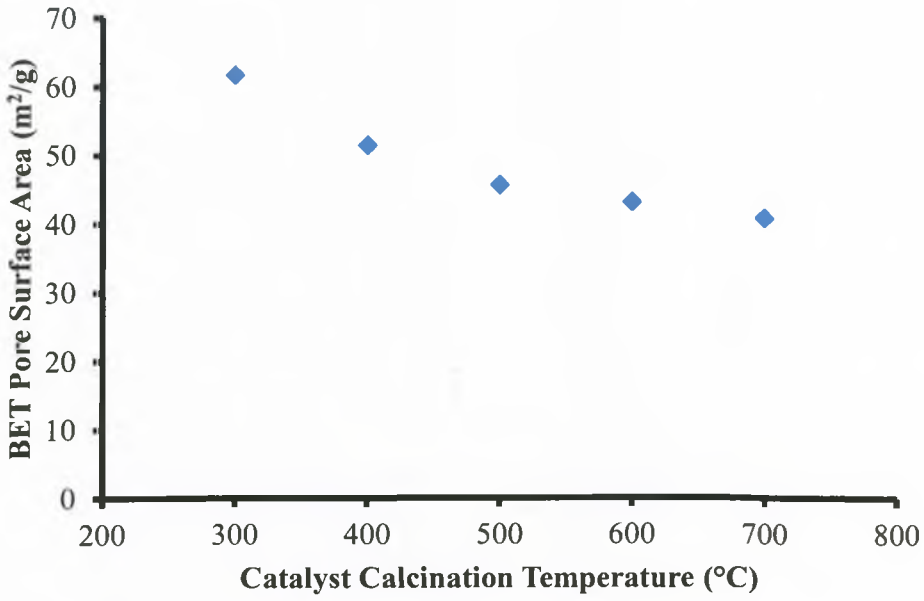


**Figure 11: BET Surface Area at Varying Catalyst Calcination Temperatures**

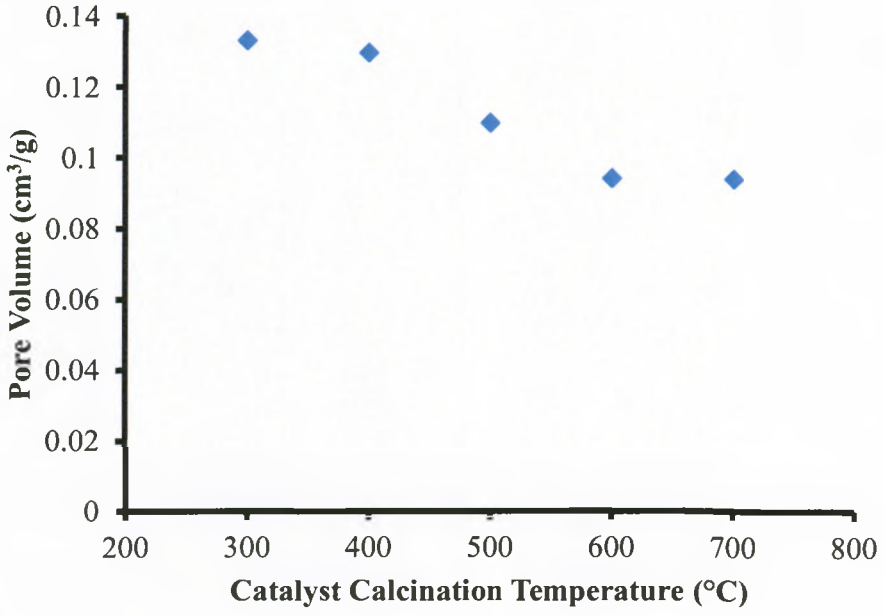


**Figure 12: BET Pore Volumes at Varying Catalyst Calcination Temperatures**

Figure 12 presents the change in pore volume with changing calcination temperatures. It can be observed that the volumes of the pores decreased with increased calcination temperatures. At a calcination temperature of 300 °C, the pore volume was 0.1329 $cm^3/g$. The volume decreased

slightly by 2.63 % to 0.1295 $cm^3/g$ at 400 °C. A drastic reduction is observed when the calcination temperature was increased further to 500 °C and 600 °C resulting in pore volumes of 0.1096 and 0.0939 $cm^3/g$, respectively. There was a 15.37 % and 14.32 % decrease in pore volume when the calcination temperature was increased to 500 °C and 600 °C, respectively. A pore volume of 0.0938 $cm^3/g$ is observed at 700 °C, a decrease of only 0.11 % from 600 °C. The decrease in pore volume and increase in pore size presented in Figure 13 are complementary because these properties directly affect each other.

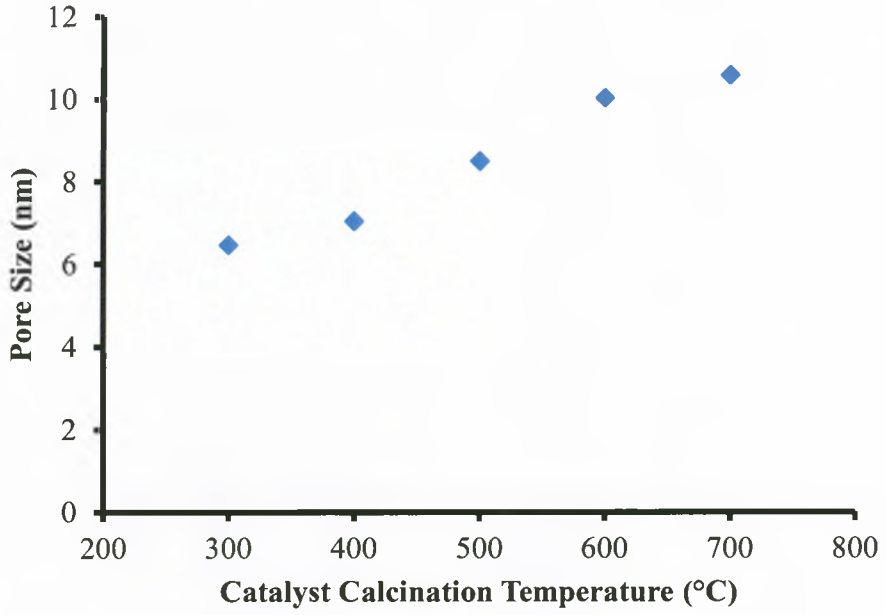


**Figure 13: BET Pore Sizes at Varying Catalyst Calcination Temperatures**

It can be observed from Figure 13 and Table 5 that the catalyst pore size increased with increased calcination temperature. The pore size slightly increased by 1.3 % from 6.951 to 7.0414 nm when the temperature was increased from 300 °C to 400 °C. When the calcination temperature was further increased to 500 °C, there was a drastic increase of pore size by 20.49 % to 8.4842 nm. There was a another significant increase in the pore size when the temperature was increased to 600 °C, after which the size increase started to decline towards a temperature of 700 °C. At 600 °C and 700 °C the pore sizes were 10.0274 nm and 10.5734 nm, respectively. The successive increments reduced to 18.19 % and 5.45 %, in that order. These results suggests that the pore sizes increases with increasing calcination temperature up to a maximum point after which the pore size will start decreasing. Kamyab (2016) suggested that 500 °C is the optimum

calcinated temperature for Ni-Mo/$Al_2O_3$ catalysts. A literature study suggested that the pore size increase with increasing calcination temperatures of Ni-Mo/$Al_2O_3$ catalysts above 500 °C was due to volatilization of Mo, which results in a loss in catalytic activity. At these temperatures, $MoO_3$ is vulnerable to sublimation (Kasztelan *et al.*, 1986). Hence, when the pore size increases, the pore volume will decrease, as observed from Figures 12 and 13.

### 4.2.4 Scanning Electron Microscopy (SEM)

Scanning Electron Microscopy (SEM) micrographs present a basic analysis for the structural activity of the catalysts. To determine the difference in texture and morphology of the catalysts as a result of the difference in Ni-loading, SEM characterisation was employed. The presented images are at a magnification of 200 μm. The collective physical form and appearance of the catalyst particles is pellets. The shapes of the particles are a mixture of square and triangular extrudes/pellets.

#### 4.2.4.1 Effect of Ni-loading on the texture and morphology of catalysts

The SEM micrographs for catalysts with varying Ni-loadings are presented in Figure 14. The bigger particles are rounded and edgy around the surface, while the smaller particles reveal flaky and sharp edged textures. It can be observed from Figures 14, a-e, that the particle size distribution is non-uniform with different degrees. There is an uneven distribution of Ni and Mo species dispersed over the catalyst support, which means that the mixing of the active components and the support was not done thoroughly. Aggregated structures and less homogeneity can be observed. This phenomenon can adversely reduce the access of the reaction fluid raw material to the catalyst active sites. The aggregated structures come as a result of preparing the catalysts by the impregnation process. It can be observed from the images that there was formation of crystals due to the agglomeration of the loaded metals. The size of the crystals increases from the catalyst with the lowest Ni-loading of 5 wt. %, to the catalyst with the highest loading of 25 wt. %. Lui *et al.* (2007) suggested that the increase in crystal sizes was due to the evaporation of the solvent during the drying of the catalyst. While drying the catalysts, the precursors crystalized and thus promoted the growth of the crystals to varying degrees, which resulted in the particles sizes distributed over a wide range (Liu *et al.*, 2007). An uneven distribution of the active sites and promoter do not effectively minimize film mass transfer and diffusional resistances.

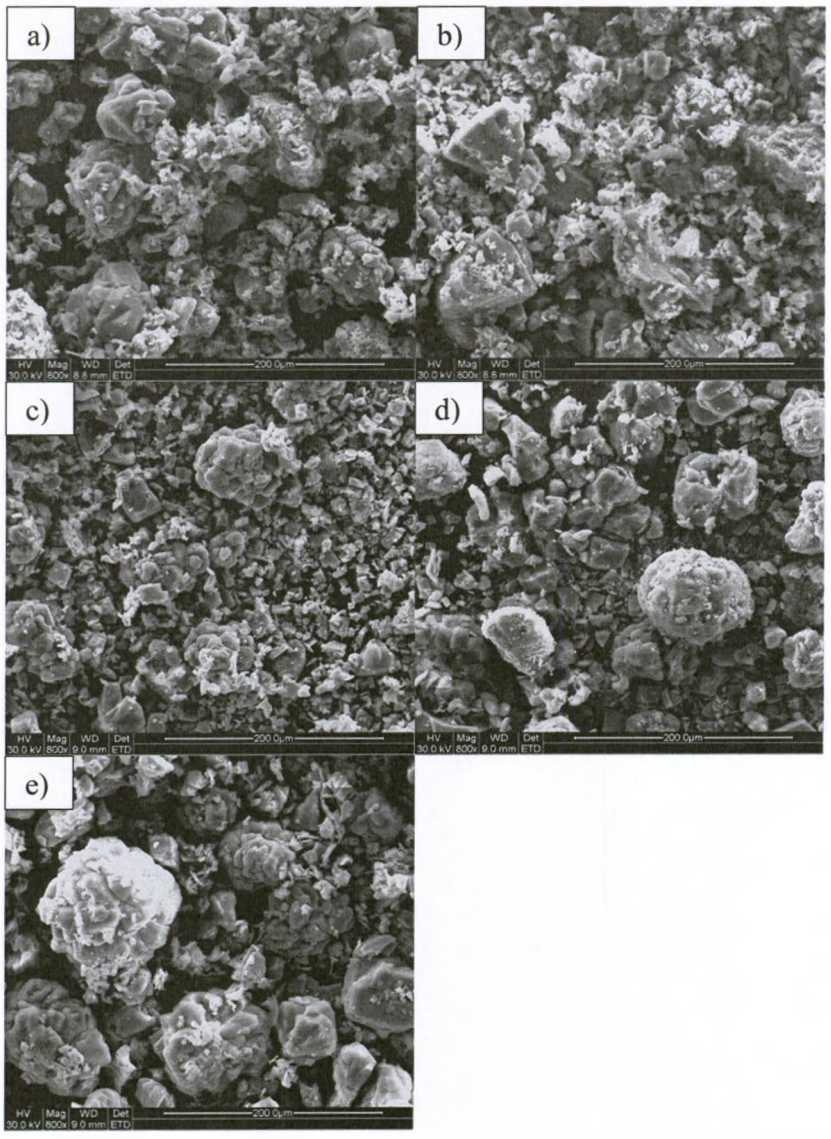


**Figure 14: SEM Images for catalysts with varying Ni-loading a) Catalyst A (5 wt. % Ni), b) Catalyst B (10 wt. % Ni), c) Catalyst C (15 wt. % Ni), d) Catalyst D (20 wt. % Ni) and e) Catalyst E (25 wt. % Ni).**

At lower Ni-loadings, there is a high dispersion of the active species. It is because of the dispersion that Figure 14 a shows less non-uniformity in comparison to the other catalysts under the same category. It can also be seen that the area between the particles, which are the pores, is getting larger with increased Ni-loading. At increased Ni-loadings, the active species occur in bulks, as presented in Figure 14 e.

#### 4.2.4.2 Effect of Calcination Temperature on the Texture and Morphology of Catalysts

The effect calcination temperature has on the physical structure and morphology was investigated. Prior to characterisation, it was noticed that the catalysts calcinated at 300 °C had a dark-grey colour. The colour faded with increasing calcination temperature until a snow-white colour was observed for the catalyst calcinated at 700 °C. This indicates that there was a riddance of some organic matter during calcination.

The SEM images for catalysts with varying calcination temperatures are presented in Figure 15. It can be seen from this figure that with increasing calcination temperature, there was breakage of the catalysts. At a low calcination temperature of 300 °C, there are more crystals and significant agglomerated particles. There was a notable decrease in the crystal sizes when the calcination temperature was increased to 400 °C, 500 °C and 600 °C. It can be said that higher calcination temperatures result in small and more uniform sized catalyst particles. This is evident from the catalyst calcinated at the highest temperature of 700 °C as there is increased particle size uniformity. This is a desirable effect as it results in a wide particle size distribution and promotes increased contact between the Ni and Mo particles and their dispersion over the support. Al-Fatesh and Fakeeha (2012) suggested that for the salts used in the catalyst preparations to be decomposed, high temperatures must be employed.

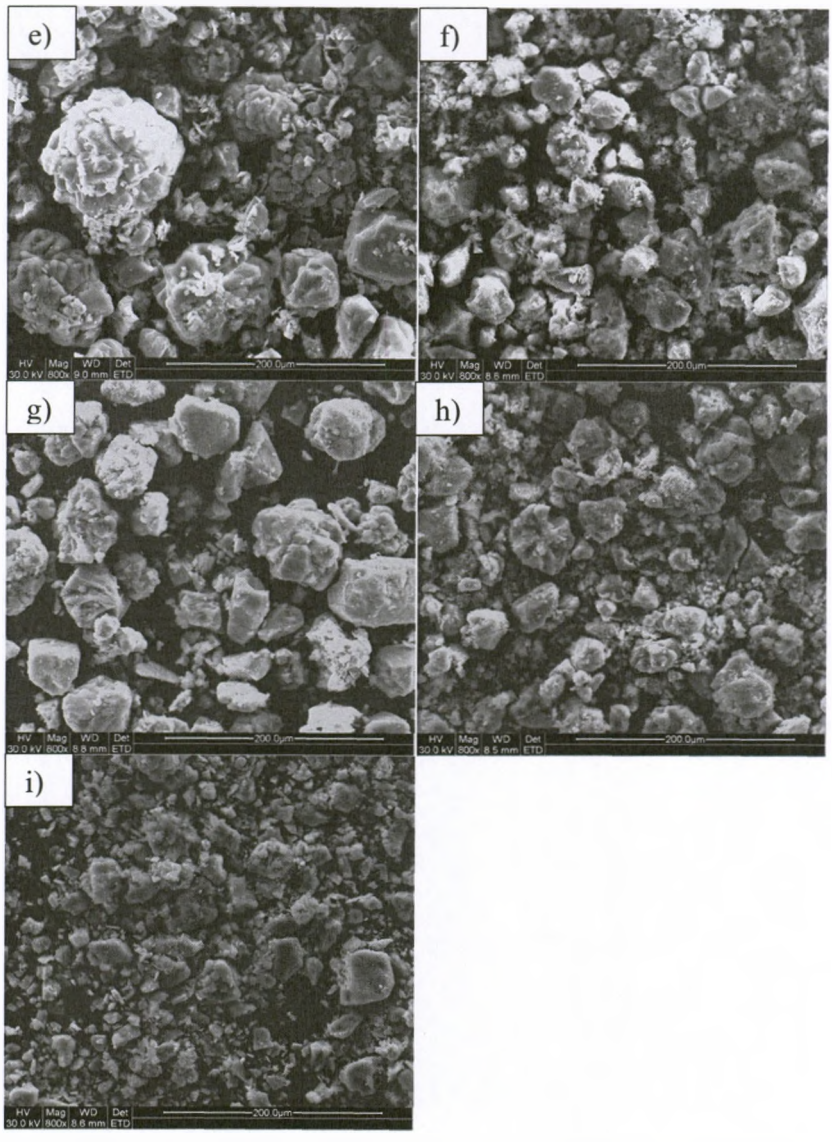


**Figure 15: SEM Images for catalysts with varying calcination temperatures e) Catalyst A (300 °C), f) Catalyst F (400 °C), g) Catalyst G (500 °C), h) Catalyst H (600 °C) and i) Catalyst I (700 °C)**

### 4.2.5 Fourier Transform Infrared (FT-IR) Spectrometry

In order to investigate the phase developments brought upon by the increase in Ni-loading and calcination temperature, the catalysts were characterised by FT-IR and Raman spectroscopy. The results of the two characterisations will be presented and discussed. FT-IR is limited because it cannot detect low frequency vibrations which can be detected by Raman Spectroscopy.

#### 4.2.5.1 Effect of Ni-loading on Catalyst Phase Change

The effect Ni-loading has on the phase change of the catalysts is presented and discussed. Figure 16 shows how the intensity displayed by the catalysts changes with increasing Ni-loading using FT-IR characterisation.

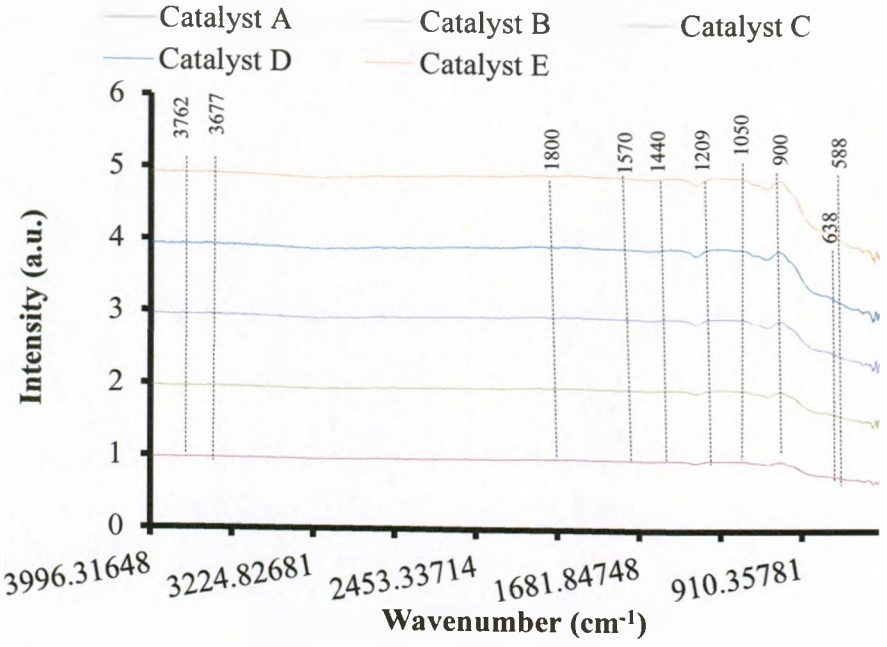


**Figure 16: FT-IR Spectra for catalysts with varying Ni-loading a) Catalyst A (5 wt. % Ni), b) Catalyst B (10 wt. % Ni), c) Catalyst C (15 wt. % Ni), d) Catalyst D (20 wt. % Ni) and e) Catalyst E (25 wt. % Ni)**

For Ni-Mo/$Al_2O_3$ catalysts, a band at 3762 and 3677 $cm^{-1}$ is characteristic of stretching of –OH groups on the surface of the catalyst. This band is not evident from Figure 16. Escobar *et al.* (2017) suggests that the absence of these bands is due to the preference of Mo deposition over surface –OH groups during impregnation. The vibrational bands that are present in within the wavelength range of 1440 to 1570 $cm^{-1}$ indicate that there is water that is dissociated on the surface of the carrier (Escobar *et al.*, 2017). The peaks at 588, 638 and 1050 $cm^{-1}$ are characteristic of Mo-O-Mo bridging bonds (Kaluža *et al.*, 2012). There is no significant shift in intensity by the catalysts from low to high Ni-loading. There is a dip band between 1050 and 1209 $cm^{-1}$. Kaluža *et al.* (2012) suggested that this band occurred as a result of a partial reaction of loaded Ni-Mo and the formation of Al-Mo from the interaction of Mo particles with the surface of the support.

### 4.2.5.2 Effect of Calcination Temperature on Catalyst Phase Developments

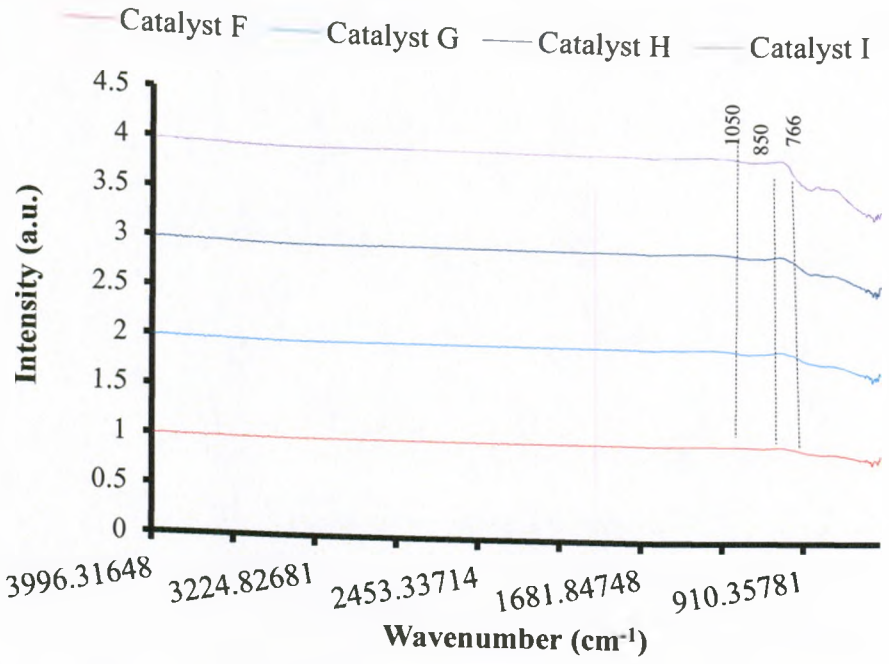


**Figure 17: FT-IR Spectra for Catalyst A with varying calcination temperatures a) Catalyst F (400 °C), b) Catalyst G (500 °C), c) Catalyst H (600 °C) and d) Catalyst I (700 °C)**

Figure 17 presents the FT-IR spectra for the catalyst A calcinated at varying temperatures. The catalysts have fairly similar trends in their spectra. The spectra are almost entirely horizontal and smooth. There appears to be a change in intensity at the interval of approximately 900 $cm^{-1}$ and 1050 $cm^{-1}$, which reflects the $Al_2O_3$ peak. A shift of the 1050 $cm^{-1}$ to higher intensities is observed. The absence of numerous peaks suggests that the catalysts are relatively homogeneously dispersed. There are no significant separations between the Ni and Mo species in the catalysts. The formation of *cis*-$MoO_2$ band between 766 and 850 $cm^{-1}$ contributes to the formation of $MoO_3$ crystallite particles, which was also observed by Kaluža *et al.* (2012). It can be said that the FT-IR spectra do not give in-depth information relating to the phase changes that the catalysts undergo. It is for this reason that Raman Spectroscopy was employed to supplement the results obtained from FT-IR.

### 4.2.6 Raman Spectroscopy

Raman spectroscopy was employed to characterise the nature and type of phases shown by the active metals in the catalysts.

#### 4.2.6.1 Raman Spectra for Catalysts with varying Ni-loadings

The Raman spectra for the prepared catalysts with varying Ni-loadings are presented in Figure 18. The catalysts displayed similar spectra with some small differences in peak intensities. The peaks for the spectra presented in Figure 18 are lower intensities than those in Figure 19, which indicates that these catalysts are less dispersed and there are more Ni and Mo interactions. The spectra have peaks at wavelengths of 966, 824, 341 and 290 $cm^{-1}$. The peaks confirm that the dispersion was non-uniform as a result of the impregnation method of catalyst preparation. These peaks correspond to the presence of $MoO_3$ crystallites in the catalysts. It can be observed that even though the spectra are similar, there is an increase in peak intensity when the Ni-loading is increased. This implies that there was an increase in the size if $MoO_3$ crystallites. The symmetrical stretch at 871 $cm^{-1}$ indicates a Mo-O bond (Badoga, 2015). The tailings of the spectra wavelengths below 290 $cm^{-1}$ shows increased polymerization of the species.

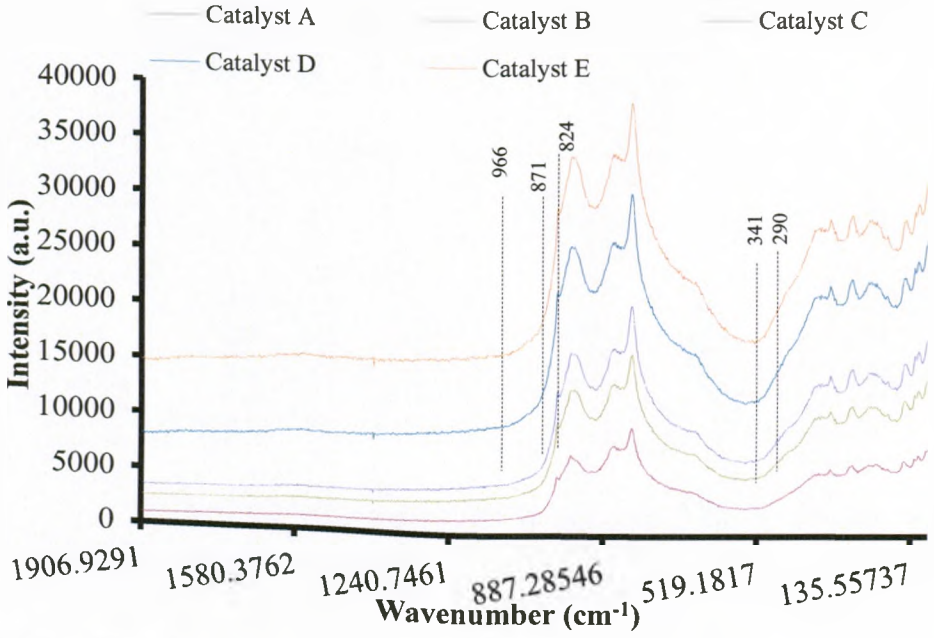


**Figure 18: Raman Spectra for catalysts with varying Ni-loading a) Catalyst A (5 wt. % Ni), b) Catalyst B (10 wt. % Ni), c) Catalyst C (15 wt. % Ni), d) Catalyst D (20 wt. % Ni) and e) Catalyst E (25 wt. % Ni)**

#### 4.2.6.2 Raman spectra of Catalysts Calcinated at varying Temperatures

Figure 19 displays the Raman spectra for Catalysts F to G calcinated at varying temperatures. Similar to the catalysts with varying Ni-loading, these catalysts display relatively similar spectra. The characteristic peaks for these catalysts can be seen at 962, 820, 379, 220 and 150 $cm^{-1}$. These peaks correspond to the presence of $MoO_3$ crystallites, which a feature literature studies have attributed the presence of the peaks to (Badoga, 2015; Kamyab, 2016). The intensity of the peaks has increased with increased calcination temperature. This suggests that high temperatures promote the formation of $MoO_3$, which also reflects that the dispersion is getting poorer with increasing calcination temperature. Kamyab (2016) suggested that the poor dispersion can be attributed to the sequence followed for the loading of the active metals during catalyst preparations. Improved dispersion is achieved when Mo is loaded before Ni. When Mo is loaded first, there is increased accessibility to Ni to form Ni-Mo-O interactions. The inhibition of these interactions results in the separation of the active Ni and Mo species (Kamyab, 2016). In this study, the nickel was loaded first, the results of which supports the suggestion.

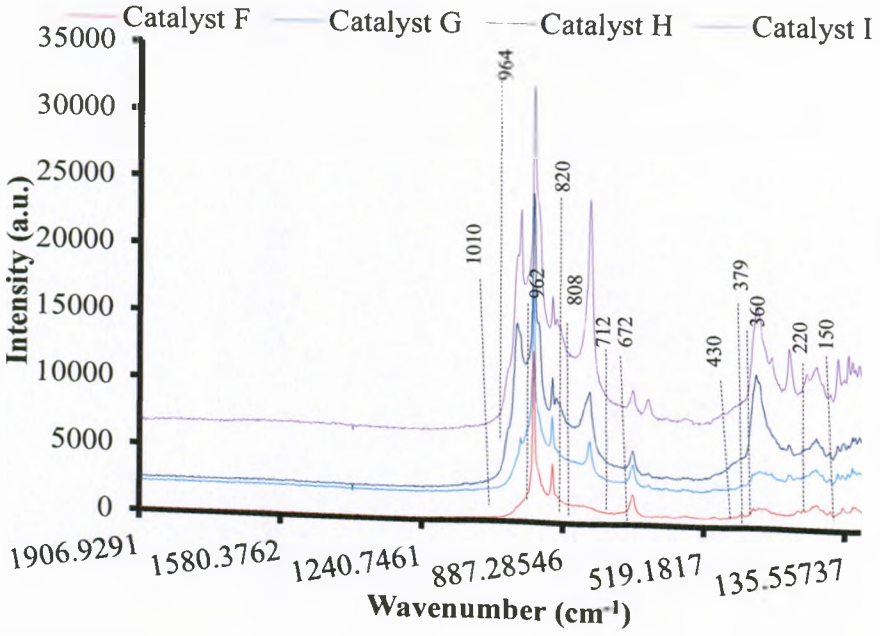


**Figure 19: Raman Spectra for Catalyst A with varying calcination temperatures e) Catalyst A (300 °C), f) Catalyst F (400 °C), g) Catalyst G (500 °C), h) Catalyst H (600 °C) and i) Catalyst I (700 °C)**

The sharp, high intensity peaks in Figure 19 suggests that the support is present in the $\alpha$-$Al_2O_3$ phase as a result of phase transformation of the support when temperature is increased. The peak at 964 $cm^{-1}$ is characteristic of the crystallization of $Al_2O_3$ support species. On the other hand, catalysts in Figure 18 show shallow and broad bands which are characteristic of the $\gamma$-$Al_2O_3$ as a result of being calcinated at a lower temperature (300 °C). The peaks at 712 $cm^{-1}$are characteristic of $NiMoO_4$ crystallites present in the catalysts. The intensity of the successive peaks remained fairly constant with increased calcination temperature. This confirms that higher dispersion of active Ni-Mo species is higher in catalysts calcinated at lower temperatures (e.g. 300 °C) than it is for high temperatures (e.g. 700 °C) as seen from the SEM micrographs.

A peak at 430 $cm^{-1}$ is characteristic of surface polymolybdates. The absence of this peak indicates that there was an inhibition of the formation of this species in all the catalysts. The bands at 1010 and 808 $cm^{-1}$ present the symmetrical and asymmetrical vibrations of Mo-O-Mo bonds, respectively. The band between the peaks at 672 and 430 $cm^{-1}$ are characteristic of Al-O-Ni vibrations. The bands at 150, 220 and 360 $cm^{-1}$ also correspond to the formation of polymolybdate species (Zepeda *et al.*, 2008).

## 4.3 Characterisation of Liquid Fuel Products

The production of biogasoline was preceded by the pre-treatment of the waste cooking oil through dehydration and de-salting. Deoxygenation reactions occurred during both the pre-treatment and catalytic hydrocracking, more so in the latter than the former. The main purpose was to eliminate any species such as alkali metal, water and salt particles that can potentially poison and/or deactivate the catalysts.

### 4.3.1 Pre-treated Waste Cooking Oil: GC-MS Analysis

It was required for the waste cooking oil to be pre-treated prior to being used for the catalytic hydrocracking reactions. Figure 20 and 21 present the chromatograms for the untreated and treated waste cooking oil, respectively. The chromatogram presented in Figure 20 is very similar to the one obtained by Khalisanni *et al.* (2008) when analyzing waste cooking oil for use as a biofuel raw material. Their study found that the WCO was composed mainly of n-hexadecanoic and oleic acid. This study confirms the presence of the two major components of the oil with a presence of other compounds.

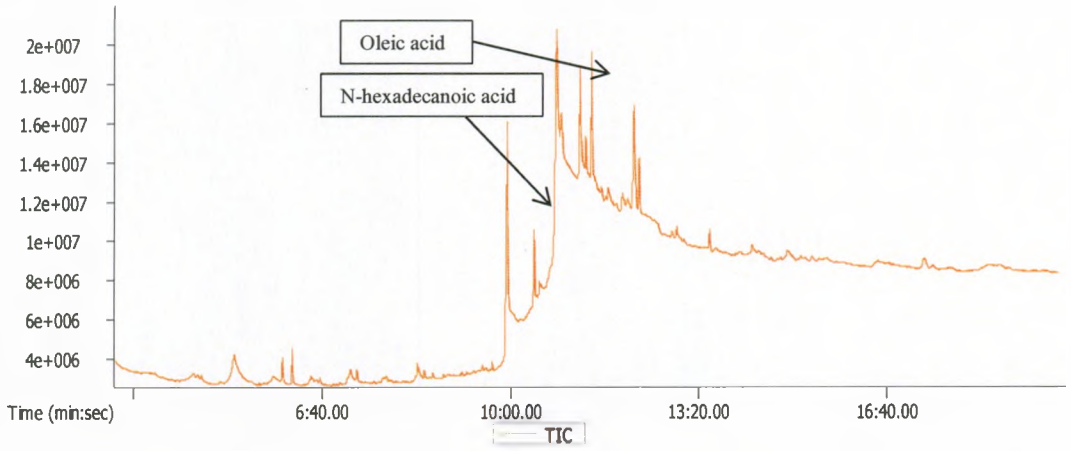


**Figure 20: Total Ion Chromatogram (TIC) for Untreated Waste Cooking Oil**

Figure 21 presents the GC-MS chromatogram for the pre-treated oil. It can be observed that there are differences between the two chromatograms, which confirm that there was a change in composition of the oil before and after the pre-treatment. It can also be said that there was cracking of the oil during pre-treatment because the chromatogram shows the presence of some short carbon chain compounds that were not there before. It can be concluded that pre-treatment of the oil is beneficial.

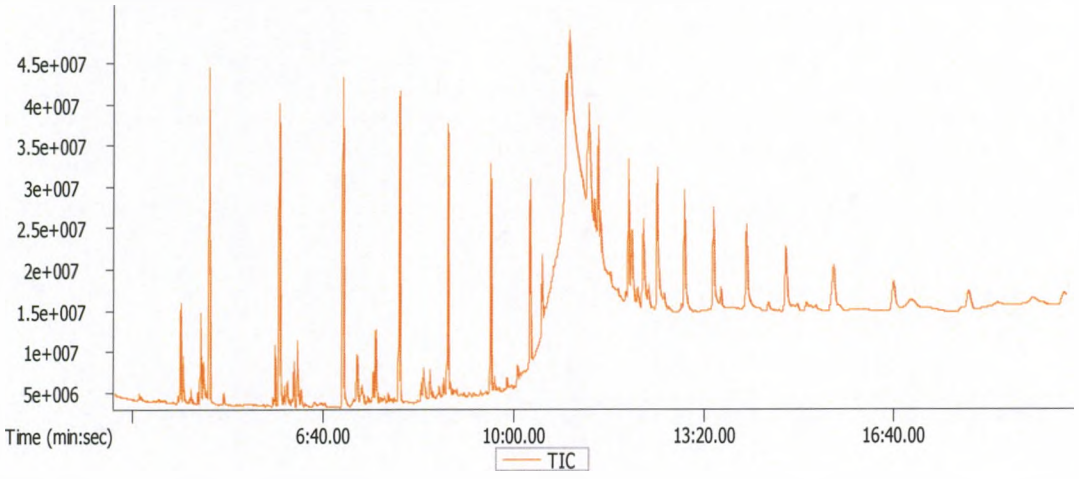


**Figure 21: Total Ion Chromatogram (TIC) for Pre-treated Waste Cooking Oil**

### 4.3.2 Biogasoline: GC-MS Analysis

This section outlines and discusses the results obtained from a GC-MS analysis. For the purposes of this study, biogasoline was produced following methods adapted and adjusted, where applicable, from best technology practices currently utilized within petroleum refineries, same as using similar catalysts and hydro-conversion processes. Therefore the biogasoline was classified as having the same chemical nature as that of petroleum-based gasoline. Figure 22 presents the chromatogram for the biogasoline liquid products obtained from this study.

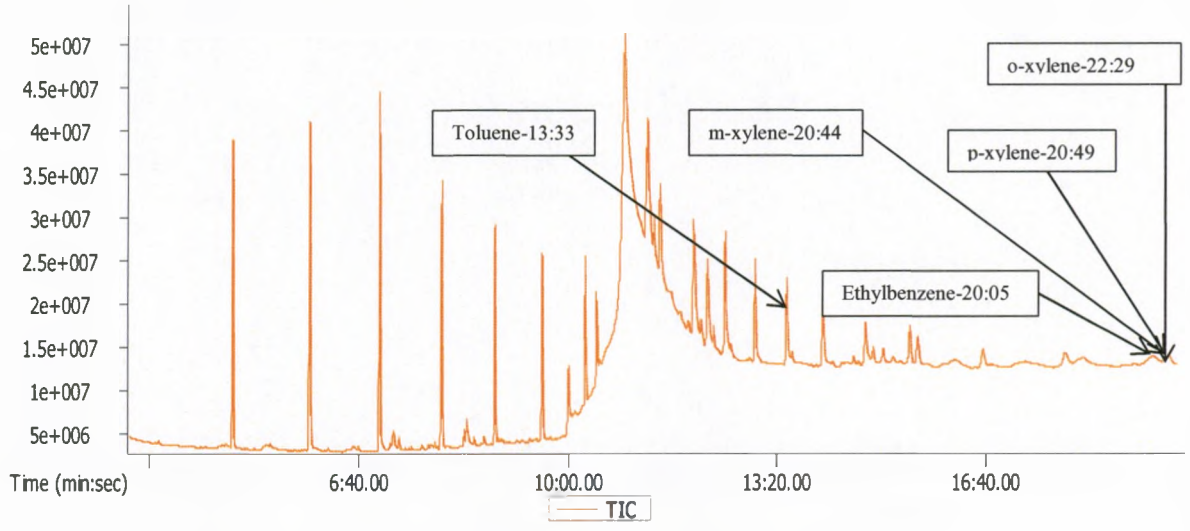


**Figure 22: Total Ion Chromatogram (TIC) Chromatography for Biogasoline**

It can be seen that the chromatogram for biogasoline product is very similar to the one for the pre-treated oil. The major difference lies in the reduction of the noise presented by the shorter peaks. This indicates that there was further refining of the feedstock during catalytic hydrocracking. The presence of important components of gasoline, i.e. toluene, xylenes and methyl ethyl benzenes, are evident from the chromatogram. Wang *et al.* (2013) conducted a study to produce biogasoline by co-cracking the distilled fraction of bio-oil and ethanol. The chromatogram of their liquid product is presented in Figure 23, which only shows the gasoline phase. Figure 23 shows the presence of a higher concentration of short chain hydrocarbons in comparison to Figure 22. After a time period of 10 minutes, both chromatograms show a rise in the baseline of the absorbance, the rise being more pronounced in Figure 22 than in Figure 23. This can be attributed to the difference in raw materials used for the production.

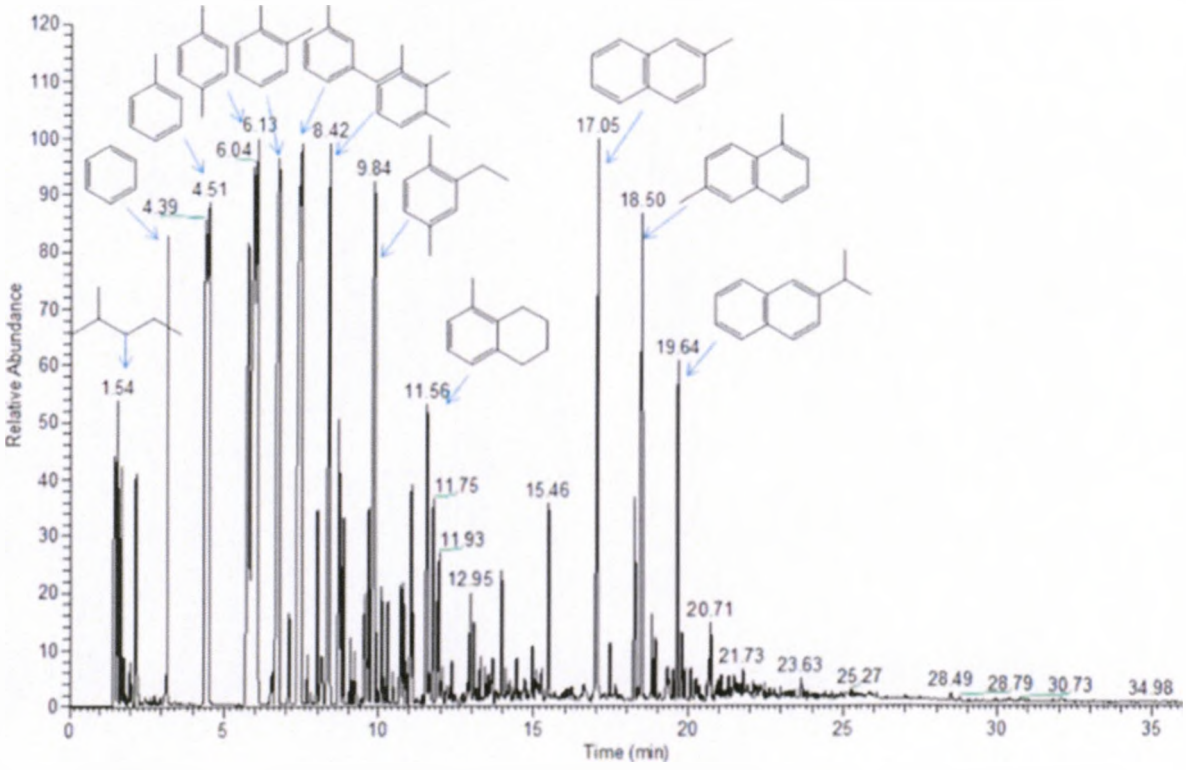


**Figure 23: Total Ion Chromatogram (TIC) Chromatography for Gasoline/Petrol Phase (adapted from Wang *et al.*, 2013)**

The GC-MS characterisation results of the liquid fuel products from this study show that the products were a complex mixture of compounds with carbon numbers ranging from $C_1$-$C_{31}$. This allowed for the classification of the different compounds within the product according to the carbon number range into which they fall. From the classes, gasoline-grade hydrocarbons (biogasoline) where totaled to give the concentration of biogasoline in the product of each experiment run. Different literature sources assign different carbon number ranges for gasoline-grade hydrocarbons. For instance, according to Aakko-Saksa *et al.*( 2011), biogasoline is within the carbon number range $C_4$-$C_{12}$(Aakko-Saksa *et al.*, 2011), while Nasikin *et al.* (2009) considers it to be within the carbon number range of $C_8$-$C_{15}$. For purposes of this study, the classifications were done following the carbon number ranges outlined by Fahim *et al.* (2010), as shown in Figure 24. According to Figure 24, biogasoline, which is analogous to "automobile gasoline" as depicted in the figure, is composed of hydrocarbons of the carbon number range of $C_3$-$C_{12}$ (Fahim *et al.*, 2010). It can also be seen from Figure 24 that there are overlaps in carbon number ranges from one class of hydrocarbons to the other. From Figure 24, liquid petroleum gasses

(LPG) are within $C_1$-$C_5$, automobile gasoline is within $C_3$-$C_{12}$, while diesel fuel is within $C_{11}$-$C_{20}$ and the heavier hydrocarbons and composed of $C_{n\geq21}$.

The results obtained from this study show that using a petroleum hydrocracking catalyst, waste cooking oil was converted into a hydrocarbon liquid fuel mixture. The GC-MS results of the various liquid products revealed the presence of significant amounts of both gasoline/petrol and diesel carbon range hydrocarbons. For this study, the results are presented on the basis of carbon-atom number ranges. Biogasoline was classified as the gasoline-grade hydrocarbon corresponding with the carbon number range of $C_6$-$C_{12}$, while liquefied petroleum gas (LPG) was given as $C_1$-$C_5$, diesel fuel $C_{13}$-$C_{20}$, and all carbons with carbon numbers $C_{n\geq21}$ where classified as heavier oils and waxes.

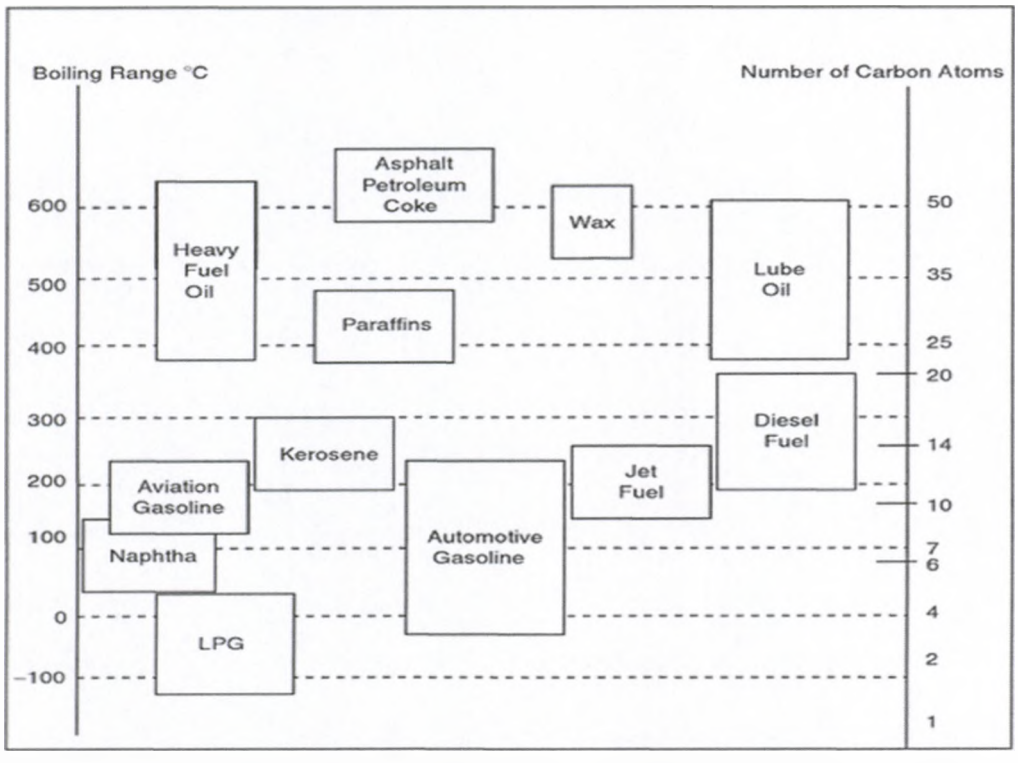


**Figure 24: Petroleum Fractions by carbon-atom number range (extracted from Fahim *et al.*, 2010).**

The liquid products were a mixture of straight chain alkanes and alkenes, as well as cycloalkanes and aromatics. The effects of reaction temperature, reaction time, catalyst: oil ratio, ratio of Ni-

loading (wt. %) in the catalyst and catalysts calcination temperature on the selectivity towards biogasoline and the distribution of the hydrocarbon boiling range classes within the liquid products will be presented and discussed.

#### 4.3.2.1 Effect of Reaction Temperature

The yield and quality of the hydro-processed oil depends on the reaction temperature, among other vital reaction conditions and parameters. Reaction temperature was one of the parameters whose effect on the yield of biogasoline was investigated. For the reaction temperatures, Catalyst A was used. A constant catalyst: oil ratio of 1:75 was used, and the reactions lasted for 1 hour each, with hydrogen gas at 0.5 kPa. The reaction temperatures studied are 180 °C, 200 °C, 220 °C, 240 °C and 250 °C.

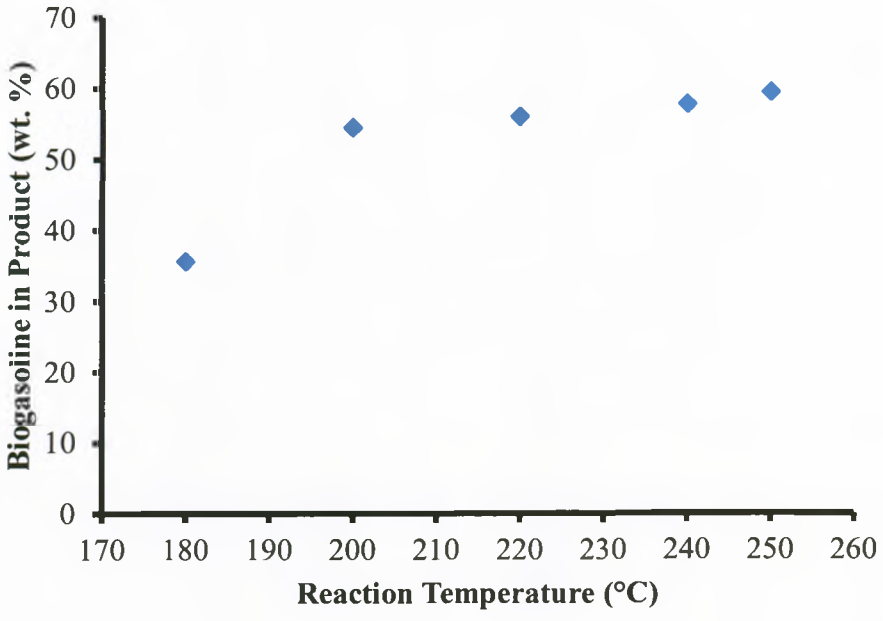


**Figure 25: Effect of reaction temperature on the hydrocracking of WCO over Ni-Mo/$Al_2O_3$ catalyst for biogasoline production**

From Figure 25, it can be observed that there was a pronounced increase in the yield of biogasoline with increased reaction temperature from 180 °C to 200 °C from 35.7 wt. % to 54.50 wt. %, respectively. At temperatures between 200 °C and 250 °C, the increase in biogasoline yield was less pronounced and rather increased almost steadily up to a maximum yield of 59.50 wt. % at 250 °C. The increase in biogasoline yield with increasing temperature is a common

trend that was expected because higher temperatures favour the yield of hydrocarbons with carbon-atom numbers within the gasoline petroleum fraction. This is in line with the results of the study by (Sotelo-Boyas *et al.*, 2010), who were hydro-treating rapeseed oil using Ni-Mo/$Al_2O_3$ as catalyst. At an initial hydrogen pressure of 9 MPa, the results of the study showed that at 350 °C, the selectivity of gasoline range hydrocarbons, defined as $C_5$-$C_{12}$, was less than 5 wt. %. The biogasoline selectivity increased to approximately 32 wt. % at 400 °C.

The carbon range of vegetable oils is similar to that of normal diesel; therefore the increased temperature is responsible for the cracking of the diesel range hydrocarbons, giving rise to lighter hydrocarbons such as those in gasoline/petrol, naphtha and jet fuel. In principle, the yield of biogasoline should increase drastically with increasing temperatures up to 420 °C, but the steady and slow increase observed in Figure 25 is attributed to the use of alumina ($Al_2O_3$) as a catalyst support. Literature sources have reported even though alumina has a high hydrogenation activity, it also considered to be a mildly acidic catalyst that favours the yield of hydrocarbons within the boiling point of diesel rather than the corresponding lighter products (Sotelo-Boyás *et al.*, 2012).

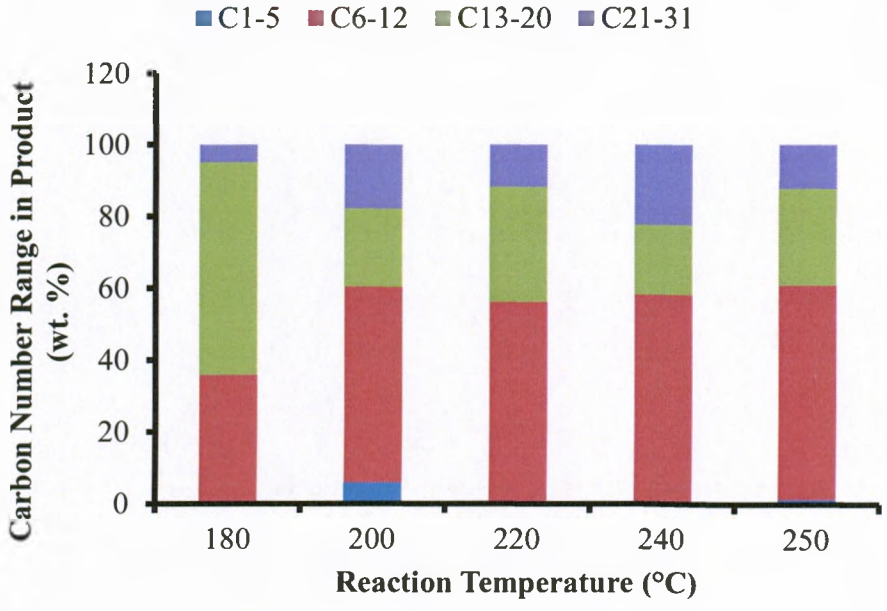


**Figure 26: Effect of reaction temperature on distribution of hydrocarbon fractions on the basis of carbon number range**

Figure 26 shows the change in yield distribution of the different hydrocarbon fractions obtained with increasing temperature. It was observed that biogasoline alone contributes to an average of about 50 wt. % of the products across the temperatures from 180 °C to 250 °C. Hydrocarbons within the diesel boiling range are more dominant at the lowest temperature, and steadily decreasing with increasing temperature. The presence of heavier hydrocarbons of carbon ranges $C_{n>20}$ were noticed. The content of these molecules does not present a distinct relationship with increasing temperature in this study. According to Sotelo-Boyás *et al.* (2012), high temperatures combined with strong catalysts yield naphtha, whereas mild temperatures and catalysts give rise to products within the boiling point of diesel.

#### 4.3.2.1.1 Comparison of Zeolites and Alumina as Hydrocracking Catalysts Support

Zeolites and alumina are common supports for hydro-treating catalysts in crude oil refineries. Alumina possesses well characterised amorphous or crystalline structures with acidic surfaces, making it a moderately acidic catalyst or catalyst support (Fahim *et al.*, 2010). Zeolites are also acidic substances that are compatible for promoting simultaneous cracking and hydrogenation reactions (Nasikin *et al.*, 2009). In this study, parallel experiments where performed to investigate the effect that $Al_2O_3$ and zeolites as Ni-Mo supports have on the biogasoline yield along with the increase in reaction temperature.

Figure 27 presents the results obtained from use of zeolite and alumina as catalyst supports for Ni-Mo with increasing temperature while other parameters remained constant, i.e. catalyst: oil ratio, hydrogen initial pressure and reaction time. When using zeolite as a catalyst support, a minimum biogasoline selectivity of 24.5 wt. %, increasing marginally up to a maximum biogasoline selectivity of 30.5 wt. % were achieved at 180 °C and 250 °C, respectively. Therefore it can be concluded that under similar reaction conditions, the alumina supported catalyst gave a better performance than the zeolite support. It should be stated that the opposite outcome was expected. The reason for this is that zeolites possess stronger acidic sites and are selective towards lighter hydrocarbons within the boiling range of jet fuel or gasoline and they have a more severe cracking activity in comparison to alumina (Sotelo-Boyás *et al.*, 2012). The results of this study contradict with those of Sankaranarayanan *et al.* (2011), who studied the effect that zeolites have on the severity of cracking long chain molecules into shorter chains. Their study showed that the incorporation of β-zeolite in a sulfided NiO (3 wt. %)-$MoO_3$ (12 wt.

%) supported on $\gamma$-$Al_2O_3$ was able to achieve nearly 100 % conversion of sunflower gas-oil mixture into diesel hydrocarbons. In the absence of β-zeolite in the catalysts, 95.5 % conversion was achieved (Sankaranarayanan *et al.*, 2011).

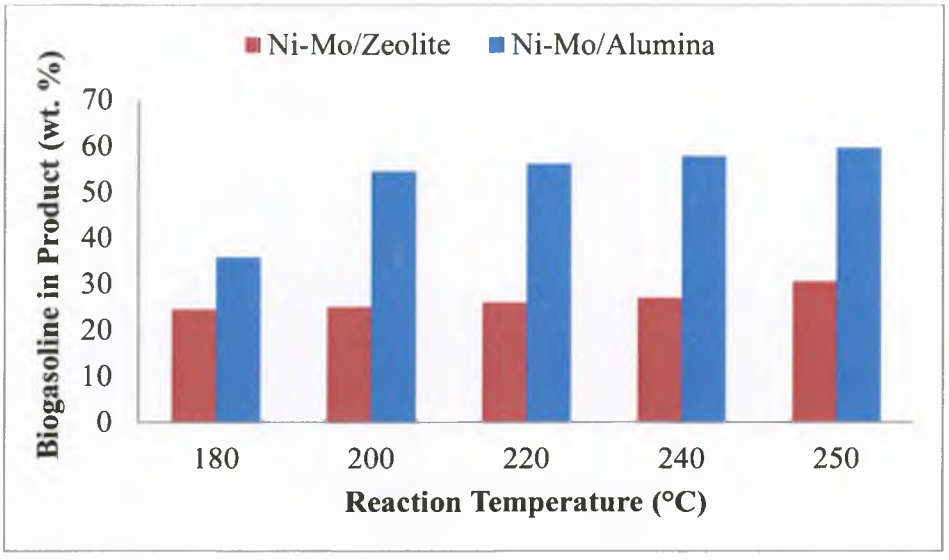


**Figure 27: Comparison of Alumina and Zeolite as catalytic supports for Ni-Mo**

Liu *et al.* (2011) conducted a study to produce bio-hydrogenated diesel (BHD) from jatropha oil, which's results support that the use of zeolite supported Ni-Mo catalysts provides more cracking activity than alumina supported catalysts because the former produced a large number of gasoline hydrocarbons than the latter. The study looked into the effect of different supports for Ni-Mo based catalysts on the cracking of jathropha oil into BHD. From the results of their study, they concluded that Ni-Mo supported on H-Y and H-ZSM-5 zeolites were not suitable for producing the desired product (BHD). The catalysts rather produced a large amount of $C_5$-$C_{10}$ gasoline range hydrocarbons. On the other hand, the use of Ni-Mo/$SiO_2$-$Al_2O_3$ produced a liquid product that had a similar composition to that of normal diesel purchased from a petrol station. This observation was supported by a $NH_3$-TPD characterisation of the catalysts that were employed for the study, which showed that the acidic strength of the catalysts supports was of the order H-ZSM-5> H-Y> $SiO_2$-$Al_2O_3$> $\gamma$- $Al_2O_3$> $SiO_2$ (Liu *et al.*, 2011). It was therefore expected that the zeolite supported catalysts will give a higher yield of the biogasoline range hydrocarbon than the alumina support. In this study, the opposite holds true, as shown in Figure 27.

#### 4.3.2.1.2 Comparison of Co-Mo/$Al_2O_3$ and Ni-Mo/$Al_2O_3$ as Hydrocracking Catalysts

The type of catalyst used in a reaction has much significant effect on the composition and quality of the liquid products as the reaction conditions (Morgan *et al.*, 2012). Co-Mo and Ni-Mo are common petroleum hydro-treating catalysts used in crude oil refineries. In both catalysts, Co-Mo and Ni-Mo promote the hydrogenation while the alumina provides the cracking activity. Before this study, prior experiments were conducted by Mabika (2016) who investigated the selectivity and hydrocracking activity of Co-Mo/$Al_2O_3$ in producing biogasoline from WCO. Figure 27 reveals the results obtained when varying the reaction temperature. The trend observed here shows that like with Ni-Mo/$Al_2O_3$ as a catalyst, selectivity towards the production of biogasoline increases with increasing reaction temperature. Majority of the experiments conducted by Mabika (2016) took place at lower temperatures than those compared to in this study. A common reaction temperature was at 200 °C, which in this instance Ni-Mo performed better than Co-Mo, with biogasoline selectivities of 54.7 wt. % and approximately 43 wt. %, respectively. Nevertheless, the data from both these studies is insufficient for the direct comparison and eventual conclusion regarding which catalyst has the optimum selectivity towards biogasoline.

Veriansyah *et al.* (2012) studied the effects of six different catalysts on the production of renewable diesel by hydro-processing soybean oil. Among the six catalysts studied were Co-Mo/$Al_2O_3$ and Ni-Mo/$Al_2O_3$. At a constant reaction temperature of 400 °C, reaction time of 2 hrs and catalyst/oil ratio of 0.044, the results of this study revealed that Co-Mo/$Al_2O_3$ was more selective towards hydrocarbons of the boiling point range of jet fuel/kerosene and naphtha, than Ni-Mo/$Al_2O_3$. The combined boiling point ranges of jet fuel/kerosene and naphtha are similar to that of gasoline. Co-Mo/$Al_2O_3$ gave a liquid product with a composition of approximately 20 wt. % for both jet fuel/kerosene and naphtha, while with Ni-Mo/$Al_2O_3$ the composition of the liquid product was approximately 6 wt. % and 18 wt. % for naphtha and jet fuel/kerosene, respectively. On the other hand, Ni-Mo/$Al_2O_3$ showed to be more selective towards diesel boiling point range hydrocarbons when compared to Co-Mo/$Al_2O_3$. Reference and comparison to the study by Veriansyah *et al.* (2012) is valid in relation to the current study because the hydrocarbons referred to have a similar carbon number range to that of gasoline i.e. $C_5$-$C_{12}$. Under the described reaction conditions, the conversion of soybean oil was 92.9 wt. % and 78.9 wt. % for Ni-Mo/$Al_2O_3$ and Co-Mo/$Al_2O_3$, respectively (Veriansyah *et al.*, 2012b). These results suggest that with regards to gasoline hydrocarbons selectivity, Ni-Mo/$Al_2O_3$ and Co-Mo/$Al_2O_3$ perform

differently at different temperatures, with the former more active at lower temperatures and the latter at higher temperatures.

#### 4.3.2.2 Effect of Reaction Time

The effect of reaction time on the hydrocracking of WCO over of Ni-Mo/$Al_2O_3$ was studied by experiments with durations of 0.5 hrs, 1 hr, 1.5 hrs, 2 hrs and 2.5 hrs. For this series of experiments, hydrogen pressure (0.5 kPa), catalyst calcination temperature (300 °C), reaction temperature (250 °C), and catalyst: oil ratio (1:75) were kept constant. The catalyst with commercially defined specifications was used for these experiments.

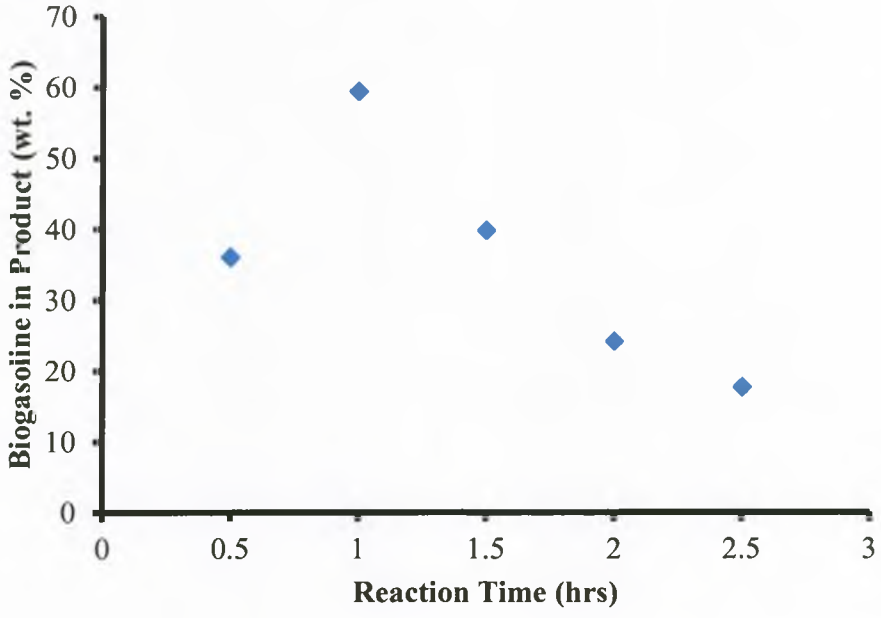


**Figure 28: Effect of reaction time on the hydrocracking of WCO over Ni-Mo/$Al_2O_3$ catalyst for biogasoline production.**

From Figure 28, it can be seen that the reaction time affects the composition of the liquid product. There was a significant increase in the production of biogasoline from 0.5 hrs to 1 hour, after which there was a significant decrease with each time interval. A maximum production of biogasoline of 59.5 wt. % was achieved at a time period of 1 hour, and the minimum production was obtained from the longest reaction time of 2.5 hrs with 17.7 wt. %. The occurrence of this trend can be attributed to the fact that the feedstock composed mainly of unsaturated

triglycerides (oleic and linoleic acids) with single and double C-C bonds which tend to result in a high consumption of hydrogen. In a batch reactor, the initial hydrogen pressure decreases with time due to an increase in the content of lighter hydrocarbons and a high rate of initial cracking activity which consumed the hydrogen. This then implies that the hydrogen/carbon (H/C) molar ratio decreases with longer contact times. The reduced cracking activity and reduced hydrogen pressure are both undesirable because the extended presence of molecules with unsaturated double bonds tend to react further with other molecules, resulting in the production of impurities to bigger molecules through polymerization reactions.

Morgan *et al.* (2012) suggests that the decrease in biogasoline production over longer periods of time comes as a result of unsaturated triglycerides in the feedstock leading to more cracking and coking, which then limits the cracking activity of the catalysts as compared to saturated triglyceride. The occurrence of polymerization reactions is evident from Figure 29, which reveals that while the production of gasoline boiling point range hydrocarbons decreases with longer reaction periods, there was an increase in the production of diesel boiling point range and heavier hydrocarbons.

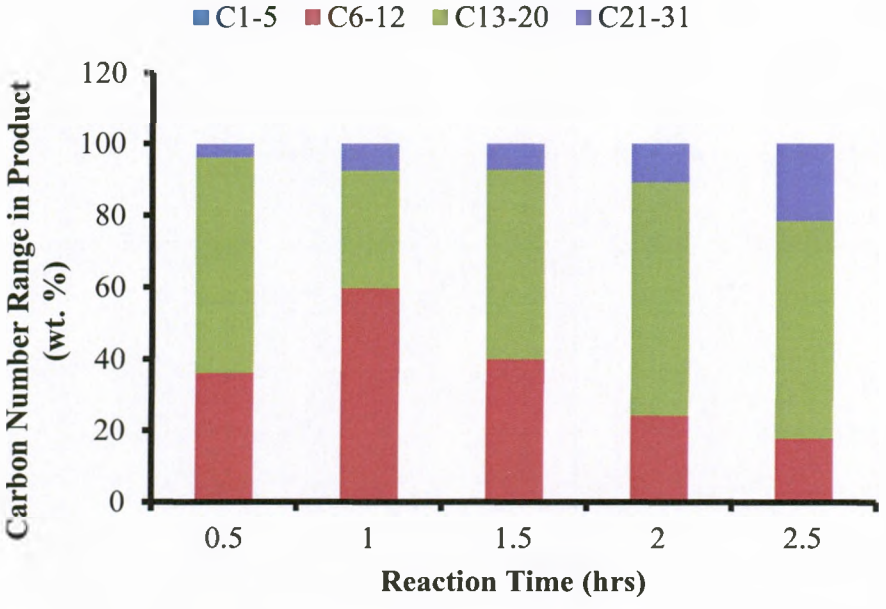


**Figure 29: Effect of reaction time on distribution of hydrocarbon fractions on the basis of carbon number range**

A similar trend was observed by Mabika (2016) when studying the hydrocracking of WCO to produce biogasoline using Co-Mo/$Al_2O_3$ as catalyst. For his series of experiments, Mabika (2016) kept constant hydrogen pressure (0.5 kPa), reaction temperature (210 °C), catalyst calcination temperature (700 °C) and catalyst: oil ratio (1:75). Figure 30 shows that using Co-Mo/$Al_2O_3$, there was a significant increase in the production of biogasoline from a time period of 0.5 hrs to 1 hour, increasing from approximately 40 wt. % to a maximum of 75.7 wt. %. At time periods longer the 1 hour, there was a marginal decrease in the production of biogasoline down to approximately 69 wt. % at 2.5 hrs. At a time period of 2 hrs, the production was revealed to be approximately 32 wt. %, which was considered as an outlier in this regard.

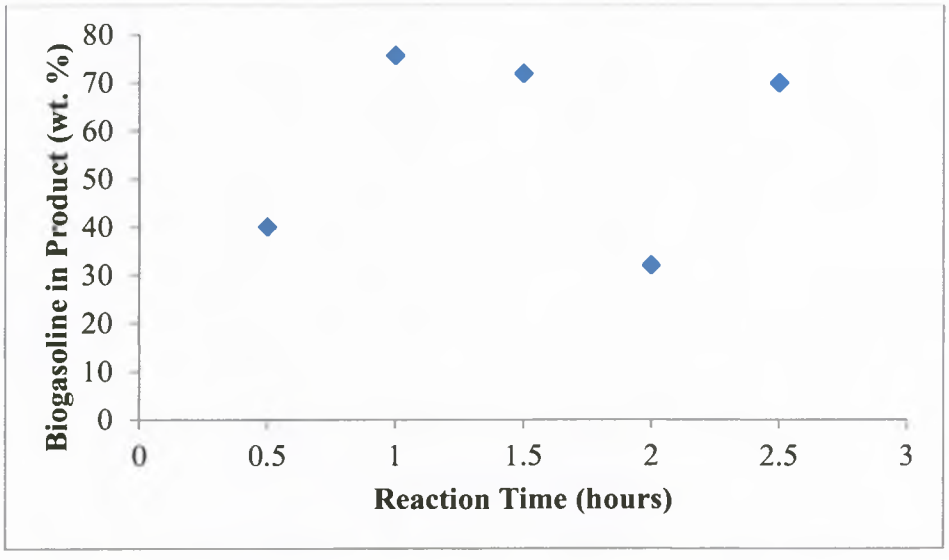


**Figure 30: Effect of reaction time on the hydrocracking of WCO over Co-Mo/$Al_2O_3$ catalyst for biogasoline production.**

#### 4.3.2.3 Effect of Catalyst: Oil ratio

Another parameter investigated for its effect on the production of biogasoline by cracking WCO in the presence of hydrogen in the catalyst: oil weight ratio. Nasikin *et al.*(2009) used a catalyst: oil weight ratio of 1:75 for the successful hydrocracking of palm oil into biogasoline over Ni-Mo/zeolite catalyst (Nasikin *et al.*, 2009). To study the effect of the catalyst: oil ratio, the same ratio was used and modified to ratios less and more than the one suggested by the above mentioned researchers. The catalyst: oil weight ratios investigated were 0:75, 0.5:75. 1:75 and 1.5:75. For this series of experiments, parameters kept constant are hydrogen pressure (0.5 kPa), reaction temperature (250 °C), reaction time (1 hour) and catalyst calcination temperature (300

°C). In Figure 31, the effect of catalyst to oil ratio used has on the catalytic hydrocracking activity and production of biogasoline is shown.

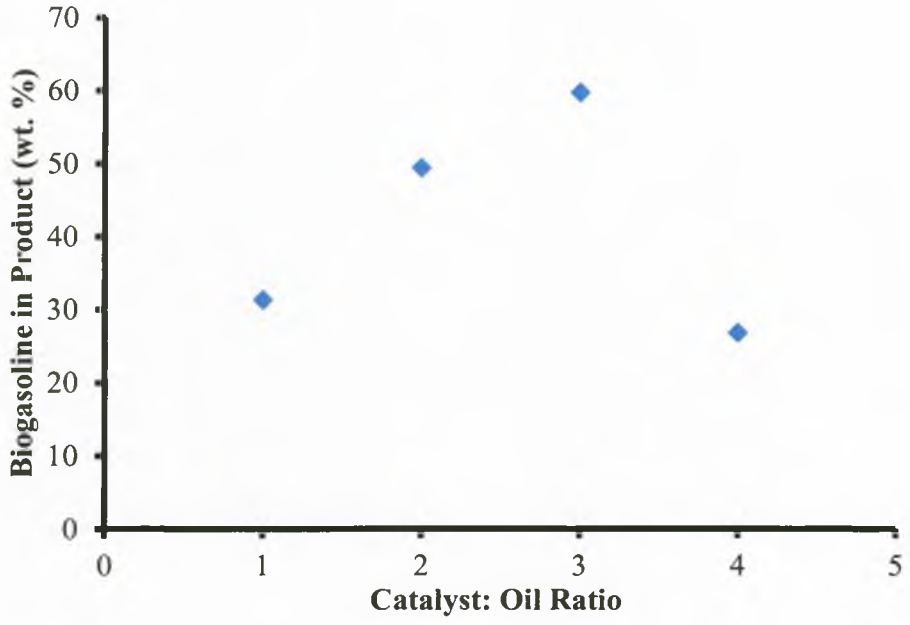


**Figure 31: Effect of catalyst to oil ratio on the hydrocracking of WCO over Ni-Mo/$Al_2O_3$ catalyst for biogasoline production.**

The catalyst to oil weight ratio of 1:75 (3) gave the maximum selectivity towards biogasoline production. It can also be noticed that some hydrocracking activity in the absence of a catalyst at a ratio of 0:75 (1) with a selectivity of 31.4 wt. % towards biogasoline production was achieved. In this instance, the production of the biogasoline was as a result of thermal hydrocracking. This shows that the presence of catalysts in reactions enhances the cracking of the larger molecules. The increase in the amount of catalyst increased the production of biogasoline from 49.5 wt. % at a ratio of 0.5:75 (2) up to a maximum at 1:75 (3), above which a declining production outcome is evident. There was a significant decline in production to 26.9 wt. % at a ratio of 1.5:75 (4). This trend is accounted for by the suggestion that the amount of hydrogen gas available for continued hydrocracking reactions in the batch reactor reduces with a high cracking activity, which comes as a result of the increased catalyst: oil ratio. The results from these series of experiments suggest that the production of biogasoline increases with increasing catalyst: oil weight ratio up to a particular optimum ratio, after which the production decreases. A somewhat contradictory outcome was noticed by Veriansyah *et al.* (2012) when hydro-processing soybean oil into

renewable diesel. When using Ni-Mo/$\gamma$-$Al_2O_3$ at a catalyst/oil weight ratio of 0.044 and 0.088, the conversion of the soybean oil was 92.9 % and 91.9 %, respectively.

In another study by Mabika (2016), a series of parallel experiments to investigate the effect of the same parameter on biogasoline production through thermal cracking and hydrocracking over Co-Mo/$Al_2O_3$ catalyst were conducted at different reaction conditions. In this study, the amount of waste cooking oil was increased with every successive experiment while keeping the amount of catalyst constant. The thermal cracking experiments were conducted at a constant reaction temperature of 450 °C, reaction time of 1.5 hrs and the catalyst was calcinated at a temperature of 700 °C. The results of these experiments reveal that a maximum selectivity of approximately 68 wt. % towards biogasoline was achieved at a ratio of 1:75. In the absence of a catalyst, 65 wt. % selectivity towards biogasoline production was achieved, which is attributed to the high temperature the reactions were subjected to. The succeeding experiment at a catalyst: oil weight ratio of 1:37.5 only marginally reduced the desired outcome to 63 wt. %, and the minimum ratio of 1:150 gave the least production at approximately 62 wt. %.

On the other hand, the hydrocracking experiments were conducted at a constant reaction temperature of 210 °C, hydrogen pressure of 0.5 kPa and reaction time of 1 hr., with a catalyst similar to that used for thermal cracking. For the hydrocracking experiments, Mabika (2016) achieved selectivities of 10 wt. %, 14 wt. %, 75.7 wt. % and 11 wt. % at catalyst: oil ratios of 0, 1:37.5, 1:75 and 1:150, respectively. The significant difference between the ratio of 1:37.5 and 1:75, and the succeeding ratio of 1:150 suggest that the ratio of 1:75 is the most suitable for the optimal hydrocracking in this regard. The overall results of these series of experiments indicate that the catalyst: oil ratio of 1:75 was most suitable when using both Co-Mo and Ni-Mo catalysts supported on alumina.

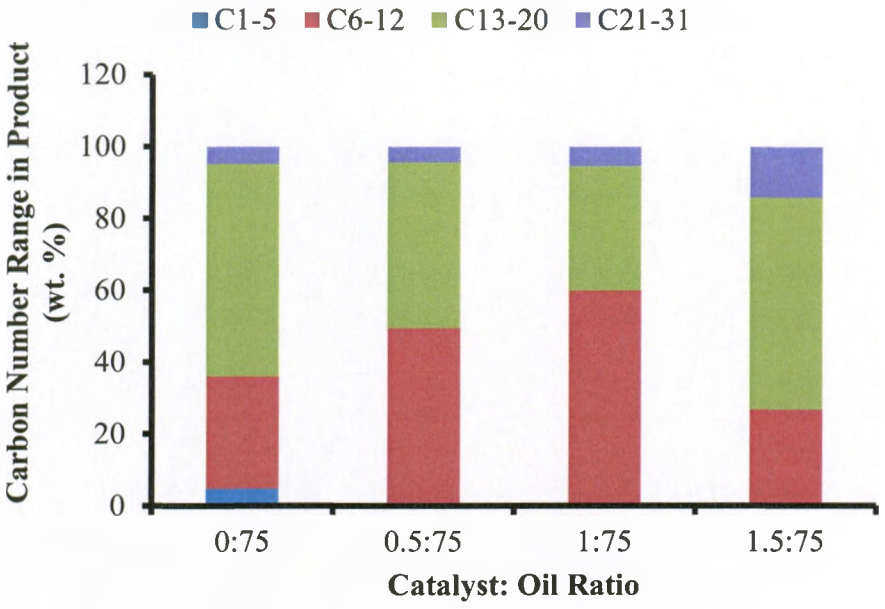


**Figure 32: Effect of catalyst: oil weight ratio on distribution of hydrocarbon fractions on the basis of carbon number range**

Figure 32 above shows the change in distribution of the hydrocarbon classes in the products with the change in catalyst: oil ratio. The liquid products resulting from the ratio of 1:75 showed to have the highest content of gasoline boiling range hydrocarbons. The presence of $C_{1\text{-}5}$ carbon range hydrocarbons in the liquid product from a catalyst: oil ratio suggests that at the low ratios there was an occurrence of severe cracking momentarily.

#### 4.3.2.4 Effect of Catalyst Calcination Temperature

The calcination of catalysts is one of the vital pre-treatment processes that play a significant role in enhancing the catalytic activity, and thus the performance of the catalyst (Al-Fatesh & Fakeeha, 2012). The effect that the calcination temperature of the catalyst has towards the production of biogasoline was investigated. A series of five experiments were performed at a constant reaction temperature (240 °C), reaction time (1 hour), initial hydrogen pressure (0.5 kPa) and catalyst: oil ratio (1:75). The catalysts were calcinated at temperatures of 300 °C, 400 °C, 500 °C, 600 °C and 700 °C.

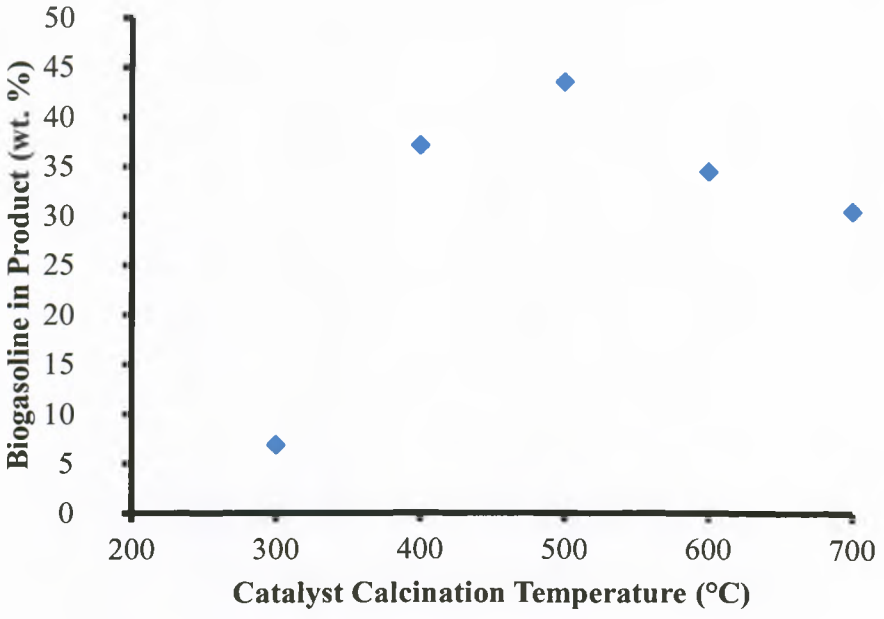


**Figure 33: Effect of catalyst calcination temperature on the hydrocracking of WCO over Ni-Mo/$Al_2O_3$ catalyst for biogasoline production.**

The observation from Figure 33 was that there was an increase in the production of biogasoline with increasing calcination temperature between 300 °C and 500 °C, after which there was a decrease down to 700 °C. This can be attributed to a number of factors, one of which is the phase change that takes place with increasing calcination temperature. At moderately low calcination temperatures, the alumina catalyst support exists in the gamma phase as $\gamma$-$Al_2O_3$. As the calcination temperature increases, the phases transition to the betta and alpha phases as $\beta$-$Al_2O_3$ and $\alpha$-$Al_2O_3$, respectively. Another key factor contributing to the change in biogasoline production is the change in the acidity and surface area of the catalysts with changing calcination temperature from 300 °C to 500 °C. The alumina is highly acidic as a result of acidic pre-treatment and has a high surface area at relatively low temperatures (Bartholomew & Farrauto, 2011). The increase in the production of biogasoline with catalysts calcinated at 300 °C to 500 °C suggests that the acidity of the alumina remained high within this calcination temperature range and therefore played a more significant role that the catalysts surface area for this observed outcome in this regard. Bartholomew and Farrauto (2011) suggested that at 500 °C alumina is in the form $\gamma$-$Al_2O_3$, at which it is most acidic but least stable.

On the other hand, Figure 11 showed that the BET surface area decreases with increasing calcination temperature. The surface area is 61.61 $m^2/g$ at 300 °C and decreased to 40.79 $m^2/g$ at 700 °C. This is due to the agglomeration of the catalyst particles. At temperatures above 500 °C up to 700 °C, the reduction in biogasoline production is attributed to a loss in acidity of the catalyst as a result of a loss in hydroxyl (-OH) groups (Bartholomew & Farrauto, 2011). The reduced catalyst surface area means that there was a limited area enabling the chemical reactions to take place. Al-Fatesh and Fakeeha (2012) pointed out that the resistance of a catalyst to carbon/coke deposition decreases with increasing calcination temperature. The increased carbon deposition results in catalyst deactivation and destruction (Al-Fatesh & Fakeeha, 2012).

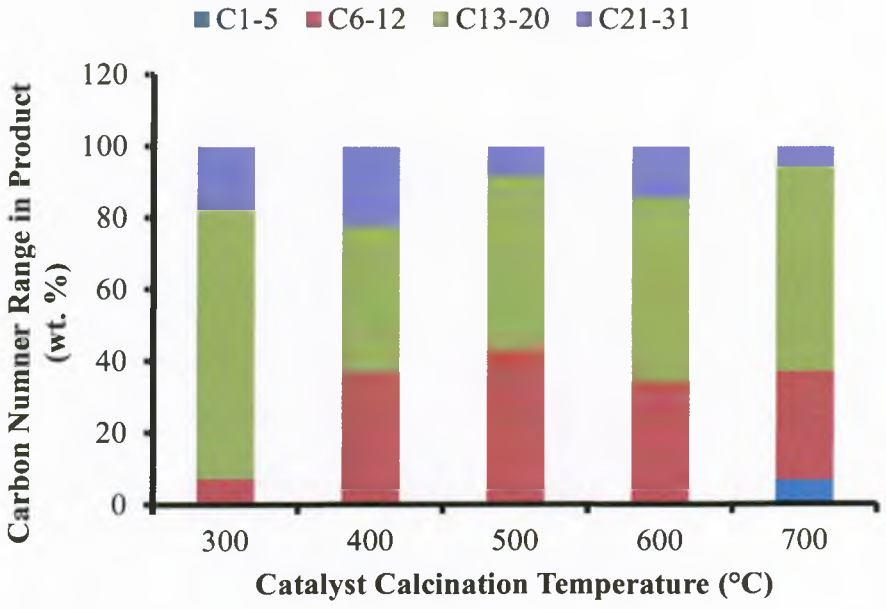


**Figure 34: Effect of catalyst calcination temperature on distribution of hydrocarbon fractions on the basis of carbon number range**

Figure 34 compares the change in composition and the distribution of the hydrocarbon classes on the basis of carbon number range in the liquid oil product, relative to biogasoline with increasing temperature. The production of diesel boiling point-range hydrocarbons was favoured more at the lowest calcination temperature of 300 °C with 75 wt. % selectivity. A significant decrease towards 41 wt. % selectivity was noticed as the calcination temperature increased to 400 °C, above which the selectivities varied slightly within an average difference of 4 wt. % between successive calcination temperatures up to 700 °C. On the other hand, a somewhat inconsistent

trend was noticed for the heavier hydrocarbon class of $C_{21-31}$. As seen from Figure 34, the production of heavier hydrocarbons fluctuates with increasing calcination temperature. The reduced acidity has evidently favoured the production of diesel boiling-point range and heavier hydrocarbons.

An interesting observation from Figure 34 is the occurrence of the $C_{1-5}$ hydrocarbon class at the calcination temperature of 700 °C. The alpha phase in which the alumina exists at this elevated temperature is what this observation is attributed to. At this phase and calcination temperature, though with the least surface area and least acidity, the catalysts is at its most stable state (Al-Fatesh & Fakeeha, 2012). The extensive agglomeration means that the catalyst is momentarily highly active, and therefore intensively cracks the liquid fuel molecules into the $C_{1-5}$ hydrocarbon molecules range.

#### 4.3.2.5 Effect of Ni-loading (wt. %) in the catalyst

The effect that the Ni-loading (wt. %) in the loaded metals has on the catalytic activity and selectivity towards the hydrocracking reactions was investigated. A series of experiments were performed and the Ni-loading (wt. %) was varied and sequentially performed as 5, 10, 15, 20 and 25 wt. %. The reaction parameters that were kept constant are the catalyst to oil weight ratio (1:75), hydrogen initial pressure (0.5 kPa), reaction temperature (250 °C), reaction time (1 hour) and catalyst calcination temperature (300 °C). The content of the catalyst support (alumina wt. %) was also kept fixed, while the Mo wt. % varied with the changing Ni-loading wt. %.

Figure 35 reveals that there was an increase in biogasoline production with increasing Ni-loading from 5 wt. % to a maximum at 15 wt. %, which gave biogasoline production outcomes of 37.7 wt. % to 46 wt. %, respectively. At Ni-loadings above 15 wt. %, there was a drastic decrease in the production of biogasoline to a minimum of 6.9 wt. % at a Ni-loading of 25 wt. %. Ni-based catalysts have proven to exhibit high activities and selectivity towards hydrogenation reactions (Chen *et al.*, 2005). Therefore, the optimum nickel loading to produce the maximum light hydrocarbon was determined, as the activity of nickel – alumina catalyst depends strongly on the interaction between catalyst and support. The higher biogasoline productions at lower Ni-loadings indicate that the chemical reactions were controlled by the reactions themselves.

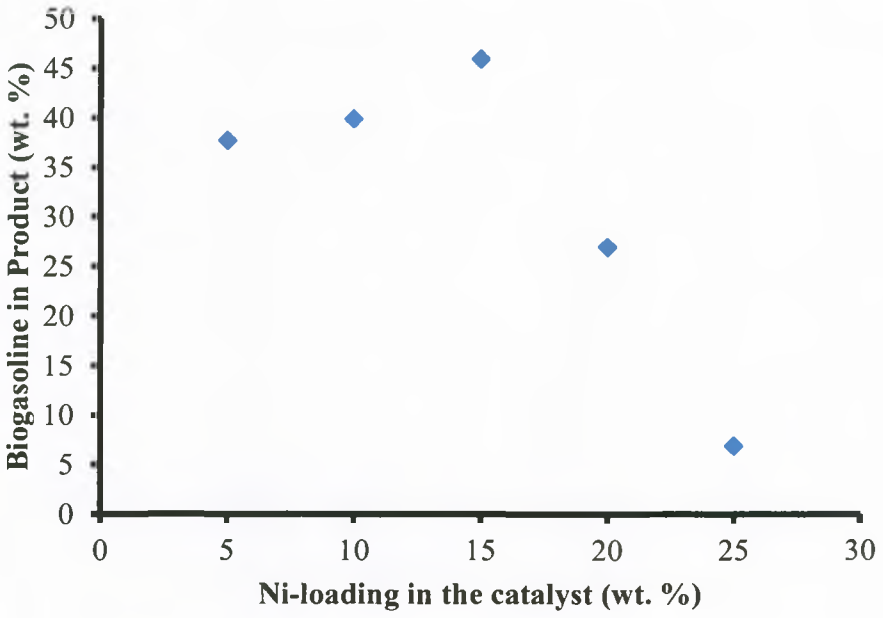


**Figure 35: Effect of Ni-loading (wt. %) in the catalyst on the hydrocracking of WCO over Ni-Mo/$Al_2O_3$ catalyst for biogasoline production.**

At Ni-loadings above 15 wt. %, a decrease in biogasoline production was observed from the maximum to a minimum production at a loading of 25 wt. %. This trend is as a result of a reduced catalyst activity due to a decline in catalysts surface area. It is also probable that this phenomenon is due to the fact that at increased Ni-loadings, the NiO grains inside the catalysts tend to aggregate, forming Ni crystals. The crystals are a result of the catalyst drying process, during which the solution retained within the pores migrates via diffusion. The solvent then evaporates and the solute precipitates, eventually becoming supersaturated and then crystallizing (Al-Fatesh & Fakeeha, 2012). The bigger size of the Ni aggravates the coking of the catalyst, thus rendering it less active. This suggests that there was catalyst deactivation from increased carbon deposition. A study performed by Chen *et al.*(2005) found that at lower Ni-loadings e.g.1 wt. %, catalysts resisted coking much better than at higher Ni-loadings e.g. 10 wt. % (Chen *et al.*, 2005).

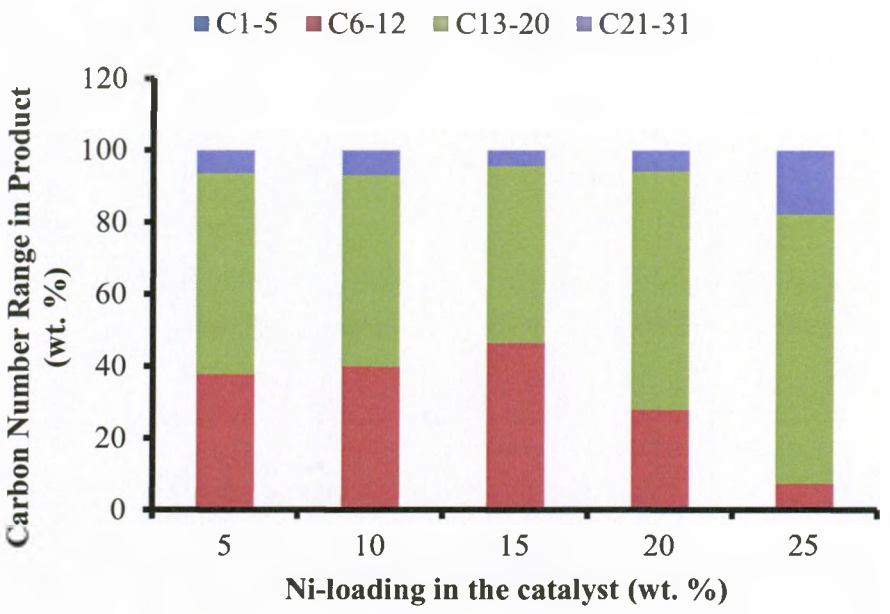


**Figure 36: Effect of Ni-loading in catalyst on distribution of hydrocarbon fractions on the basis of carbon number range**

Figure 36 compares the change in distribution and selectivity towards the various classes of hydrocarbon molecules with increasing Ni-loading relative to the production of biogasoline. It can be seen that as a result of the deactivation of the catalyst, there is an increase in the production of the diesel i.e. $C_{13\text{-}20}$ and heavy hydrocarbon ranges with increasing Ni-loading. Interestingly, the presence of the lightest hydrocarbon range of $C_{1\text{-}5}$ at less than 1 wt. % is evident, which suggests that severe cracking took place at the high Ni-loadings from 15 wt. % to 25 wt. %. This observation can be attributed to the decrease in the catalyst surface area, which contributes to the decrease in the activity of the catalyst. It is also probable that the catalyst's activity is higher when its active sites are concentrated towards the centre of the support rather than when uniformly dispersed. It might be the case that because the active sites were not evenly distributed on the entire support, then the deactivation on the catalyst occurred progressively as some sites were more active than others.

# CHAPTER FIVE: CONCLUSIONS AND RECOMMENDATIONS

## 5.1 Conclusions

Biogasoline was produced through catalytic hydrocracking of WCO over Ni-Mo/$Al_2O_3$ catalysts in the presence of hydrogen gas at a pressure of 0.5 kPa. The study for the production of biogasoline from waste cooking oil as an alternative liquid fuel has proven to be feasible. The catalysts used in this study were synthesized through successive impregnation, loading Ni followed by Mo salts over alumina. In a series of five synthesized catalysts with varying Ni-loadings (wt. %) within a range of 5-25 wt. %, the catalyst with the least Ni performed the best. Catalyst A, with a Ni-loading of 5 wt. %, showed the highest thermal stability and BET surface area of 61.61 $m^2/g$. SEM micrographs of the catalysts showed that the 5 wt. % catalyst had a high dispersion of the active metals, resulting in a high surface area of the catalyst. When the Ni concentration was increased, the SEM micrographs proved that there was agglomeration of the catalyst particles, resulting in a reduction of the catalyst surface area. FT-IR and Raman spectra also confirmed the higher dispersion of the active phase of the catalysts with the lower Ni concentrations than those with a higher concentration. Commercial Ni-Mo/$Al_2O_3$ catalysts are composed of 2.4 wt. % Ni and 9.3 wt. % Mo (Kougionas *et al.*, 1995).

By calcining the 5 wt. % Ni-loading catalyst at a temperature range of 300 °C-700 °C with intervals of 100 °C, the effect of calcination temperature of the catalyst activity was investigated. The results showed that there increased agglomeration of the catalyst particles with increased calcination temperature. There was a decrease in the BET surface area of the catalyst with increased calcination temperature, but the surface area decrease rate reduced at calcination temperatures between 500 °C and 600 °C. Literature confirmed that the optimum calcination temperature for Ni-Mo/$Al_2O_3$ is 500 °C (Kamyab, 2016).

The effects different operation parameters have on the production of biogasoline were also investigated. There was an increase in the production of biogasoline with increased reaction temperature, while keeping the other parameters constant. An optimum production of biogasoline was 59.5 wt. % at a reaction temperature of 250 °C, reaction time of 1 hr, catalyst: oil ratio of 1:75 with the 5 wt. % Ni-loading catalyst calcinated at 300 °C. When the reaction

time was investigated, a maximum production was achieved at 1hr after increasing from 0.5 hrs. After the 1 hr mark, the production dropped significantly. Literature used a catalyst: oil ratio of 1:75, which proved to give the maximum production in this study (Nasikin *et al.*, 2009). When studying the sole effect of catalyst calcination temperature, 500 °C gave the optimum production of biogasoline at 43.5 wt. %. This result is in consistent with literature (Kamyab, 2016). The Ni-loading (wt. %) also had a significant effect on the production of biogasoline. An increase in production from 5-15 wt. % was observed. At concentrations above 15 wt. %, the production decreased significantly. This confirms that for optimum production of biogasoline from waste cooking oil, low concentrations of Ni are ideal. In conclusion, the production of biogasoline from catalytic hydrocracking of WCO using a Ni-Mo/$Al_2O_3$ bifunctional catalyst was successful.

## 5.2 Recommendations for Future Work

Waste cooking oil, like petroleum crude oil is a complex mixture of different molecules combined together. It has been discovered that there is a number of ways that the Ni-Mo/$Al_2O_3$ catalyst can be modified in order to enhance its catalytic activity and increase its conversion, selectivity and yield of the desired product. The catalyst can be modified by the addition of boron, chlorine and fluorine ions to increase the acidity of the catalyst. The use of boron as a promoter is more common and favourable as it increases the resistance of the catalyst to coking, and thus deactivation (Al-Fatesh & Fakeeha, 2012; Chen *et al.*, 2005)

Studies have shown that reaction temperature and pressure play key roles in the conversion of triglycerides into hydrocarbons (Sotelo-Boyas *et al.* , 2010; Sankaranarayanan *et al.*, 2011). Therefore in order to achieve a liquid product with a high content of biogasoline boiling range hydrocarbons, the use of stainless steel reactors must be used as they can handle higher temperatures and hydrogen pressure. The results of this study gave almost equal compositions of diesel and gasoline boiling range hydrocarbons with the use of Ni-Mo/$Al_2O_3$ catalyst. Several literature studies revealed that Ni-Mo/$Al_2O_3$ catalysts are more favourable towards a higher selectivity towards diesel boiling range hydrocarbons in comparison to Co-Mo/$Al_2O_3$. In terms of catalyst supports, zeolites are more acidic and catalytically active than $Al_2O_3$. Therefore the use of Co-Mo/Zeolite catalysts will be better suited and highly favourable for selectivity towards gasoline range hydrocarbons, which correspond to biogasoline.

It was found out the method of catalyst preparation has an impact on the catalytic activity of the catalyst. Other methods of catalyst preparations such as co-precipitation can be studied and analyzed against the impregnation catalyst preparation. Under the impregnation method, different types of metal loading sequences must be explored to study the effect of loading Ni or Mo first and simultaneous loading. The effect the concentrations of Mo and $Al_2O_3$ have on the catalytic activity of the catalyst is a worthwhile investigation.

To confirm the composition and conversions of the waste cooking oil, the gas phase from reactions must be collected and take for analysis as well. This will give a more accurate interpretation of the catalytic activity and the severity of the hydrocracking catalysts.

## REFERENCES


Aakko-Saksa, P., Koponen, P., Kihlman, J., Reinikainen, M., Skyttä, E., Rantanen-Kolehmainen, L., & Engman, A. (2011). Biogasoline options for conventional spark-ignition cars. *VTT Technical Research Centre of Finland, Finland.*

Al-Fatesh, A. S. A., & Fakeeha, A. H. (2012). Effects of calcination and activation temperature on dry reforming catalysts. *Journal of Saudi Chemical Society*, *16*(1), 55–61.

Badoga, S. (2015). Synthesis and Characterisation of Ni-Mo Supported Mesoporous Materials with EDTA and Phosphorus for Hydrotreating of Heavy Gas Oil. *University of Sakatchewan.*

Bartholomew, C. H., & Farrauto, R. J. (2011). *Fundamentals of Industrial Catalytic Processes.* John Wiley & Sons.

Balat, M., Balat, H., & Öz, C. (2008). Progress in bioethanol processing. *Progress in Energy and Combustion Science*, *34*(5), 551–573.

Bezergianni, S., & Kalogianni, A. (2009). Hydrocracking of used cooking oil for biofuels production. *Bioresource Technology*, *100*(17), 3927–3932.

Blodel, D., Meyer-Ohlendorf, N., Schlosser-Allera, C., & Steel, P. (2006). United Nations Framework Convention on Climate Change: Handbook. In United Nations Framework Convention on Climate Change: handbook (pp. 220-220).

BusinessTech (2016 a). Petrol vs diesel prices in South Africa: 2006 – 2016. Business Tech SA

BusinessTech (2016 b). How far the rand has fallen: from 2000 to 2016. Business Tech SA

Cardona, C. A., & Sánchez, Ó. J. (2007). Fuel ethanol production: Process design trends and integration opportunities. *Bioresource Technology*, *98*(12), 2415–2457.

Chai, M., Tu, Q., Lu, M., & Yang, Y. J. (2014). Esterification pretreatment of free fatty acid in biodiesel production, from laboratory to industry. *Fuel Processing Technology*, *125*, 106–113.

Chen, L., Lu, Y., Hong, Q., Lin, J., & Dautzenberg, F. (2005). Catalytic partial oxidation of methane to syngas over Ca-decorated-$Al_2O_3$-supported Ni and Ni-B catalysts. *Applied Catalysis A: General*, *292*, 295–304.

Chhetri, A. B., Watts, K. C., & Islam, M. R. (2008). Waste cooking oil as an alternate feedstock for biodiesel production. *Energies*, *1*(1), 3–18.

Doronin, V. P., Potapenko, O. V., Lipin, P. V., Sorokina, T. P., & Buluchevskaya, L. A. (2012). Catalytic cracking of vegetable oils for production of high-octane gasoline and petrochemical feedstock. *Petroleum Chemistry*, *52*(6), 392–400.

Escobar, J., Barrera, M. C., Gutiérrez, A. W., & Terrazas, J. E. (2017). Benzothiophene hydrodesulfurization over NiMo/alumina catalysts modified by citric acid. Effect of addition stage of organic modifier. *Fuel Processing Technology*, *156*, 33–42.

Ferdous, D., Dalai, A. K., & Adjaye, J. (2004). A series of Ni-Mo/$Al_2O_3$ catalysts containing boron and phosphorus: Part I. Synthesis and characterisation. *Applied Catalysis A: General*, *260*(2), 137–151.

Fogler, H. S. (2006). *Elements of chemical reaction engineering* (4th ed., 3.printing). Upper Saddle River, NJ: Pearson Education International/Prentice Hall PTR.

Fu, B., Gao, L., Niu, L., Wei, R., & Xiao, G. (2008). Biodiesel from waste cooking oil via heterogeneous superacid catalyst $SO_{42}$−/$ZrO_2$. *Energy & Fuels*, *23*(1), 569–572.

Gupta, R. B., & Demirbas, A. (2010). *Gasoline, diesel, and ethanol biofuels from grasses and plants*. New York: Cambridge University Press.

Hancsók, J., Kasza, T., Kovács, S., Solymosi, P., & Holló, A. (2012). Production of bioparaffins by the catalytic hydrogenation of natural triglycerides. *Journal of Cleaner Production*, *34*, 76–81.

Kaluža, L., Palcheva, R., Spojakina, A., Jirátová, K., & Tyuliev, G. (2012). Hydrodesulfurization NiMo catalysts supported on Co, Ni and B modified $Al_2O_3$ from Anderson heteropolymolybdates. *Procedia Engineering*, *42*, 873–884.

Kamyab, A. (2016). *Preparation and evaluation of sulfided Ni-Mo/γ-$Al_2O_3$ hydrotreating catalysts*.

Kasztelan, S., Payen, E., Toulhoat, H., Grimblot, J., & Bonnelle, J. P. (1986). Industrial $MoO_3$-promoter oxide-γ-$Al_2O_3$ hydrotreating catalysts: genesis and architecture description. *Polyhedron*, *5*(1–2), 157–167.

Khalisanni, K., Khalizani, K., Rohani, M. S., & Khalid, P. O. (2008). Analysis of waste cooking oil as raw material for biofuel production.

Kim, S., & Dale, B. E. (2004). Global potential bioethanol production from wasted crops and crop residues. *Biomass and Bioenergy*, *26*(4), 361–375.

Kougionas, V., Cattenot, M., Zotin, J., Portefaix, J., & Breysse, M. (1995). Enhancement of the catalytic properties of Ni-Mo and Co-Mo alumina-supported sulfide catalysts by addition of ruthenium sulfide dispersed in Y zeolites. *Applied Catalysis A: General*, *124*(1), 153–164.

Kulkarni, M. G., & Dalai, A. K. (2006). Waste cooking oil an economical source for biodiesel: a review. *Industrial & Engineering Chemistry Research*, *45*(9), 2901–2913.

Laurent, E., & Delmon, B. (1994). Study of the hydrodeoxygenation of carbonyl, carboxylic and guaiacyl groups over sulfided Co-Mo/γ-$Al_2O_3$ and Ni-Mo/γ-$Al_2O_3$ catalysts: I. Catalytic

reaction schemes. *Applied Catalysis A: General*, *109*(1), 77–96.

Liu, Y., Sotelo-Boyás, R., Murata, K., Minowa, T., & Sakanishi, K. (2011). Hydrotreatment of vegetable oils to produce bio-hydrogenated diesel and liquefied petroleum gas fuel over catalysts containing sulfided Ni–Mo and solid acids. *Energy & Fuels*, *25*(10), 4675–4685.

Mabika, K. (2016). Biogasoline Production from Waste Cooking Oil using Nano-Cobalt Molybdenum Catalyst. University of the Witwatersrand, Johannesburg, South Africa

MacDonald, R. R., Salazar, A., Sutherland, D. A., Verma, A., & Short, M. P. (2012). Production of biodiesel and biogasoline via coupling a LBE-cooled reactor to hydrogen and biofuels plants (Vol. 107, pp. 117–120). Presented at the Transactions of the American Nuclear Society.

Maubane, M. S. (2011). *Synthesis, doping and functionalization of carbon nanotubes* (Doctoral dissertation). University of the Witwatersrand, Johannesburg, South Africa.

Mohd Addli, S. (2009). Concentration of biopetrol synthesized from palmitic acid through catalytic cracking using zeolite as catalyst.

Morgan, T., Santillan-Jimenez, E., Harman-Ware, A. E., Ji, Y., Grubb, D., & Crocker, M. (2012). Catalytic deoxygenation of triglycerides to hydrocarbons over supported nickel catalysts. *Chemical Engineering Journal*, *189*, 346–355.

Nasikin, M., Susanto, B. H., Hirsaman, M. A., & Wijanarko, A. (2009). Biogasoline from palm oil by simultaneous cracking and hydrogenation reaction over nimo/zeolite catalyst. *World Applied Sciences Journal*, *5*, 74–79.

Olivier, J. G., Janssens-Maenhout, G., & Peters, J. A. (2012). *Trends in global $CO_2$ emissions: 2012 Report*. PBL Netherlands Environmental Assessment Agency Hague.

Owolabi, R., Adejumo, A., & Aderibigbe, A. (2012). Biodiesel: Fuel for the Future (A Brief Review). *International Journal of Energy Engineering*, *2*(5), 223–231.

Pandey, A. (Ed.). (2011). *Biofuels: alternative feedstocks and conversion processes* (1st ed). Kidlington, Oxford□; Burlington, MA: Academic Press.

Phan, A. N., & Phan, T. M. (2008). Biodiesel production from waste cooking oils. *Fuel*, *87*(17), 3490–3496.

Priecel, P., Kubička, D., Čapek, L., Bastl, Z., & Ryšánek, P. (2011). The role of Ni species in the deoxygenation of rapeseed oil over NiMo-alumina catalysts. *Applied Catalysis A: General*, *397*(1), 127–137.

Sankaranarayanan, T., Banu, M., Pandurangan, A., & Sivasanker, S. (2011). Hydroprocessing of sunflower oil–gas oil blends over sulfided Ni–Mo–Al–zeolite beta composites. *Bioresource Technology*, *102*(22), 10717–10723.

Samolada, M.C., Baldauf, W., & Vasalos, I. A. (1998). Porudction of a bio-gasoline by upgrading biomass flash pyrolysis liquids via hydrogen processing and catalysts cracking. Fuel, 77(14), 1667-1675.

Šimáček, P., Kubička, D., Šebor, G., & Pospíšil, M. (2010). Fuel properties of hydroprocessed rapeseed oil. *Fuel*, *89*(3), 611–615.

Sotelo-Boyás, R., de Jesús Hernández-Loyo, F., & Trejo-Zárraga, F. (2012). *Hydroconversion of triglycerides into green liquid fuels*. INTECH Open Access Publisher.

Sotelo-Boyas, R., Liu, Y., & Minowa, T. (2010). Renewable diesel production from the hydrotreating of rapeseed oil with Pt/Zeolite and Ni-Mo/$Al_2O_3$ catalysts. *Industrial & Engineering Chemistry Research*, *50*(5), 2791–2799.

Susanto, B. H. (2014). Preparation and Characterisation Ni-Mo/Zeolite Catalyst using

Microwave Polyol Process Method for Synthesizing Renewable Diesel from Jathropa Oil. In *Sriwijaya International Seminar on Energy-Environmental Science and Technology* (Vol. 1, pp. 1–7).

Taufiqurrahmi, N., & Bhatia, S. (2011). Catalytic cracking of edible and non-edible oils for the production of biofuels. *Energy & Environmental Science*, *4*(4), 1087–1112.

Total, 2014. Engineers Technical Handbook. Total. Red Bird Media cc. ISBN: 0-620-37121-8IS

Tsuchida, T., Yoshioka, T., Sakuma, S., Takeguchi, T., & Ueda, W. (2008). Synthesis of biogasoline from ethanol over hydroxyapatite catalyst. *Industrial & Engineering Chemistry Research*, *47*(5), 1443–1452.

Veriansyah, B., Han, J. Y., Kim, S. K., Hong, S.-A., Kim, Y. J., Lim, J. S., … Kim, J. (2012). Production of renewable diesel by hydroprocessing of soybean oil: effect of catalysts. *Fuel*, *94*, 578–585.

Wang, S., Cai, Q., Wang, X., Zhang, L., Wang, Y., & Luo, Z. (2013). Biogasoline production from the co-cracking of the distilled fraction of bio-oil and ethanol. *Energy & Fuels*, *28*(1), 115–122.

Yin, C., Zhao, L., Bai, Z., Liu, H., Liu, Y., & Liu, C. (2013). A novel porous ammonium nickel molybdate as the catalyst precursor towards deep hydrodesulfurization of gas oil. *Fuel*, *107*, 873–878.

Zepeda, T. A., Pawelec, B., Fierro, J. L. G., Olivas, A., Fuentes, S., & Halachev, T. (2008). Effect of Al and Ti content in HMS material on the catalytic activity of NiMo and CoMo hydrotreating catalysts in the HDS of DBT. *Microporous and Mesoporous Materials*, *111*(1), 157–170.

# APPENDIX

## A.1 Raw Data from ICP-OES Characterisation

**Table 6: Raw data from ICP-OES Characterisation for Catalyst Samples**

| Catalyst Identification | $Al_2O_3$ (mg/g) | Ni (mg/g) | Mo (mg/g) | Ni-loading (wt %) |
|---|---|---|---|---|
| **Commercially specified** | 26.23014 | 0.901393 | 16.15653 | 2.082313085 |
| **Catalyst A** | 55.58684 | 8.507807 | 123.9665 | 4.823957838 |
| **Catalyst B** | 42.398 | 14.92008 | 107.8879 | 9.031198507 |
| **Catalyst C** | 36.934 | 32.01109 | 152.9969 | 14.42317878 |
| **Catalyst D** | 36.60087 | 25.98941 | 70.34009 | 19.55114546 |
| **Catalyst E** | 48.25697 | 58.71514 | 131.9721 | 24.57274022 |

Table 6 represents the raw data as obtained from the ICP-OES characterisation. To calculate the Ni-loading (wt %), equation A.1 was used.

$$Ni - loading\ (wt\%) = \frac{Ni}{Al2O3+Ni+Mo} \times 100 \qquad (A.1)$$

## A.2 Calculation formula for Biogasoline Selling Price

To estimate the selling price of biogasoline, formula A.2 was used

$$\frac{Selling\ Price\ of\ Unleaded\ 95\ in\ 2016}{Selling\ Price\ of\ diesel\ 0.05\%\ in\ 2016} = \frac{Selling\ Price\ of\ biogasoline\ in\ 2016}{Selling\ Price\ if\ biodiesel\ in\ 2016} \qquad (A.2)$$

## A.3 GC-MS Raw Data

Table 7 below shows the raw data from the GC-MS characterisation from one of the liquid products.

**Table 7: GC-MS Raw Data showing the range of components available in the liquid products**

| Name | Formula |
|---|---|
| 2-Heptenal, (Z)- | C7H12O |
| trisiloxane, 1,1,1,5,5,5-hexamethyl-3-[(trimethylsilyl)oxy]- | C9H28O3Si4 |
| Ethanol, 2-(2-ethoxyethoxy)- | C6H14O3 |
| Propane, 1,2-dimethoxy- | C5H12O2 |
| Undecane, 2-methyl- | C12H26 |
| Decane | C10H22 |
| Decane | C10H22 |
| 2-Octenal, (E)- | C8H14O |
| n-Tridecan-1-ol | C13H28O |
| 1-Decene, 3,3,4-trimethyl- | C13H26 |
| Undecane, 5,7-dimethyl- | C13H28 |
| Hexane, 2,3,4-trimethyl- | C9H20 |
| Oxalic acid, hexyl neopentyl ester | C13H24O4 |
| Nonanal | C9H18O |
| Octane, 2,3,6,7-tetramethyl- | C12H26 |
| 2-[(Trimethylsilyl)oxy]-2-{4-[(trimethylsilyl)oxy]phenyl}ethanamine | C14H27NO2Si2 |
| Cyclopentane, 1,3-dichloro-, trans- | C5H8Cl2 |
| 2-Nonenal, (E)- | C9H16O |
| 2-Undecanethiol, 2-methyl- | C12H26S |
| Phenylethanolamine | C8H11NO |
| Benzoic acid, ethyl ester | C9H10O2 |
| 2,4-Nonadienal, (E,E)- | C9H14O |
| Nonadecane | C19H40 |
| Bicyclo[3.1.1]heptan-3-ol, 6,6-dimethyl-2-methylene-, [1S-(1à,3à,5à)]- | C10H16O |
| Hexadecane | C16H34 |
| 3-Phenyl-3-pentanol | C11H16O |
| 1,3-Dioxolane, 2-propyl- | C6H12O2 |
| Oxanilic acid, O,O'-bis(trimethylsilyl) | C14H23NO3Si2 |
| Cyclohexasiloxane, dodecamethyl- | C12H36O6Si6 |
| Aminocaproic acid | C6H13NO2 |
| Pentadecane | C15H32 |
| Hexadecane | C16H34 |
| n-Tridecan-1-ol | C13H28O |

| | |
|---|---|
| 2,4-Decadienal, (E,E)- | C10H16O |
| n-Tridecan-1-ol | C13H28O |
| Heptacosane | C27H56 |
| Hexadecane | C16H34 |
| Fumaric acid, pentyl 2,3,5,6-tetrachlorophenyl ester | C15H14Cl4O4 |
| 2,4-Decadienal, (E,E)- | C10H16O |
| Pentadecane | C15H32 |
| Pentadecane | C15H32 |
| Heptadecane, 2,6,10,14-tetramethyl- | C21H44 |
| Benzeneacetaldehyde, à,2,5-trimethyl- | C11H14O |
| Pentadecane | C15H32 |
| Trisiloxane, 1,1,1,5,5,5-hexamethyl-3,3-bis[(trimethylsilyl)oxy]- | C12H36O4Si5 |
| Trisiloxane, 1,1,1,5,5,5-hexamethyl-3,3-bis[(trimethylsilyl)oxy]- | C12H36O4Si5 |
| Trisiloxane, 1,1,1,5,5,5-hexamethyl-3,3-bis[(trimethylsilyl)oxy]- | C12H36O4Si5 |
| 4,5-Nonadiene | C9H16 |
| Cyclooctane, ethenyl- | C10H18 |
| Pentalene, 1,2,4,5,6,6a-hexahydro-2-methylene- | C9H12 |
| 5-Decen-1-ol, (Z)- | C10H20O |
| 4-Undecene, 5-methyl-, (E)- | C12H24 |
| Hexadecane | C16H34 |
| Tridecane | C13H28 |
| 1-(4-Ethoxyphenyl)propan-1-ol | C11H16O2 |
| 4,5,6,7-Tetramethylphthalide | C12H14O2 |
| 2-Hexyl-1-octanol | C14H30O |
| Butylated Hydroxytoluene | C15H24O |
| 2,4-Di-tert-butylphenol | C14H22O |
| 7-Tetradecyne | C14H26 |
| Pentadecane | C15H32 |
| Benzoic acid, 4-ethoxy-, ethyl ester | C11H14O3 |
| Pentadecane | C15H32 |
| Pentadecane | C15H32 |
| 5,7-Dodecadiene, (E,Z)- | C12H22 |
| Pentadecane | C15H32 |
| Pentadecane | C15H32 |
| Glutaric acid, isobutyl 2-pentyl ester | C14H26O4 |
| Bicyclo[2.2.2]oct-7-en-2-one, 5-methylene- | C9H10O |
| 2,2,4-Trimethyl-1,3-pentanediol diisobutyrate | C16H30O4 |
| 1,2,3,4,7,7a-Hexahydro-2,4,7-trimethyl-6H-2-pyrindin-6-one | C11H17NO |
| Undecane, 2-methyl- | C12H26 |
| Mercaptoacetic acid, 2TMS derivative | C8H20O2SSi2 |
| 7-Tetradecyne | C14H26 |

| | |
|---|---|
| cis-2-Methyl-7-octadecene | C19H38 |
| Adipic acid, isobutyl 3-pentyl ester | C15H28O4 |
| Benzene, 1,1'-[3-(3-cyclopentylpropyl)-1,5-pentanediyl]bis- | C25H34 |
| Eicosane | C20H42 |
| Ethanone, 1-[2,3-dihydro-2-(1-methylethenyl)-5-benzofuranyl]-, (R)- | C13H14O4 |
| á-Vatirenene | C15H22 |
| Hexadecane | C16H34 |
| 2H-1-Benzopyran-2-one, 8-methoxy- | C10H8O3 |
| 2-Decen-1-ol, (E)- | C10H20O |
| Triallylsilane | C9H16Si |
| Octadecane | C18H38 |
| Silane, 9H-fluoren-9-yltrimethyl- | C16H18Si |
| 1,1,1,5,7,7,7-Heptamethyl-3,3-bis(trimethylsiloxy)tetrasiloxane | C13H40O5Si6 |
| 1-Heptadecyne | C17H32 |
| Octadecane | C18H38 |
| 1-Heptadecyne | C17H32 |
| 2-Methyltetracosane | C25H52 |
| Benzene, (3-octylundecyl)- | C25H44 |
| 6-Ethyl-4,7-dimethyl-2,3-benzofurandione | C12H12O3 |
| Hexadecane | C16H34 |
| Neophytadiene | C20H38 |
| 11,14-Eicosadienoic acid, methyl ester | C21H38O2 |
| 1,2-Benzenedicarboxylic acid, bis(2-methylpropyl) ester | C16H22O4 |
| Pentasiloxane, dodecamethyl- | C12H36O4Si5 |
| Tetramethylammonium acetate | C6H15NO2 |
| Cyclotetradecane | C14H28 |
| Octadecane | C18H38 |
| Cyclopropane, 1-(1-hydroxy-1-heptyl)-2-methylene-3-pentyl- | C16H30O |
| Undecanoic acid, methyl ester | C12H24O2 |
| Heptacosane, 1-chloro- | C27H55Cl |
| Octadecane | C18H38 |
| Octadecane | C18H38 |
| Dibutyl phthalate | C16H22O4 |
| Octadecane | C18H38 |
| n-Hexadecanoic acid | C16H32O2 |
| Octadecane | C18H38 |
| 2-Methyltetracosane | C25H52 |
| Behenyl chloride | C22H45Cl |
| 1-Butoxy-2-methyl-2-butene (Z)- | C9H18O |
| Spiro[2.4]hept-5-ene, 5-trimethylsilylmethyl-1-trimethylsilyl- | C14H28Si2 |
| Hexasiloxane, 1,1,3,3,5,5,7,7,9,9,11,11-dodecamethyl- | C12H38O5Si6 |

| | |
|---|---|
| Hexadecane | C16H34 |
| Octadecanoic acid, 2-propenyl ester | C21H40O2 |
| Palmitic acid vinyl ester | C18H34O2 |
| 1-Butanamine, 3-methyl- | C5H13N |
| Triacontane | C30H62 |
| Methyl-methoxy-hydroxymethyl-amine | C3H9NO2 |
| 1,1,1,5,7,7,7-Heptamethyl-3,3-bis(trimethylsiloxy)tetrasiloxane | C13H40O5Si6 |
| trans-13-Octadecenoic acid | C18H34O2 |
| 9,12-Octadecadienoic acid (Z,Z)- | C18H32O2 |
| Fluoranthene | C16H10 |
| Benzeneethanamine, 2-fluoro-á,3,4-trihydroxy-N-isopropyl- | C11H16FNO3 |
| Imidazolo[2,1-b]thiazole, 5-(3-indolyl)- | C13H9N3S |
| 11-Hexadecynal | C16H28O |
| 1-Hexacosene | C26H52 |
| Hexadecanoic acid, 2-hydroxy-1-(hydroxymethyl)ethyl ester | C19H38O4 |
| 2-naphthalenol, 1-[[(2-hydroxyphenyl)imino]methyl]- | C17H13NO2 |
| Cyclohexanamine, N-2-propenyl- | C9H17N |
| 4H-3,1-Benzoxazin-2-amine, 4-ethyl-N-[4-(1-methylethyl)phenyl]- | C19H22N2O |
| Octadecanoic acid, 2-propenyl ester | C21H40O2 |
| Pentasiloxane, dodecamethyl- | C12H36O4Si5 |
| 6,11-Eicosadienoic acid, methyl ester | C21H38O2 |
| Oxalic acid, allyl nonyl ester | C14H24O4 |
| Glycidyl palmitate | C19H36O3 |
| 6-Chloro-7-fluoro-4-oxo-1-(1-phenylethyl)-1,4-dihydroquinoline-3-carboxylic acid | C18H13ClFNO3 |
| 2-Methyl-3-(3-methyl-but-2-enyl)-2-(4-methyl-pent-3-enyl)-oxetane | C15H26O |
| Unknown 1 | C15H16O3 |
| Carbonic acid, 2-ethoxyethyl 2-methoxyethyl ester | C8H16O5 |
| 5,6-Dihydro-2,4,6-triethyl-4H-1,3,5-dithiazine | C9H19NS2 |
| 1-[(2-Thienylcarbonyl)oxy]-2,5-pyrrolidinedione | C9H7NO4S |
| Methyl 8,11,14-heptadecatrienoate | C18H30O2 |
| Cyclopropaneoctanal, 2-octyl- | C19H36O |
| Pentasiloxane, dodecamethyl- | C12H36O4Si5 |
| L-Serine, 3TBDMS derivative | C21H49NO3Si3 |
| 9,12-Octadecadienoyl chloride, (Z,Z)- | C18H31ClO |
| (E)-13-Docosenoic acid | C22H42O2 |
| Unknown 2 | C24H43NO |
| Octadecanoic acid, 2,3-dihydroxypropyl ester | C21H42O4 |
| Cyclopentadecanone, 4-methyl- | C16H30O |
| l-Norvaline, N-methoxycarbonyl-, methyl ester | C8H15NO4 |
| Unknown 3 | C21H28N2O4 |
| 13-Octadecenal, (Z)- | C18H34O |

| | |
|---|---|
| Glycidyl palmitate | C19H36O3 |
| Methyl 10,13,16-docosatrienoate | C23H40O2 |
| (-)-cis-Myrtanylamine | C10H19N |
| 1,1,1,5,7,7,7-Heptamethyl-3,3-bis(trimethylsiloxy)tetrasiloxane | C13H40O5Si6 |
| Cyclooctene, 3-ethenyl- | C10H16 |
| 1,15-Hexadecadiene | C16H30 |
| 2-Methyl-Z,Z-3,13-octadecadienol | C19H36O |
| Isocytosine | C4H5N3O |
| Stannane, butyldimethyl(1-methylethyl)- | C9H22Sn |
| 1-Cyclohexyldimethylsilyloxybutane | C12H26OSi |
| 1-Cyclohexyldimethylsilyloxybutane | C12H26OSi |
| Cyclododecanone, thiosemicarbazone | C13H25N3S |
| Pentasiloxane, dodecamethyl- | C12H36O4Si5 |
| Octadecanoic acid, 2-propenyl ester | C21H40O2 |
| Disiloxane, 1,1,3,3-tetramethyl-1,3-bis[3-(oxiranylmethoxy)propyl]- | C16H34O5Si2 |
| Dotriacontane | C32H66 |
| Pentasiloxane, dodecamethyl- | C12H36O4Si5 |
| 1-Butanamine | C4H11N |
| 5,10-Dioxatricyclo[7.1.0.0(4,6)]decane | C8H12O2 |
| Nonanamide | C9H19NO |
| Farnesol isomer a | C15H26O |
| Pentasiloxane, dodecamethyl- | C12H36O4Si5 |
| D-Alanine, N-ethoxycarbonyl-, tetradecyl ester | C20H39NO4 |
| 7,11-Hexadecadienal | C16H28O |
| Tridecane | C13H28 |
| Cholest-5-en-3-ol (3á)-, carbonochloridate | C28H45ClO2 |
| Hexasiloxane, 1,1,3,3,5,5,7,7,9,9,11,11-dodecamethyl- | C12H38O5Si6 |
| Cholest-5-en-3-ol (3á)-, carbonochloridate | C28H45ClO2 |
| Stigmastan-6,22-dien, 3,5-dedihydro- | C29H46 |
| 9-Octadecenal | C18H34O |
| 1,3-Benzothiazole, 2-(3-methylbutoxy)- | C12H15NOS |
| Cholest-5-en-3-ol (3á)-, carbonochloridate | C28H45ClO2 |
| Hexasiloxane, 1,1,3,3,5,5,7,7,9,9,11,11-dodecamethyl- | C12H38O5Si6 |
| dl-à-Tocopherol | C29H50O2 |
| Hexasiloxane, 1,1,3,3,5,5,7,7,9,9,11,11-dodecamethyl- | C12H38O5Si6 |
| Cyclopropane, 1-(1-hydroxy-1-heptyl)-2-methylene-3-pentyl- | C16H30O |
| Hexasiloxane, 1,1,3,3,5,5,7,7,9,9,11,11-dodecamethyl- | C12H38O5Si6 |
| Cyclopropane, 1-(1-hydroxy-1-heptyl)-2-methylene-3-pentyl- | C16H30O |
| E,E,Z-1,3,12-Nonadecatriene-5,14-diol | C19H34O2 |
| Cholest-4-en-3-one | C27H44O |